NTNU

Norwegian University of
Science and Technology

Feasibility study on Subsea Power Generation from Wellstream Heat using a Binary Organic Rankine Cycle

Roger Jakobsen Gleditsch

Petroleum Geoscience and Engineering
Submission date: June 2018
Supervisor: Milan Stanko, IGP

Norwegian University of Science and Technology
Department of Geoscience and Petroleum

Preface

This master's thesis "*Feasibility study on Subsea Power Generation from Wellstream Heat using a Binary Organic Rankine Cycle*" was written to fulfill the graduation requirement of the Petroleum Engineering program at the Norwegian University of Science and Technology. The idea of using the selected topic as basis for my thesis came while working an internship at Equinor ASA, after seeing how committed the company is to finding new, innovative and environmental friendly technological solutions. The research objectives were formulated based on input from my main faculty supervisor Milan Stanko, my company contact Lars Brenne and my personal requests. Work on the project was conducted during my final semester at the university, from middle of January 2018 to start of June 2018.

Performing work and writing the thesis were some of the most challenging tasks I have experienced, but as I find the research topic highly interesting I was able to enjoy every minute of the endeavor. The investigation resulted in answers to the main research objectives, and I want to take this opportunity to thank my supervisors who helped in making this thesis possible by giving their input, guidance and providing access to real field data.

It is my hope that the reader will find reading this thesis interesting. As the author I have truly enjoyed my part in this project, and I am optimistic and looking forward to starting as a graduate employee in Equinor ASA this summer.

Trondheim, 2018-06-11

Roger Gleditsch

Acknowledgment

My biggest thanks go out to my thesis advisor Associate Professor Milan Stanko of the Norwegian University of Science and Technology. He made it possible for me to spend my final semesters working on a topic that has really piqued my interest for a long time. Finding a way of utilizing waste heat offshore has been a personal dream of mine, which led to my request of doing my specialization project fall 2017 dealing with this field of science. The specialization project was titled "*Thermal Energy Conversion Methods for Subsea Power Generation*[1]" and involved looking into existing technologies for thermal energy conversion, such as thermoelectric materials and different power cycles, and it was found that binary organic Rankine cycles had very high potential for thermal energy conversion using oil-based wellstreams. The specialization project laid ground work for much of the thermodynamic theory presented in this thesis.

I especially appreciate how my supervisor allowed me to work very independently and was still able to quickly respond to any question I have had, and his excellent guidance when it came to define the research objectives and how to fulfill them. I would also like to extend my thanks to my external contact in Equinor ASA, Lars Brenne. The research would not have been feasible without the field data he provided, and I am thankful that he made it possible for me to conclude my education at NTNU by doing research for the company I will be working for in the future.

My peers at NTNU, my family and my friends also deserve a special thank you for making the last five years in Trondheim not only possible, but also engaging and fun. As I am typing this I only have two more weeks in Trondheim before moving to Northern Norway to work, and I am sure I will be looking back at my time at the university as some of the best years of my life. Looking forward, I can almost not wait to kick-off my career in Equinor ASA as I am sure the next coming years will be great too.

R.G.

[1] TPG4560 Petroleum Engineering, Specialization Project. Roger Gleditsch, December 2017.

Executive Summary

Geothermal heat from the subsurface can potentially be used as a clean energy source for offshore oil and gas producing facilities in the future. This thesis investigates the feasibility of thermal energy conversion by the use of a binary organic Rankine cycle offshore, with the aim to see if on-site power generation based on waste heat may be viable for utilization. This study uses wellstream data from the Tordis and Midgard fields to evaluate the energy conversion potential from oil- and gas-based reservoirs, respectively. A comparison of the raw power potential between the two reservoirs at different wellhead temperatures have been quantified, to investigate which reservoir type is more suitable for geothermal energy exploitation. It was found that the liquid-based Tordis wellstream has larger thermal potential than Midgard saturated gas for any wellhead temperature when production mass rates and other conditions were equalized. A large amount of fluids were screened as potential working fluids for a thermodynamic cycle operating at the Tordis field. The working fluid selection criteria were based on performance, accessibility and environmental impact. The fluids R134a and butane were found to be the most suitable for an organic Rankine cycle placed topside at Tordis. For a cycle placed on the sea floor, a binary mixture of 10 mol-% propane and 90 mol-% ethane performed well at the high-pressure subsea ambient. The necessary operating conditions for optimal net power output have been defined using a subsea cycle at Tordis as a base case. This involved estimating the pressure and temperature requirements for each stage of the cycle along with optimizing the working fluid mass flow rate, which was performed using the thermodynamic software Aspen HYSYS. The simulation of the subsea power generation system involved using a rigorous model for the shell and tube evaporator heat exchanger, to get a realistic estimate for the heat transfer potential from wellstream to cycle. The highest thermal energy transfer was achieved using a series of five dual-pass heat exchangers totalling an effective heat transfer area of 1397.8 m^2, which would transmit 23.2 MW of heat to the cycle. The cycle thermal efficiency was 9%, effectively producing approximately 2.1 MW worth of power. Rough basic design features of the cooling system and turbine were also determined. It was opted to use a passive system for working fluid cooling by making use of natural convection with the surrounding sea water, and the required effective heat transfer area of the passive cooling manifold was estimated to a minimum of 950.0 m^2. Sizing of the turbine was performed based on the energy state of the working fluid to calculate the optimum lengths of the rotor blades to produce electricity at the Norwegian grid frequency of 50 Hz. The unit was modelled as a simple axial turbine, and it was found that with inlet binary working fluid velocity at 260.8 m/s, using initial rotor blade lengths of 0.19 meters, grid frequency is achieved. The outlet velocity was calculated to 98.1 m/s, yielding an overall maximum energy utilization efficiency of 85.8% for the proposed turbine. It was investigated which control requirements are necessary to run a subsea organic Rankine cycle, and the following elements were found as the most efficient actuators for output optimization and cycle supervision. Installation of a by-pass

valve circumventing the heating train for pressure control, a turbine by-pass that can be opened to route the working fluid in case of condensate droplets occurring, pump speed control and a gear box for the generator to ensure energy production at constant frequency. The thermodynamic feasibility of a power generation unit at the Tordis field has been assessed qualitatively after an extensive literature review, and is deemed as plausible. The energy requirement for subsea boosting at the field was used as evaluation criteria. Tordis requires approximately 4 MW of power supply for its boosters, and the results from the literature study suggested that a net energy output of up to 4.65 MW is achievable based on a realistic cycle thermal efficiency factor. When the thermodynamic feasibility was assessed quantitatively based on the proposed dynamic model for subsea cycle, it is deemed non-viable. The calculated net energy output of 2.1 MW from the rigorous model does not suffice to cover the boosting power requirement.

Executive Summary in Norwegian

Geotermisk varme fra undergrunnen kan potensielt brukes som en ren energikilde for fremtidige olje- og gassproduksjonsanlegg. Denne masteroppgaven undersøker muligheten for å konvertere termisk energi til elektrisitet ved bruk av en binær organisk Rankine syklus installert offshore, med formål om å se om kraftproduksjon på sokkelen basert på spillvarme kan være bærekraftig. Studien bruker brønnstrømdata fra Tordis og Midgard-feltene for å evaluere energikonverteringspotensialet fra henholdsvis olje- og gassbaserte reservoarer. En sammenligning av det rå kraftpotensialet mellom de to reservoarene ved forskjellige brønnhodetemperaturer er blitt kvantifisert for å undersøke hvilken reservoartype som er best egnet for utnyttelse av geotermisk energi. Det ble funnet at den væskebaserte Tordis-brønnstrømmen har større termisk potensial enn Midgard mettet gass for en hvilken som helst brønnhodetemperatur når produksjonsmasseratene og andre parametere var satt til samme verdi. En stor mengde fluider ble undersøkt som potensielle arbeidsfluider for en termodynamisk syklus som opererer på Tordis. Fluidene ble sammenlignet basert på ytelse, tilgjengelighet og miljøpåvirkning for å finne et egnet arbeidsmedium for bruk i en syklus installert på feltet. Fluidene R134a og butan ble funnet til å være de mest hensiktsmessige mediene for en organisk Rankine-syklus som opererer ved Tordis når syklusen er installert på overflaten. For en syklus plassert på sjøbunnen ble det vist at en binær blanding av 10 mol-% propan og 90 mol-% etan fungerte godt under operasjon ved det høye trykket og de lave temperaturene som er tilfellet 250 meter under havoverflaten. De nødvendige driftsforholdene som vil gi optimal netto ytelse av elektrisitetsproduksjonen er definert for en undersjøisk syklus ved Tordis. Dette innebar estimering av trykk- og temperaturforhold for hvert trinn i syklusen samt optimalisering av arbeidsfluidets massestrømningshastighet, kalkulasjoner som ble utført ved hjelp av den anerkjente termodynamiske programvaren Aspen HYSYS. Simuleringen av det subsea kraftgenereringssystemet inkluderer en detaljert modell for skall og rør-varmeveksler, da dette var spesielt viktig for å få et realistisk estimat for varmeoverføringspotensialet fra brønnstrømmen til syklusen. Den høyeste termiske energioverføringen ble oppnådd ved bruk av en serie bestående av fem varmevekslere, som totalt utgjorde et effektivt varmeoverføringsområde på 1397.8 m^2, en konfigurasjon som overfører 23.2 MW varmeenergi til syklusen. Syklusens termiske effektivitetsfaktor var 9 %, og den produserte effektivt omtrent 2.1 MW strøm. Grunnleggende designfunksjoner av kjølesystemet og turbinen ble også bestemt ved hjelp av matematiske modeller. Det ble valgt å bruke et passivt system for kjøling av arbeidsmediet for å utnytte naturlig konveksjon med det kalde omkringliggende sjøvannet, og det nødvendige effektive varmeoverføringsområdet for en passiv kjølemanifold ble estimert til minimum 950.0 m^2. Dimensjonering av turbinen ble utført på grunnlag av energitilstanden til arbeidsfluidet for å beregne optimal lengde av rotorblad for å produsere elektrisitet på den norske nettfrekvensen på 50 Hz. Enheten ble modellert som en enkel to-stegs aksialturbin, og det ble funnet at grensefrekvensen oppnås ved innløpshastighet av arbeidsmediet på

260.8 m/s når rotorbladene ved innløpet er 0.19 meter lange. Utløpshastigheten fra turbinen ble beregnet til 98.1 m/s, hvilket ga en total maksimal energiutnyttelse på 85.8 % for den foreslåtte turbinen. Det ble undersøkt hvilke former for kontroll som er nødvendige for å drive en subsea organisk Rankine-syklus, og følgende elementer ble funnet som de mest effektive aktuatorene for optimalisering samt syklustilsyn. En bypassventil som omgår oppvarmingsvarmeveksler for å kunne benyttes til utførelse av trykkregulering samt et turbinbypass som kan åpnes for å lede arbeidsfluidet forbi turbinen (i tilfelle det oppstår kondensatdråper) vil måtte være integrert i syklusen subsea. I tillegg vil hastighetsregulering av pumpe og girkasse for generatoren være nødvendig for å sikre energiproduksjon ved konstant frekvens på 50 Hz. Den termodynamiske gjennomførbarheten av en kraftgenereringsenhet på Tordis-feltet har blitt vurdert kvalitativt etter en omfattende litteraturgjennomgang, og anses som plausibel. Energibehovet for subsea boosting på feltet ble brukt som evalueringskriterie for å dømme om elektrisitetsutbyttet er godt nok eller ikke. Tordis krever omtrent 4 MW strømforsyning for å drive boosting, og resultatene fra litteraturstudien antydet at en nettoproduksjon på opptil 4.65 MW er oppnåelig basert på en realistisk effektivitetsfaktor. Når den termodynamiske gjennomførbarheten ble vurdert kvantitativt basert på den foreslåtte dynamiske modellen for undersjøisk syklus, anses den ikke å være levedyktig. Nettoeffekten på 2.1 MW kalkulert med den detaljerte modellen er ikke tilstrekkelig til å dekke strømforbruket som kreves til subsea boosting.

Contents

List of Tables

List of Figures

Acronyms

Acronyms referenced in Text

BP Bubble Point

CGR Condensate Gas Ratio

DP Dew Point

FSCC Future Subsea Controllable Cooler

GOR Gas Oil Ratio

GHG Greenhouse Gas

ID Inner Diameter

IHE Internal Heat Exchanger

NCG Non-Condensable Gas

NCS Norwegian Continental Shelf

OD Outer Diameter

ORC Organic Rankine Cycle

PT Pressure Temperature

ROV Remotely Operated underwater Vehicle

SPE Society of Petroleum Engineers

UNFCCC United Nations Framework Convention on Climate Change

VBA Visual Basic for Applications

WC Water Cut

WF Working Fluid

WHP Wellhead Pressure

WHT Wellhead Temperature

Abbreviations referenced as subscripts in Equations

CMTD Corrected Mean Temperature Difference

H Horizontal

LMTD Logarithmic Mean Temperature Difference

SD Super Duplex

SS Shell Side

TS Tube Side

V Vertical

e Empty

f Full

g Gravity

hf-i Heating Fluid-i

i Inner

o Outer

qua quadratic or square tube pattern

t Turbulent

tc Turbulence Correction

tri Triangular tube pattern

w Wavy

wf-i Working Fluid-i

Chapter 1

Introduction

1.1 Background

One of the most significant challenges for our modern world is to find ways to cover a rapidly increasing need for energy, without harming the environment that surrounds us. At 12th of December 2015, *The Paris Agreement* was signed by 194 United Nations Framework Convention on Climate Change (UNFCCC) members. The agreement sent a strong message to people all over the world that the involved countries want to battle greenhouse gas (GHG) emissions and climate change together, through an increased global effort. The oil industry is often portrayed by the media as the biggest hindrance to achieving long term climate goals. Equinor ASA is a Norwegian oil company that has set strict CO_2 intensity goals to reduce the carbon footprint from their operations at the Norwegian continental shelf (NCS) and other locations around the world. Research and development of new technology that increase operational efficiency while reducing GHG emissions is unequivocally supported and heavily funded, with the aim for a greener energy future. A large part of the emissions coming from the oil industry is in relation to offshore combustion of fuels for energy production, which means GHG output on the NCS can be directly influenced by increasing the energy conversion efficiency. As it is challenging to improve modern power generators to significant effect, more companies have started looking for alternative energy sources to cover their offshore energy requirements. Green electricity produced onshore is a possibility for some fields, but for very remote installations it would imply very high umbilical costs. To find cost-efficient ways of producing clean energy on-site is a dream for many. Wind and wave energy is often talked about as potential energy sources, but also thermal energy from the reservoirs represents possibilities. This thesis evaluates the feasibility of using an organic Rankine cycle (ORC) installed subsea to generate a net power output from the raw thermal energy in the wellstream. The research objectives were developed in joint effort by a cooperation agreement between Equinor ASA and NTNU.

Problem Formulation

High amounts of thermal energy are wasted to the environment on daily basis in relation to hydrocarbon production offshore. The energy is mainly lost as the fluids flow from reservoir to surface by heat transfer to the surroundings or in processing when the fluids are cooled for storage and/or transportation. Using waste heat for electricity generation offshore can potentially serve as a means of reducing GHG output from the oil industry in the future. As fields grow old they often tend to produce more and more water, which is a fluid with very high thermal heat capacity. In addition, the need for subsea boosting is generally larger over time as reservoirs get more depleted. As the increasing water cut could lead to more thermal energy potential over time, a positive synergy effect would be if the energy could be used to supply duty to the submerged boosters or other equipment, and lessen the need for the company to burn fuels for electricity. This master's thesis aim is to look at the already proven energy conversion technology *organic Rankine cycle* (ORC) to see if it may be considered viable for offshore installation and to get an idea of its potential net power output. The scope is to do the thermodynamic feasibility evaluation based on fields producing mainly oil, but a comparison between the raw thermal heat potential of both gas and oil producers is also analyzed.

Related work

A literature study was performed in relation to working on this project, and an annotated bibliography of papers concerning low temperature ORCs has been written to be included in the thesis. The annotated bibliography is found in Section 2.4 and gives the reader insightful information on the effectiveness of applying the thermodynamic cycle energy conversion technology on geothermal resources with temperatures lower than 130°C. Since an overview of some of the key papers from the literature research is reviewed in detail in the theory chapter, this section will only contain a summary of the work and honorable mentions of other authors that also have been referenced in the thesis.

- The published textbook *Organic Rankine cycle (ORC) power systems: Technologies and Applications* by Astolfi and Macchi (2017) provided helpful information of details regarding the thermodynamic cycle on a general level, and showed many examples of real ORC power plants around the world utilizing brine as a geothermal resource.

- DiPippo (2016) authored the book *Geothermal Power Plants: Principles, Applications, Case Studies and Environmental Impact* which deals with ORCs at a high technical level, and has served as a very useful resource for the thesis in multiple aspects.

- It is shown by Dong et al. (2017) that the performance of low temperature ORCs can be improved using mixtures as cycle working fluid as opposed to running the cycle with a

pure fluid. In light of the finds, this thesis investigates the use of both singular component and binary working fluids for the subsea cycle.

- In the paper *Geometry Optimization of Power Production Turbine For A Low Enthalpy ($\leq 100^{\circ}C$) ORC System* Efstathiadis et al. (2015) developed a turbine optimization model that was run under the assumption of extreme conditions. The internal geometry and required turbine volume was compared between using pure and binary working fluids, and it was found that a binary mixture of i-butane and i-pentane could outperform R134a significantly without having a large impact on turbine dimensions.

- Hettiarachchi et al. (2007) presents a cost-effective design criterion for low temperature ORC. The developed model uses a function of the ratio between required heat exchanger area to net power output to estimate the most efficient cycle operating conditions. Special emphasis is made on optimizing condensation and evaporation temperatures.

- The recently published textbook *Turbomachinery Concepts, Applications, and Design* by Murty (2018) is a great resource for information on how to determine required design features of turbines and other rotating equipment.

- Rudh et al. (2016) gives detailed review of different kinds of subsea cooling equipment, both state of the art technology and recently explored concepts.

- In the paper *Working fluids for low-temperature organic Rankine cycles* Saleh et al. (2007) screens a large amount of working fluids using cycles with and without internal heat exchanger. A table summarizing some of the most important results have been included in the annotated bibliography of this report, and the calculated cycle efficiencies from the Saleh et al. (2007) screening gave useful information on what fluids are of high potential.

- Toffolo et al. (2014) used a multi-criteria approach to optimize cycle design parameters. The paper evaluates a large amount of working fluids at different cycle configurations and answers which cycle designs are usually most fitting to specific fluids.

What Remains to be Done?

Geothermal plants are outputting power with ORC technology all over the world by production of brine from the subsurface as an energy source. The working fluids used in the industry today are generally pure substances, but studies suggest that the thermal efficiency of plants built in the future can be increased by using working fluids based on multiple components. This thesis investigates the implications of using ORC *subsea* exploiting thermal energy in hydrocarbon wellstreams, which is an unexplored application area so far. The potential for using a binary working fluid composition for the subsea cycle is also assessed.

1.2 Objectives

The main objective of this master's project is to perform a feasibility study on subsea power generation with ORC technology using heat from reservoir fluids produced at the Tordis field. The secondary objectives are:

1. To determine the difference in raw heat potential between fields producing mainly oil or mainly gas, using Tordis and Midgard compositional data for comparison.
2. To screen suitable working fluids for the Tordis field thermodynamic cycle and select one.
3. To define flow rates, temperatures and pressures as operating conditions for the thermodynamic cycle.
4. Determine control requirements for the subsea power generation unit.
5. To perform a rough pre-design of the heat exchangers and other elements of the thermodynamic cycle.
6. To evaluate qualitatively and quantitatively the thermodynamic feasibility of a subsea power generation unit based on extracting heat using a thermodynamic cycle.

1.3 Approach

A literature review of general thermodynamic phenomena and low temperature organic Rankine cycles have been performed. The reasoning behind the review was not only to understand the core concepts, but also to help determine the qualitative feasibility of a subsea ORC by finding answers to 'if', 'how' and 'why' it would work. A quantitative feasibility analysis of subsea ORC was performed using the Tordis field as a base case for study. This involved creating several numerical models which helped estimate the raw thermal potential, evaluate the thermal efficiency of eligible working fluids, calculate the cycle net power output and roughly estimate the necessary component sizes. Two computational routines where the software Aspen HYSYS was interlinked with Excel VBA were used for the raw thermal potential estimation, one investigating the effect on heat flow potential when the wellhead temperature changes and the other calculating the raw thermal heat potential through field lifetime using data from NPD. The methodology for the working fluid screening was to create a basic cycle ORC with the Tordis field constraints and limitations, linking it with an Excel spreadsheet that allowed for changing cycle working fluid. This way it was possible to use a macro for iteration through the eligible fluids, calculating cycle thermal efficiencies and net power outputs for the entire realistic Tordis wellhead temperature range, and write the data back to Excel. The cycle component sizing was performed using

known equations for convective and conductive heat transfer, with a precise model for the shell and tube heat exchanger designed using Aspen EDR. With the rigorous model for the evaporator it was possible to calculate realistic heat transfer from the Tordis wellstream to the cycle working fluid, and the ORC operating conditions were determined based on this state of enthalpy. Cycle control requirements were determined based in part on specifications in NORSOK P-002 (2014) and the main cycle control elements were chosen based on the limited amount of actuators present in a subsea ORC.

1.4 Contributions

The main contributions from this thesis is determining the operational requirements for a subsea power generation plant using ORC technology with the Tordis wellstream as an energy source. The potential net power output of the system has been estimated and the necessary minimum sizes of various cycle elements have been assessed. Code implemented in Excel VBA to communicate with the thermodynamic software program Aspen HYSYS has been tested extensively, and used for cycle optimization and working fluid selection.

1.5 Limitations

This work evaluates the *thermodynamic* feasibility of a subsea power generation unit. Other factors that have not been evaluated play a significant role in a complete feasibility study concerning establishing a power plant offshore. These are things as cost analysis and payback period calculation, environmental risk assessment, energy conversion technology reassessment, detailed component design, geothermal resource analysis to name some of the most important ones. This study aims to answer if the wellstream as an energy source is of sufficient size for meaningful power generation, and not evaluate if it is the commercially correct thing to do so.

1.6 Outline

- **Chapter 2. Theory:**
  This chapter includes an introduction to the base principles of heat transfer and energy conversion using low temperature organic Rankine cycles. The heat transfer part is based on widely known thermodynamic theory which makes the following chapters more easily understandable, and the part about low temperature organic Rankine cycles is based on a literature review of published papers.

- **Chapter 4. Methodology:**
  This chapter presents models that have been made to compute raw thermal power potential of a wellstream, to screen potential working fluids for the thermodynamic cycle and to evaluate equipment design requirements.

- **Chapter 5. Results:**
  Here key results from the numerical simulations and calculations are presented, along with information about the inputs used to generate them.

- **Chapter 6. Conclusions:**
  This chapter summarizes the main findings from the master's project, and discusses what conclusions that can be safely drawn from them.

- **Appendix A. Code associated with the Raw Power Model:**
  The scripts written for the raw power numerical calculations have been included here.

- **Appendix B. Code associated with the Subsea ORC Model:**
  The scripts written for the simulations of subsea organic Rankine cycle to generate optimum properties for maximum cycle net power output have been included here.

- **Appendix C. Heat Exchanger Design Illustration:**
  Figure of cross section of the proposed shell and tube evaporator is included here.

- **Bibliography:**
  List of references to the sources used for this report.

Chapter 2

Relevant Thermodynamic and Heat Transfer Theory

In this report several models are presented that estimate a variety of thermodynamic properties, depending on user input and what process is being investigated. Thermodynamic software packages make it easy to produce numbers for a process, but that does not automatically mean that the user understands what is going on and what calculations are taking place. One of the scopes of this master's project is to develop and show understanding of the core concepts at work in thermal energy conversion processes, and a natural way of doing so is to start by making a description. Most of the theoretical physics in this chapter is referenced to the specialization project work leading up to this thesis, contained in the unpublished paper "*Thermal Energy Conversion Methods for Subsea Power Generation*" by Gleditsch (2017).

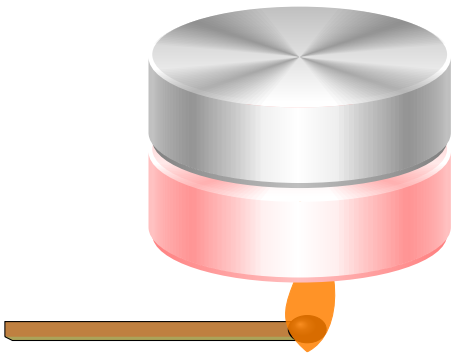

Figure 2.1: Heat transferred through direct contact by conduction. The bottom metal disc is heated by the burning matchstick, eventually causing the temperature of both discs to rise.

2.1 Heat Transfer in General

The amount of thermal energy that is added to or removed from a system is what we call *heat*. Heat can be defined as the energy that is transferred between systems, when they are at different temperatures. It is common to label heat with the letter Q, and use the SI unit Joules. The flow of heat changes the temperature of a system, but how much it is changed depends on two things. The first thing it is dependent on is the systems mass; if the mass is increased more heat is required to change its temperature. The second thing it is dependent on, is the *specific heat* of the system. The specific heat is defined as a measure of how well a substance stores heat, and every substance has its own value. When the specific heat of a substance is increased, it means that more energy transfer in the form of heat is required to induce a temperature change. Equation (2.1) defines heat for an in-compressible substance, and shows that the amount of thermal energy transferred is equal to the mass multiplied with specific heat c_p and temperature change. A positive Q means that the energy is flowing into the system, and a negative prefix would indicate that heat is flowing out. For gases it must be taken into account that pressure-volume work in addition to heat transfer affects the internal energy of a substance, which can be expressed by the first law of thermodynamics (Equation (2.2)). During a phase change the internal energy of a substance will change even as its temperature is held fixed ($\Delta T = 0$). A way to calculate how much heat is flowing in or out of a system during phase changes is to use an entity called *latent heat*. Latent heat reflects the changes in internal energy during a phase change, and in Equation (2.3) it is labelled with the letter L.

$$Q = m \cdot c_p \cdot \Delta T \tag{2.1}$$

$$\Delta U = W + Q = P\Delta V + Q \tag{2.2}$$

$$Q = m \cdot L \tag{2.3}$$

Heat spreads in three different ways, by conduction, convection or by radiation. These occur depending on the circumstances that are taking place, and several of these types of heat transfer can happen simultaneously. In the remainder of this section conduction and convection will be explained, as they are phenomena of great importance to the topics of this thesis.

Conduction is the heat transfer related to direct contact between atoms or molecules, where kinetic energy is transferred as they vibrate. A good example of conduction would be when solid metal discs are in contact with each other, here illustrated in Figure 2.1 where the bottom disc is heated due to some source of energy. Because of direct contact between the discs, both discs are expected to become of higher temperature. In metals the phenomenon of conduction is especially prominent, because the atoms sit very neatly packed together and allows the kinetic

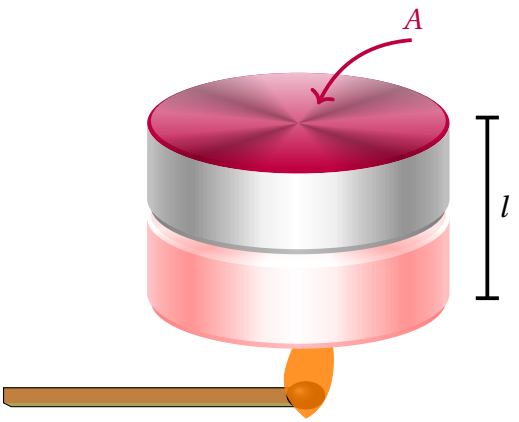

Figure 2.2: Cross-section and travel distance related to heat flow by conduction. If both discs are made of the same metal, they possess the same κ.

energy to spread rapidly from one atom to the next. In thermodynamics, the letter κ is commonly used for *thermal conductivity* and represents how fast a material is at conducting heat. Equation (2.4) shows how rate of heat transfer between two points by the means of conduction can be calculated. In the equation, the letter A means cross sectional area, t is time and the letter l is the distance between two points, see it illustrated in Figure 2.2.

$$\frac{Q}{t} = \frac{\kappa \cdot A \cdot \Delta T}{l} \tag{2.4}$$

Convection is another type of heat transfer mechanism, which has some similarities to conduction in the sense that it also is dependent on molecular contact. In conduction the molecules collide because they are closely packed nearby each other, but in the case of convection they tend to travel much greater spatial distances. The typical example of convection is when a tea kettle is warmed on the stove. Since the kettle is warmed from below, the tea water at the bottom will become warm first which causes the arrangement of molecules to expand to a lower density and make them spread away from the heat source. As soon as the warm molecules have moved, cooler molecules from higher up in the kettle will move downwards and take their place, thus creating heat transfer in the kettle. Another example of convection is when hot fluids from a reservoir below the ground come towards the surface through a production well, effectively moving away from the heat source to a cooler environment. The basic relationship for heat transfer by convection is given in Equation (2.5), where λ is the *heat transfer coefficient*, t is time and A_s is the surface area of the substance. It should be noted that convection can be divided into two types, *forced* convection and *natural* convection. Forced convection is heat transfer that happens when a substance is forced into contact with another substance, like when a liquid is forced to flow through a pipe. Natural convection happens naturally, for example when sea water comes into contact with stationary subsea equipment. To perform calculations on convection, one must rely on empirical *Nusselt number*-correlations to determine the heat transfer

coefficient λ. There are many different correlations to choose from depending on the situation, and in Sections 2.3.5 and 3.5 of this thesis some are shown. For natural convection, the geometry of the contact surface becomes of importance and must be determined. If we are looking at forced convection like flow through a pipe, one must determine the flow conditions possibly by calculating the Reynolds number manually. If the convection happens naturally or forced under laminar conditions, the heat transfer coefficient would be determined by the use of the Prandtl, Grashof and Rayleigh numbers along with an empirical correlation fitting to the situation. The Prandtl, Grashof and Rayleigh numbers are defined by Equations (2.6)-(2.8). If the convection happens forced but under turbulent conditions, one would have to estimate the friction coefficient for the interface as well, and rely on a different correlation for λ.

$$\frac{Q}{t} = \lambda \cdot A_s \cdot \Delta T \tag{2.5}$$

$$Ra = Gr \cdot Pr \tag{2.6}$$

$$Gr = \frac{g L_{gr}^3 \beta \Delta T}{\nu^2} \tag{2.7}$$

$$Pr = \frac{\mu c_p}{\kappa} \tag{2.8}$$

Nomenclature for Chapter 2.1

Q	Heat (J)	l	Distance (m)
m	Mass (kg)	λ	Heat transfer coefficient ($W/m^2 \cdot K$)
c_p	Specific heat ($J/kg \cdot K$)	A_s	Surface area (m^2)
ΔT	Temperature differential (K)	g	Gravity (m/s^2)
L	Latent heat (J/kg)	L_{gr}	Flat plates: Vertical length (m)
t	Time (s)		Pipes: Diameter (m)
κ	Thermal conductivity ($W/m \cdot K$)	β	Coefficient of thermal expansion (1/K)
A	Cross-sectional area (m^2)	ν	Kinematic viscosity (m^2/s)
ΔU	Change in internal energy (J)	μ	Dynamic viscosity ($Pa \cdot s$)
W	Pressure volume work (J)		

2.2 Potential Heat Energy in a Produced Hydrocarbon Mixture

In Section 3.1, an Aspen HYSYS routine that estimates the raw thermal power potential from a fluid stream that is cooled is presented. The goal in that exercise is to see how much thermal energy that has to transfer out of a fluid stream if the core temperature of the stream is reduced by a set amount. This section will show why HYSYS is used for the numerical calculation with an example that shows how difficult it is to solve accurately manually. Kindly find the nomenclature for the equations in the table at the end of the section.

The enthalpy H of a system is a measure of its internal energy U plus the product of its pressure and volume, as defined by Equation (2.9). If we assume that a fluid has constant pressure, an enthalpy change can be induced by heat, work or a volume change. If we make another assumption that all the work done in the system is what the pressure does to change the volume, then we end up with Equation (2.12) that shows that the change in enthalpy is effectively equal to heat. When doing thermodynamic analysis often the letter h for specific enthalpy is used as opposed to H. The specific enthalpy is defined as enthalpy divided by mass, and is convenient because it changes the value into an intensive property, here given by Equation (2.13).

$$H = U + P \cdot V \tag{2.9}$$

$$\Delta H = Q + W + \Delta(P \cdot V) \tag{2.10}$$

$$\Delta H = Q + -\Delta(P \cdot V) + \Delta(P \cdot V) \tag{2.11}$$

$$\Delta H = Q \tag{2.12}$$

$$h = \frac{H}{m} \tag{2.13}$$

Below are equations necessary to analytically express heat flow from a fluid stream that passes through a cooler, as illustrated by Figure 2.3. Equations (2.14), (2.15) and (2.17) are derived from the first law of thermodynamics, which states that the energy of an isolated system is constant. The internal energy u and enthalpy h have here been expressed as intensive properties, therefore lower-case letters have been used.

$$\sum E_{in} = \sum E_{out} + \Delta E_{storage} \tag{2.14}$$

$$\dot{W} + \dot{m}_{in}(u_{in} + P_{in}V_{in} + \frac{v_{in}^2}{2} + gz_{in}) = \dot{Q} + \dot{m}_{out}(u_{out} + P_{out}V_{out} + \frac{v_{out}^2}{2} + gz_{out}) \tag{2.15}$$

$$h = u + PV \tag{2.16}$$

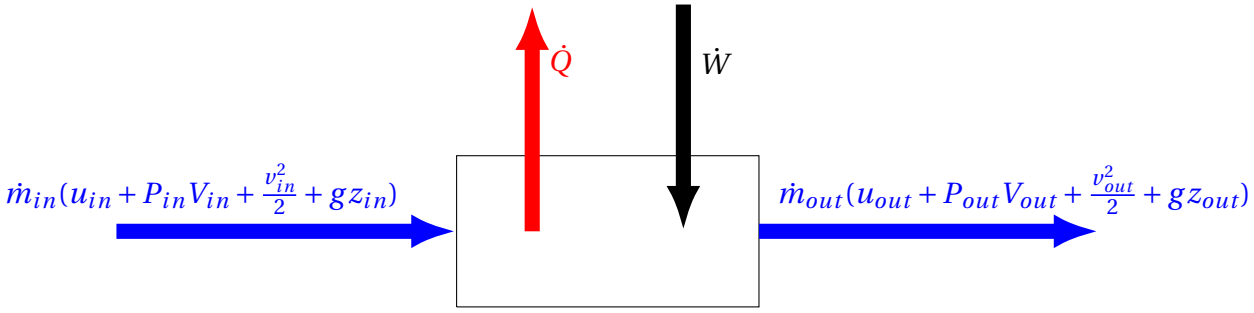

Figure 2.3: Cooling process illustrated by a box that acts as control volume for energy conservation considerations.

$$\dot{W} + \dot{m}_{in}(h_{in} + \frac{v_{in}^2}{2} + gz_{in}) = \dot{Q} + \dot{m}_{out}(h_{out} + \frac{v_{out}^2}{2} + gz_{out}) \tag{2.17}$$

Equation (2.17) shows that the difference in enthalpy between inlet and outlet streams of a cooler can be used to calculate a value for heat. With constant rates, no work and no elevation difference between the sides of the cooler, the terms for kinetic and potential energy will cancel out and leave heat solely as a function of enthalpy difference. The enthalpy of a mixture of different fluids can then be expressed based on the mass fraction of each phase times its enthalpy. The enthalpy of liquid (and solid) phase is equal to the product of c_p and ΔT, but the enthalpy of gases is not as easily expressed. When we are dealing with a hydrocarbon mixture, the total heat flux will be the sum of the contribution from each fluid, see Equation (2.18). Equation (2.19) shows the expression for the total heat flux based on the mass fraction and enthalpy change of each phase of a fluid stream consisting of water, oil and gas.

$$\frac{Q}{t} = \dot{Q} = \dot{Q}_g + \dot{Q}_o + \dot{Q}_w \tag{2.18}$$

$$\dot{Q} = (\dot{m}_g \Delta h_g + \dot{m}_o \Delta h_o + \dot{m}_w \Delta h_w) \tag{2.19}$$

To make numeric estimations by hand it is found convenient to write the mass flow rate in terms of density and volumetric flow rate, as shown in Equation (2.20). Here the product of heat capacity and temperature difference has been substituted in for enthalpy change for the liquid phase, but the same simplification can not be done for the gas.

$$\dot{Q} = (\dot{m}_g \Delta h_g + \rho_o \dot{V}_o c_{p,o} \Delta T + \rho_w \dot{V}_w c_{p,w} \Delta T) \tag{2.20}$$

There are multiple reasons that the simplifications done in the equations above could cause large errors, and manual calculation of Equation (2.20) is never performed in this report because of these. In the previous section it was mentioned that if a substance was subject to phase change, a property called latent heat is necessary to perform the calculation of heat and that

its temperature would remain unchanged during the transition. And as we now have seen, the thermal potential of the hydrocarbon flow is a combination of multiple fluids in two different phases. Further expressing the rate of heat transfer analytically quickly becomes very tedious, as it must be taken into account that phase change may occur in one of the fluids while others stay within their current phase. In theory, phase changes between hydrocarbons in gaseous and liquid state could occur, thus keeping the temperature constant between them, whilst a temperature drop indeed could take place for the water simultaneously. When it comes to the energy calculation of heat from the gaseous phase, it also has to be taken into account that as heat is transferred to the surroundings the gas will have a tendency to contract in volume, which means the surroundings will do pressure-volume work on the system. Aspen HYSYS will be used for further analysis as it is an extremely powerful tool that can predict thermodynamic properties based on equation of state, and makes it easier to detect enthalpy changes in a system and get realistic estimates for the rate of heat transfer.

2.2.1 Early Evaluation of Tordis Raw Heat Potential

In Sections 4.1 and 4.2 the results from calculations on raw thermal heat potential from the Tordis produced fluids are presented, where Aspen HYSYS was used to model the duty. This section is included mainly to give the reader early understanding on the magnitude of the power potential that is dealt with, which is done using relationships we have seen so far.

The heat source at Tordis is a fluid in mainly liquid state, which means Equation (2.21) can be used to calculate an approximate of the heating potential. A more precise expression is given in Equation (2.22) that requires knowledge of the enthalpy values of the wellstream at inlet and outlet states, and can be used to calculate the potential accurately when a fraction of the wellstream is in gaseous state. Table 2.1 contains the necessary data to calculate the raw thermal heat potential of Tordis with the given conditions, here shown in Equation (2.23). The enthalpy values were generated by flashing the brine and hydrocarbons at 75°C and 20°C in PVTsim and among the data supplied by Equinor. As shown in the calculation, the Tordis raw thermal power potential is approximately 46.5 MW.

$$\dot{Q} = \dot{m} C_p \Delta T \tag{2.21}$$

$$\dot{Q} = \dot{m} \Delta h \tag{2.22}$$

Table 2.1: Mass rates and wellstream enthalpy values at possible cycle inlet and outlet conditions

	Mass rate	**Enthalpy at 40 bara and 75°C**	**Enthalpy at 37 bara and 20°C**
Water	161 kg/s	-2320.56 kj/kg	-2585.4 kj/kg
HC fluid	31.5 kg/s	-176.44 kj/kg	-299.86 kj/kg

$$\begin{aligned} \dot{Q} &= \dot{m}_{water}\Delta h_{water} + \dot{m}_{HC}\Delta h_{HC} \\ \dot{Q} &= \dot{m}_{water}(h_{w,in} - h_{w,out}) + \dot{m}_{HC}(h_{HC,in} - h_{HC,out}) \\ \dot{Q} &= 161 \cdot (-2320.56 - -2585.4) + 31.5 \cdot (-176.44 - -299.86) \\ \dot{Q} &= 46.5\,MW \end{aligned} \tag{2.23}$$

Approximate Power Output Potential

Without going into the implications involving Tordis specifically, one can make an approximation for the net power output potential from ORC thermal heat conversion by multiplying the raw power available with realistically achievable thermal efficiency factors. According to Hettiarachchi et al. (2007), possible cycle efficiency for power generation based on low temperature geothermal resources (in the 70-100°C range) is approximately 5-10%. Equation (2.24) was therefore calculated for cycle efficiency within the realistic range, in order to give an idea of the plausible power output from Tordis thermal heat conversion. Realistic figures for net power output for an ORC system at the field are seen to be between 2.33 MW and 4.65 MW. The energy requirements for boosting at Tordis are approximately 4 MW, so a cycle with 9% or higher thermal efficiency would cover a target output of this figure.

$$W = \dot{Q} \times \eta_{thermal} \tag{2.24}$$

Table 2.2: Tordis power output potential based on raw power availiable and cycle efficiencies from 5-10%

$\dot{Q}$	46.5 MW	46.5 MW	46.5 MW	46.5 MW	46.5 MW	46.5 MW
$\eta_{thermal}$	0.05	0.06	0.07	0.08	0.09	0.10
W	2.33 MW	2.79 MW	3.26 MW	3.72 MW	4.19 MW	4.65 MW

2.3 Binary Organic Rankine Cycle

In power plants all around the world geothermal resources are exploited by producing hot water from the subsurface and using it as an energy source to generate power. Many of these facilities are using an organic Rankine cycle for converting thermal energy into electricity, and to look at how the geothermal plants are operating onshore would be a good idea before attempting anything subsea. The plants that are using ORC can be further divided into two main groups; those that are operating with a *direct cycle* and those that run a *binary cycle*. The binary cycle method will be reviewed in detail in this chapter since it is directly relevant to the Tordis field which produces mainly liquids, but both methods are highly relevant when it comes to hydrocarbon thermal energy conversion in general. In fact, geothermal energy conversion companies deal with limitations and challenges some of which are very similar to those of oil companies. As an example of the similarities it is referred to DiPippo (2016) that lists the following five necessary features that should be present in order to have a commercially viable geothermal resource.

- A large heat source
- Permeable reservoir
- Water supply
- Overlaying impervious rock
- A reliable recharge mechanism

As seen from the list, the hydrothermal reservoir characteristic requires many of the qualities similar to what is expected of a hydrocarbon reservoir with the main difference being the composition of the hot fluid. The hot fluid can be referred to as the geothermal resource, and according to Astolfi and Macchi (2017) the enthalpy is the most important parameter for geothermal resource classification. The in-situ phase of the resource is also important when different development options for the geothermal plants are considered. If dealing with mainly vapor it is common to use direct expansion in a steam turbine for energy conversion, but if the water is mainly liquid phase or 2-phases there is a range of binary configurations that needs to be considered. When thermal heat is converted to electricity with a binary subcritical cycle, that entails having the hot fluid heat exchange with a secondary *working fluid* that has a low boiling point, thus making the working fluid evaporate within a closed cycle. The evaporated working fluid is then passed through a turbine to extract energy, before it is cooled back to liquid state by heat exchanging with a coolant. As mentioned in the previous section, the binary cycle solution is common when dealing with a geothermal resource that is in the in-situ state of liquid or a combination of liquid and vapor, such as Tordis. But the specific configuration of the binary cycle varies between power plants, so it is necessary to have a look on the design options and main factors determining the design choice.

Astolfi and Macchi (2017) states that the thermodynamic analysis of a thermal fluid is based mainly on the amount of non-condensable gases (NCG) and its enthalpy, which has to be considered in combination with the WH conditions to determine cycle configuration and an optimal working fluid. A typical example of a NCG found in a geothermal resource is CO_2, which is not easily condensed by cooling unless the pressures are very high. Due to the detailed description by Astolfi and Macchi (2017), it acts as the main source of the theoretical information contained further in this section, unless stated otherwise.

The main parameters affecting the binary cycle design are the following

- Enthalpy of the geothermal fluid at bottom hole conditions
- Amount of non-condensable gases
- Pressure at wellhead
- Phase at wellhead
- Fluid composition
- Size of the reservoir

The binary power plants are mainly characterized by what working fluids are in the cycles, what cycle configurations are actually run, cooling media used and turbine technology applied. In fact, there are five common binary cycle system configurations that can be used to extract heat from resources in both gaseous and liquid phase. Three of these configurations are variations of subcritical systems, and the other two are supercritical and combined cycles. The single pressure level subcritical cycle (see Figure 2.5) is the least complex configuration of them all, and will be of the main focus here due to its simplicity, it being very common in the industry and its low amount of required parts.

The next few pages show how one would conduct thermodynamic analysis on such a cycle, by going through each component and describing the flow of energy by equations. The main goal is to give the reader an overview of how the binary cycle works, and what part the individual components play in the energy conversion system. This analysis begins with looking at the material and energy flow through and from the turbine, and then moves clockwise through the cycle as it is shown in Figure 2.5, and analysing every component in a similar manner.

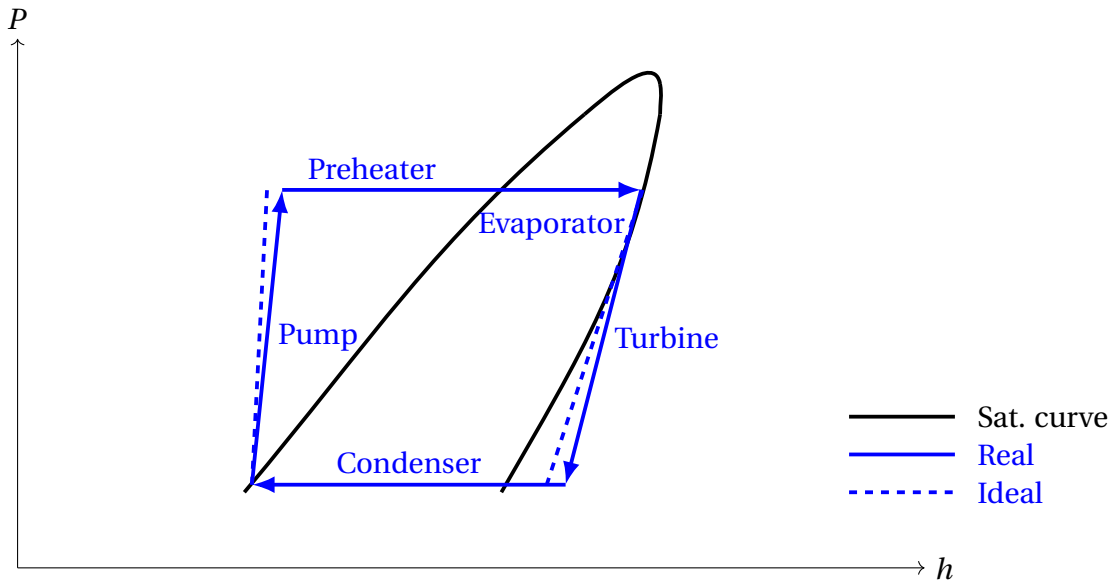

Figure 2.4: Pressure-enthalpy diagram of a subcritical binary thermal conversion process.

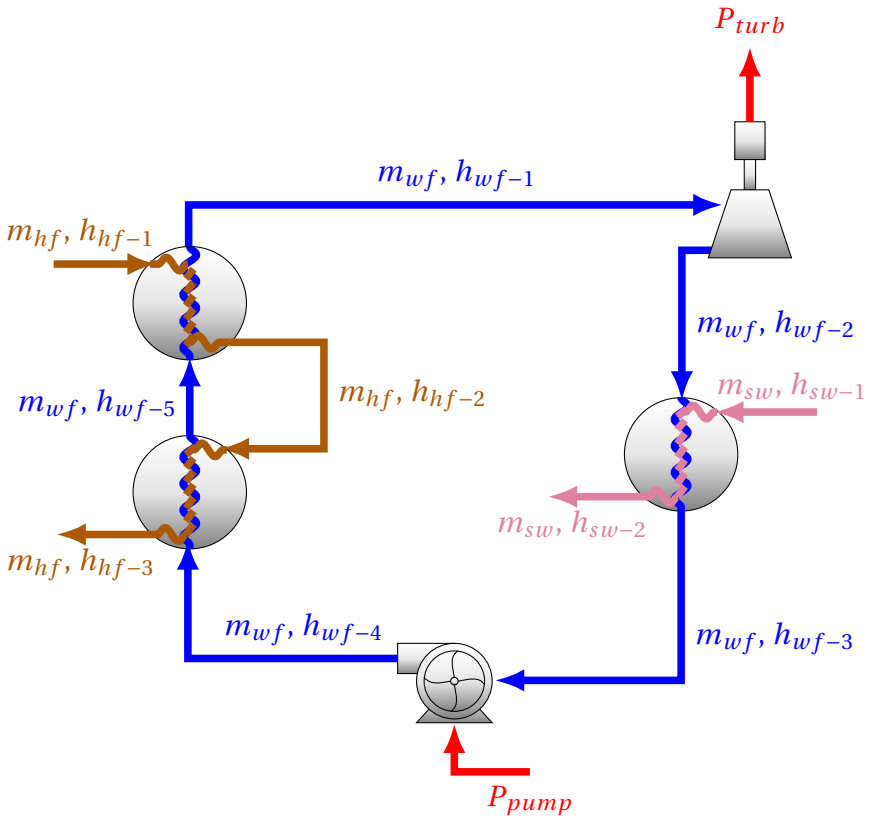

Figure 2.5: Single pressure binary cycle with subcritical configuration.

2.3.1 Turbine Function and Analytic Thermodynamic Description

For an ORC application such as this it is necessary to have a turbine that can convert vapor energy into mechanical energy that can do work. Three forms of energy associated with the vapor are of interest, namely energy associated with kinetic movement, pressure and temperature. The vapor enters the turbine through the main inlet valve from the evaporator. The turbine consists of multiple sets of blades with alternating shapes. The odd number of bladerows counting from the first set in axial direction are called rotors and can rotate, and even numbers are called stators and are stationary. Figure 2.7 shows an industrial scale gas turbine. The rotor parts of the turbine has airfoil shaped blades, that are located in spatially increasing sizes. The vapor energy induces rotation onto the blades, because of lift force due to the pressure difference between each side of every blade. After passing through a rotor, the velocity of the vapor is reduced. Therefore, the stator that follows acts as a nozzle to increase vapor velocity and kinetic energy, thus decreasing vapor pressure and temperature due to the laws of energy conservation. As the reader may be well aware of, pressure is inversely proportional to volume when it comes to gases which leads to a necessity of a volumetric expanding shape as pressure goes down since the vapor will occupy more space. The reader is referred to Figure 2.4 to see conceptual turbine pressure decrease effect on specific enthalpy. So, as the vapor moves through the multiple compartments it expands as it transfers energy onto the rotor blades, and each rotor stage has bigger blades than the previous to ensure capture of more energy. The expanding shape also helps in regard to the efficiency, because the gas expands as the pressure is reduced, and if the blade length span was left unchanged the velocities would be too high and cause increased frictional losses. Since the potential energy from a geothermal ORC system can not be considered constant in time, but instead varies, it is smart to install a vapor flow governing mechanism before the vapor inlet. This means that the rates into the turbine can be regulated, keeping the rotor rpm close to constant. As a matter of fact, the frequency of electric power produced is directly proportional to the generator speed. Once the vapor has passed through all stages, it can be exhausted into the condenser for regeneration.

When it comes to turbine (and pump) engineering, an entity called the *isentropic efficiency* is often used to convert from ideal to real conditions. It is defined as the ratio between real work and isentropic work, and is given by Equation (2.25). The turbine power can be expressed as by Equation (2.26), but note that this value represents mechanical power and needs to be converted to grid power by multiplication by generator efficiency. When performing calculations, one must be careful to consider the real turbine operating conditions, specifically making a note of the working fluid phase. Even though the fluid has undergone preheating and evaporation processes before passing through the turbine, it is possible that it retains some liquid in form of droplets. The presence of liquid has a negative effect on the turbine efficiency, and also leads to

increased wear of the physical equipment. According to Baumann (1921) it is relatively simple to take the presence of moisture into account when calculating turbine efficiency. His rule is still considered as valid, and it states that one percent moisture leads to one percent lower turbine efficiency, in general. The rule was given by Equation (2.27) as a function of wetness y_{wf}, but can easily be expressed as a function of dryness by multiplication of the dry isentropic efficiency value with average dryness of the working fluid x_{wf}. The constant a can vary, but in most cases it can safely be assumed equal to one. That gives Equations (2.28) and (2.29). In Figure 2.6 blue arrows represents the material streams composed of the working fluid, while the red arrow represents turbine energy output.

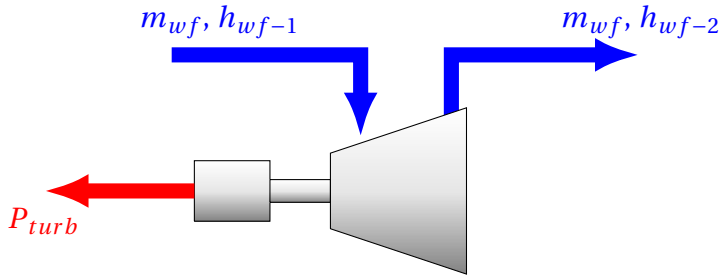

Figure 2.6: Simple sketch of a turbine.

$$\eta_{turb} = \frac{h_{wf-1} - h_{wf-2}}{h_{wf-1} - h_{2,ideal}} \tag{2.25}$$

$$P_{turb} = m_{wf}(h_{wf-1} - h_{wf-2}) = m_{wf}\eta_{turb}(h_{wf-1} - h_{2,ideal}) \tag{2.26}$$

$$\eta_{turb,wet} = \eta_{turb} \cdot (1 - a \cdot \frac{y_{wf-1} + y_{wf-2}}{2}) \tag{2.27}$$

$$\eta_{turb,wet} = \eta_{turb} \cdot (1 - \frac{y_{wf-1} + y_{wf-2}}{2}) \tag{2.28}$$

$$\eta_{turb,wet} = \eta_{turb} \cdot \frac{x_{wf-1} + x_{wf-2}}{2} \tag{2.29}$$

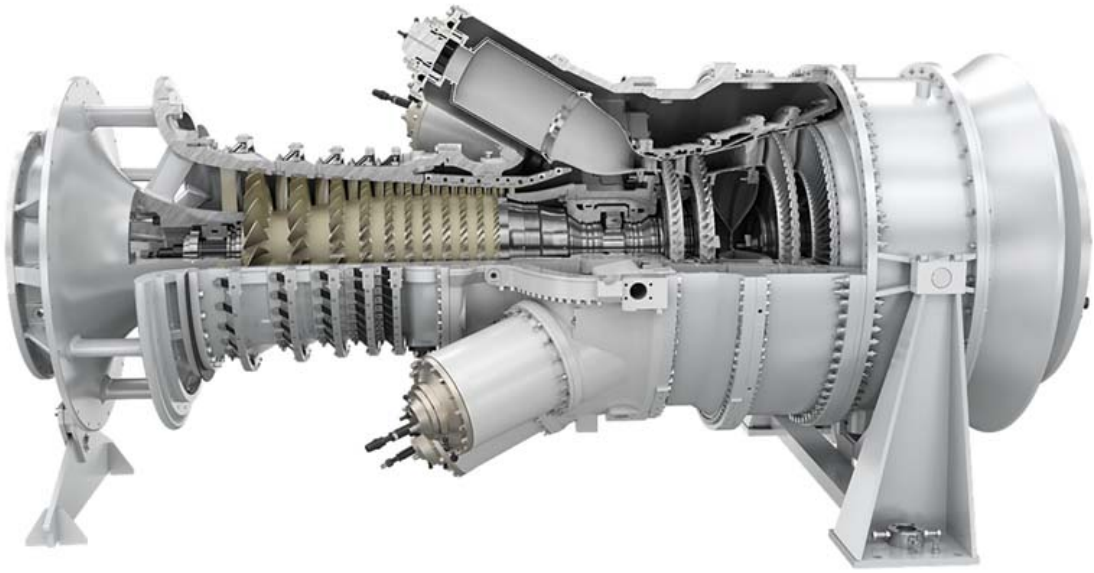

Figure 2.7: Siemens SGT-400, 14.3 MW industrial gas turbine. Photo taken from Siemens.com

Figure 2.8: Amarinth U Series industrial centrifugal pump, rated for 10 bar. Photo taken from amarinth.com

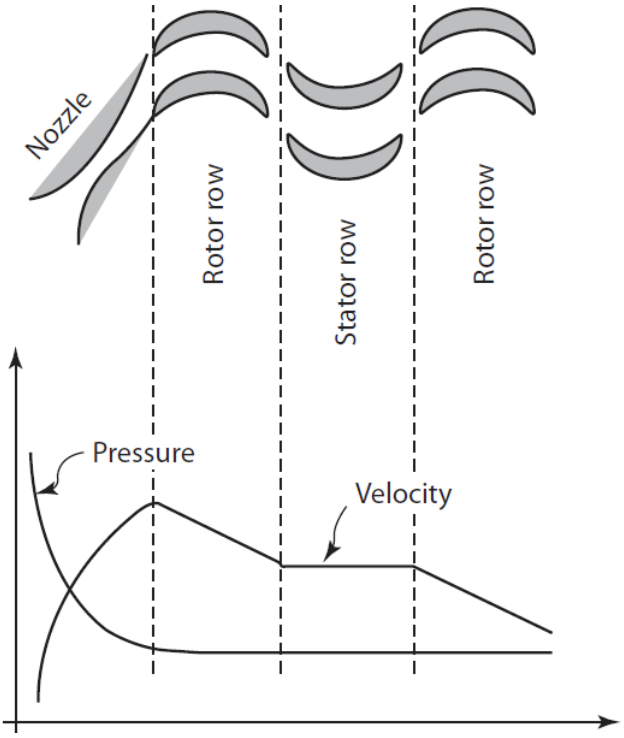

Figure 2.9: Turbine pressure and velocity profiles shown for initial two stages. Figure taken from Murty (2018).

Velocity Compounding in Turbine Design

The ORC turbine must be designed such that the required energy transfer can be achieved by having a sufficiently high isentropic efficiency factor. Velocity compounding is an alternative design method commonly used in modern turbines to obtain high enthalpy drop and reasonable rotor tip speeds, by compounding the energy generation process into multiple smaller stages. An illustration of the method is shown in Figure 2.9 and it can be seen how the entire pressure drop happens when the gas passes through the nozzle, then flow velocity is decreased with every rotor row until the kinetic energy becomes negligible at the final stage (Murty (2018)). The physical setup guides the working fluid through the stages after the nozzle without making impact on the pressure state, and the corresponding velocity diagrams are shown in Figure 2.10. These diagrams are very useful because equations can be derived for calculation of the energy transfer related to each stage based on the changes in fluid velocity. Equation (2.30) shows how the energy transfer of the first stage E_1 can be simplified to an expression which is only based on blade velocity u, absolute fluid velocity V and nozzle inlet angle α_1. A similar derivation can be done for the second stage, here shown in Equation (2.31). For following the derivation, it should be noted that the following relationships holds true; relative velocities $w_1 = w_2$ and $w_3 = w_4$, blade angles $\beta_1 = \beta_2$ and $\beta_3 = \beta_4$, fluid velocities $V_2 = V_3$ and nozzle angles $\alpha_2 = \alpha_3$.

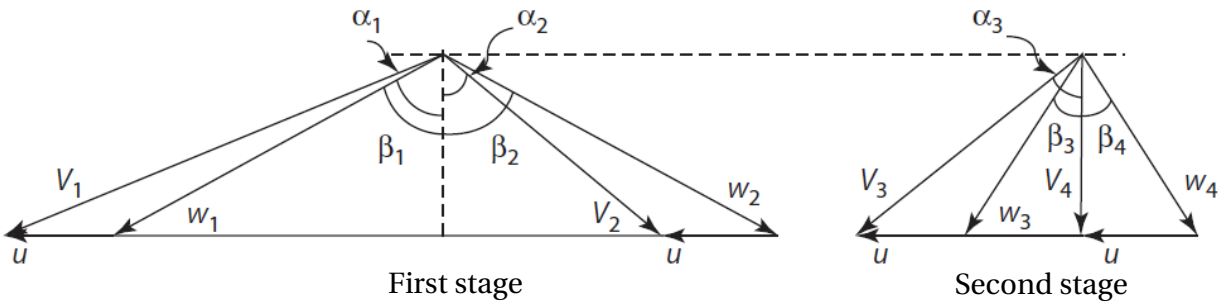

Figure 2.10: Velocity triangles for first and second stages. Figure taken from Murty (2018).

$$\begin{aligned} E_1 &= u \times V_1 \sin(\alpha_1) + u \times V_2 \sin(\alpha_2) \\ &= u \times (V_1 \sin(\alpha_1) + w_2 \sin(\beta_2) - u) \\ &= u \times (V_1 \sin(\alpha_1) + w_1 \sin(\beta_1) - u) \\ &= u \times (V_1 \sin(\alpha_1) + V_1 \sin(\alpha_1) - u - u) \\ &= 2u \times (V_1 \sin(\alpha_1) - u) \end{aligned} \tag{2.30}$$

$$\begin{aligned} E_2 &= u \times V_3 \sin(\alpha_3) + u \times 0 \\ &= 2u \times w_3 \sin(\beta_3) \\ &= 2u \times (V_3 \sin(\alpha_3) - u) \\ &= 2u \times (V_2 \sin(\alpha_2) - u) \\ &= 2u \times (w_2 \sin(\beta_2) - u - u) \\ &= 2u \times (w_1 \sin(\beta_1) - u - u) \\ &= 2u \times (V_1 \sin(\alpha_1) - u - u - u) \\ &= 2u \times (V_1 \sin(\alpha_1) - 3u) \end{aligned} \tag{2.31}$$

The resulting expressions from each stage can be combined to a final formula for calculation of the turbine energy transfer as shown in Equation (2.32).

$$\begin{aligned} E_{Total} &= E_1 + E_2 \\ &= 2u \times (V_1 \sin(\alpha_1) - u) + 2u \times (V_1 \sin(\alpha_1) - 3u) \\ &= 4u \times (V_1 \sin(\alpha_1) - 2u) \end{aligned} \tag{2.32}$$

It must be clear that E_{Total} represents energy production if the turbine operates under ideal conditions and a certain amount of potential exits the turbine outlet as kinetic energy proportional

to $V_{out}^2/2$. Equation (2.33) shows how this fact is used to express (and simplify) the utilization factor ϵ for the turbine in question.

$$\begin{aligned}\epsilon &= \frac{E_{total}}{E_{total} + V_{out}^2/2} = \frac{E_{total}}{E_{total} + V_4^2/2} = \frac{E_{total}}{V_1^2/2} \\ &= \frac{4u \times (V_1 \sin(\alpha_1) - 2u)}{V_1^2/2} \\ &= 8 \times \frac{u}{V_1}(sin(\alpha_1) - 2 \times \frac{u}{V_1})\end{aligned} \tag{2.33}$$

The factor needs to be maximized to obtain the highest possible turbine efficiency, which is done by setting its derivative with respect to u/V_1 to zero and according to Murty (2018) the term u/V_1 can be referred to as *peripheral speed factor* or a turbine's *speed ratio*. Equation (2.34) shows this expressed mathematically, and is solved with respect to the speed ratio for maximum utilization in Equation (2.35).

$$\frac{d\epsilon}{du/V_1} = \frac{d}{du/V_1}[8 \times \frac{u}{V_1}(sin(\alpha_1) - 2 \times \frac{u}{V_1})] = 0 \tag{2.34}$$

$$\frac{u}{V_1} = \frac{\sin(\alpha_1)}{4} \tag{2.35}$$

The resulting speed ratio is inserted into the original expression for the utilization factor in order to express its maximum, and it is shown how the factor is simplified greatly such that it is only a function of the inlet nozzle angle, as in Equation (2.36).

$$\begin{aligned}\epsilon_{max} &= 8 \times \frac{\sin(\alpha_1)}{4}(sin(\alpha_1) - 2 \times \frac{\sin(\alpha_1)}{4}) \\ &= 2\sin^2(\alpha_1) - \sin^2(\alpha_1) \\ &= \sin^2(\alpha_1)\end{aligned} \tag{2.36}$$

From earlier it was found that $E_{Total} = 4u \times (V_1 \sin(\alpha_1) - 2u)$, which means that the maximum energy transfer from the turbine in question can be calculated by inserting the relation of maximum utilization $4u = V_1 \sin(\alpha_1)$ in the formula, as shown in Equation (2.37). This means that for the two-stage turbine, the energy transfer can be expressed purely as a function of blade velocity which is a very useful find as the speed is directly proportional to electricity generation from the generator.

$$E_{Max} = 4u \times (4u - 2u) = 8u^2 \tag{2.37}$$

Murty (2018) performed velocity compounding analysis based on n amount of stages and showed that the method could easily be expanded to any turbine size and keep the simple relationships

for energy transfer calculation that was found for two stages, and the formulas are given here by Equation (2.38) and Equation (2.39). With the turbine energy transfer being proportional to the number of stages squared, it is clear that every added stage gives a significant benefit to its overall efficiency.

$$E_n = 2n^2u^2 \tag{2.38}$$

$$\frac{u}{V_1} = \frac{\sin(\alpha_1)}{2n} \tag{2.39}$$

2.3.2 S&T Condenser Function and Analytic Thermodynamic Description

A condenser is a type of shell and tube (S&T) heat exchanger designed to convert gases or vapors into a liquid state commonly referred to as condensate or distillate depending on the process. In the process considered here, cool sea water from the tube side of the condenser enters through what's commonly called the inlet head, and then passes through a number of tubes before it flows out of the condenser through the outlet head. On the shell side of the condenser, vapor passes through an inlet and flows around the tubes. The surfaces of the tubes are cold due to the sea water that passes through them, so when the vapor comes in contact with the tubes heat starts to flow from vapor to water. As heat is rejected to the cooling water, the vapor starts to condense on the surfaces of the tubes. Droplets of condensate starts to drip from the tubes towards the bottom of the shell, before it flows out of an outlet at the bottom.

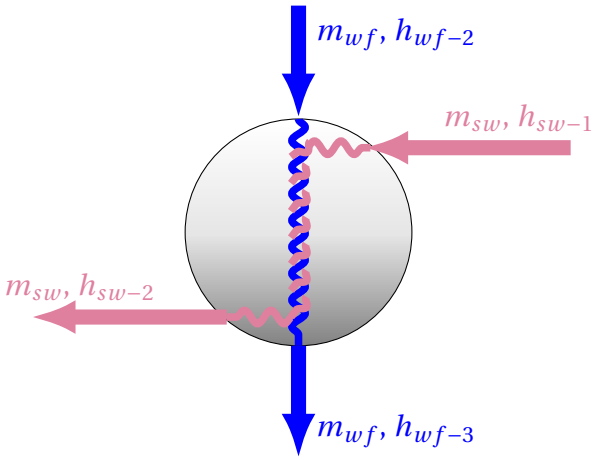

Figure 2.11: Simple sketch of condenser. Heat exchange between working fluid and sea water.

$$Q_{cooling} = m_{wf}(h_{wf-2} - h_{wf-3}) = m_{sw}(h_{sw-2} - h_{sw-1}) \tag{2.40}$$

$$Q_{cooling} = m_{wf}(h_{wf-2} - h_{wf-3}) = m_{sw} \cdot Cp_{sw} \cdot (T_{sw-2} - T_{sw-1}) \tag{2.41}$$

A good illustration of a shell and tube heat exchanger is given in Figure 2.21. It is worth mentioning that as the vapor condenses a low pressure is created inside the condenser, which means that the engineer must make sure the vapor entry pressure is sufficiently high at all times to ensure inflow. Since the heat that leaves the hot vapor is equal in amount to the heat received to the cool water, the rate of heat transfer can be expressed as in Equation (2.40). If we consider a case where the specific heat capacity of the sea water is not changing, the heat flow can be expressed in terms of the corresponding temperature increase which is easily measured, as shown in Equation (2.41). The working fluid material stream is illustrated in blue color as in previous figures, and the sea water material stream is shown in pink in Figure 2.11.

Condensation

When the organic Rankine cycle is designed based on using a working fluid operating on a subcritical pressure condition it means that phase change of the fluid will occur in the heating and cooling systems. To calculate realistic values for the heat transfer coefficients when the working fluid condenses or evaporates one needs to use some additional empirical correlations to accommodate the latent heat involved in these processes. The Kern equations for heat transfer coefficient to be used for condensation processes are shown below. For an ORC with access to cooling brine the heat sink is to be considered isothermal and Equation (2.42) is used for gravitation driven isothermal condensation. The value for G in the Kern method is dependent on the condenser geometric configuration of which there are four main choices, horizontal tubes, horizontal tube bundle, vertical tubes and vertical tube bundle which are shown in their respective order in Equations (2.43)-(2.46). If the condensation is vertical under turbulent and wavy flow, the correction factor f_{tc} defined in Equation (2.47) is multiplied with the initial heat transfer coefficient as seen in Equation (2.48). If vertical condensation happens under conditions of very high turbulence, Kern proposes Equation (2.49) for the heat transfer coefficient.

$$\alpha_g = 0.925\frac{\kappa\rho^2 g}{\eta G} \tag{2.42}$$

$$G_{ts,H} = \frac{M_{liquid}}{1800 n\pi l_{tube}} \tag{2.43}$$

$$G_{ss,H} = \frac{M_{liquid}}{3600 n^{0.66} l_{tube}} \tag{2.44}$$

$$G_{ts,V} = \frac{M_{liquid}}{3600 n\pi D_i} \tag{2.45}$$

$$G_{ss,V} = \frac{M_{liquid}}{3600 n\pi D_o} \tag{2.46}$$

$$f_{tc} = 0.8(\frac{Re}{4})^{0.11} = 0.8(\frac{G_V}{\eta})^{0.11}, \quad 40 < Re \tag{2.47}$$

$$\alpha_w = f_{tc}\alpha_g \tag{2.48}$$

$$\alpha_t = 0.0076(\frac{\kappa^3\rho^2 g}{\eta^2})^{1/3} \times (\frac{4G_V}{\eta})^{0.4}, \quad 2100 < Re \tag{2.49}$$

Nomenclature for the Kern equations

List of variables:

α_g	Heat transfer coeff. for grav.-driven isothermal cond. (W/m$^2\cdot$k)
κ	Thermal conductivity (W/m$\cdot$K)
g	Gravity (m/s^2)
ρ	Density (kg/m^3)
η	Dynamic viscosity (Pa$\cdot$s)
M_{liquid}	Mass rate (kg/h)
n	Number of tubes (−)
l_{tube}	Tube length (m)
D_i	Inner diameter (m)
D_o	Outer diameter (m)
f_{tc}	Turbulence correction factor (−)
Re	Reynolds number (−)
α_w	Corrected heat transfer coeff. (W/m$^2\cdot$k)
α_t	High turb. flow heat transfer coeff. (W/m$^2\cdot$k)

2.3.3 Other Types of Subsea Cooling Equipment

A traditional flow assurance challenge has been to maintain a certain level of temperature in the flow lines in order to ensure that problems related to things like wax, asphaltenes and hydrates do not occur. But sometimes an opposite problem needs solving for optimum field development, the problem of cooling the wellstream subsea to accommodate a certain need. An example situation is when compression subsea is performed and subsea cooling is required to counteract the corresponding temperature rise, or when very high temperature crude is cooled to the point where less expensive piping is applicable due to less corrosion. Because of challenges such as these, a number of subsea cooling systems have been developed by oil service companies in the later years. In this section an overview of some of these systems and their main principles are shown, since the systems potentially could be applied in subsea organic Rankine cycles in place of a regular condenser.

In the SPE published paper *Subsea Cooling; Passive, Active or Sea Current Controlled?* Rudh et al. (2016) has listed passive manifold coolers, sectioned passive coolers, by-pass coolers, sea current controlled coolers and shell and tube coolers as the main cooling technologies to be used subsea. Shell and tube coolers are not reviewed in this section due to having been introduced earlier in this thesis and neither is sea current controlled coolers because of not yet being commercially available.

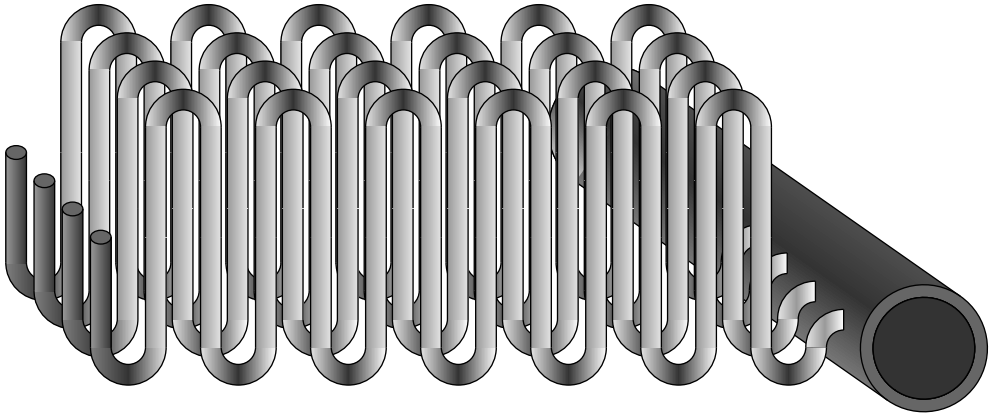

Figure 2.12: Passive Manifold Cooler principle illustration. Fluid enters the coils from main pipeline and sea water cools it down by means of natural convection.

Passive Manifold Cooler

A passive manifold cooler is illustrated in Figure 2.12. It is based on splitting the main flow line into numerous smaller less isolated tubes that are coiled in parallel. A high degree of natural convection will occur to cool the medium inside the coils while requiring no powering of the apparatus. The main reason behind splitting the stream into multiple channels is to deal with potential multi-phase flow, and when the passive cooler is applied in a traditional manner one needs to be aware that the temperature distribution will not be completely even between the different coils. This means that certain local temperature minimums may cause flow assurance issues, but this would be less of a concern when the unit is run in a ORC since no deposits are to be expected from the working fluid. According to Rudh et al. (2016) the size of the coils used are usually between 1 and 2 inches and usually made of super duplex stainless steel with no coating. Figure 2.13 show a passive manifold cooler that is developed by Future Technology AS.

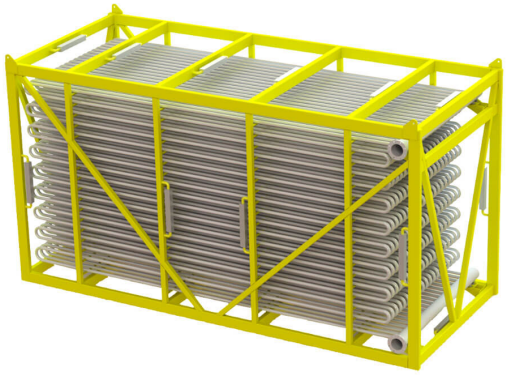

Figure 2.13: A Future Technology AS passive subsea cooler. Cools up to 50 MW and can be scaled to customer needs. Image taken from http://futuretechnology.no/fscc/.

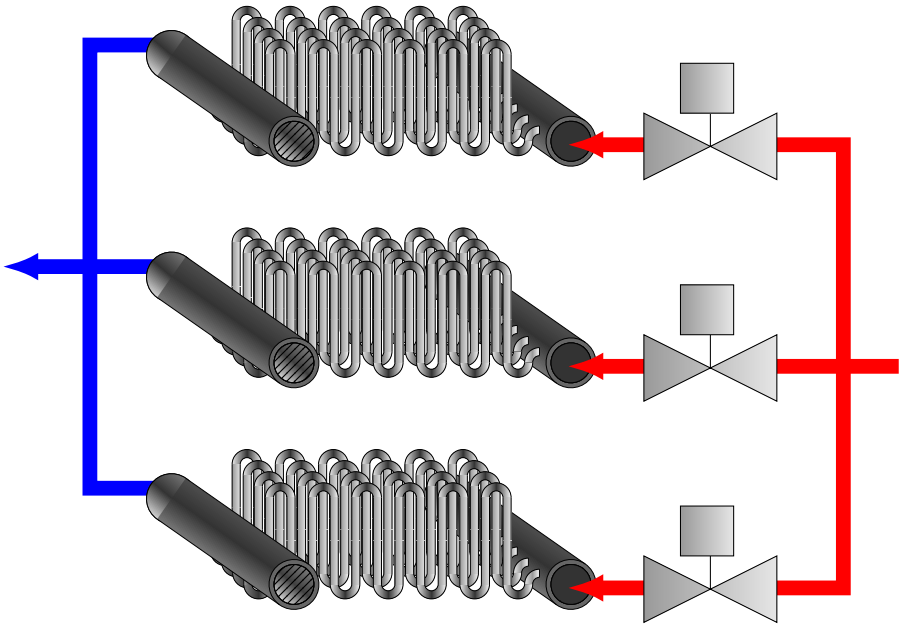

Figure 2.14: Principle illustration of a sectioned passive manifold cooler. Operator can control the cooling duty by routing the working fluid through the chosen coils based on need.

Figure 2.15: A Future Technology AS 5-100% controllable subsea cooler. Cools up to 50 MW and can be scaled to customer needs. Image taken from http://futuretechnology.no/fscc/.

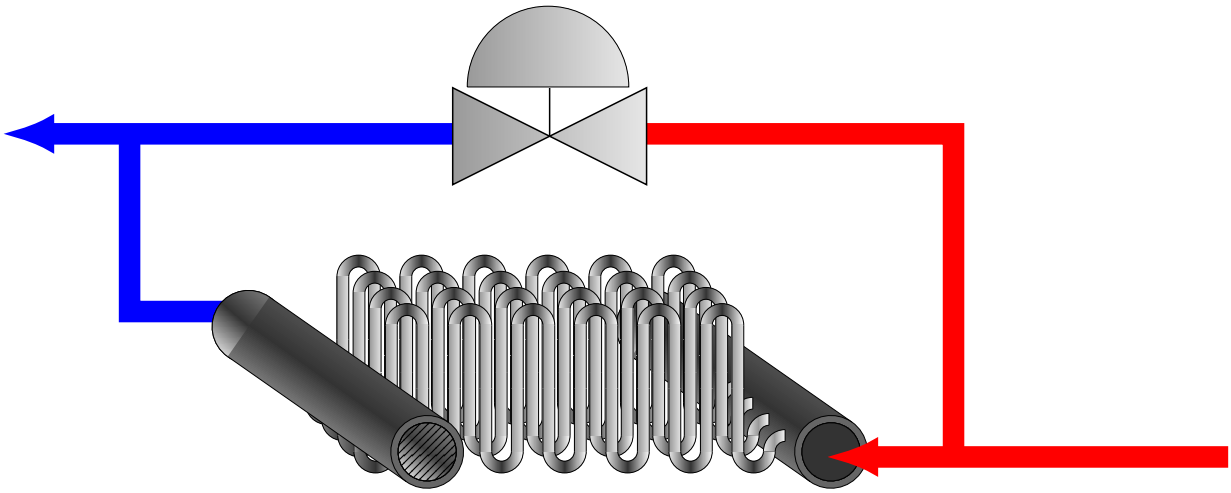

Figure 2.16: Principle illustration of a by-pass cooler. Outlet temperature can be controlled with high accuracy using the choke.

Sectioned Passive Cooler

Figure 2.14 shows the principle behind the sectioned passive cooling manifold, red colored arrows here represents a fluid of original temperature and blue arrows represents the cooled fluid that leaves the heat exchanger. As seen from the illustration, a setup like this allows for some control of the condition of the outlet fluid. The isolation valves can be operated by ROV or similar to adjust the area of heat transfer and hence the heat duty of the cooler. Since having accurate cooling duty is very important for any thermodynamic cycle, using a sectioned cooler would be preferable as compared to basic passive cooling. Future Technology AS developed the FSCC - Future Subsea Controllable Cooler that is shown in Figure 2.15, and it is suited to transfer up to 50 MW worth of thermal energy.

By-pass Cooler

Figure 2.16 illustrates the concept of the by-pass cooler. Rudh et al. (2016) states that even though this setup allows the temperature to be controlled with very high accuracy, there are potential problems if operation is under high turn-down and most of the fluid is directed through the choke. This is because the minor fraction of fluid that actually passes through the cooling system will be very cold and can pose a flow assurance challenge.

2.3.4 Pump Function and Analytic Thermodynamic Description

There are multiple pump types to choose from when selecting a pump for a ORC cycle. In this section we focus on understanding how a single stage centrifugal pump works, due to its simple nature and wide range of application areas. The pump utilizes the centrifugal force to move liquids, which is the force that pushes away from the centre of rotation when an object or material moves in a circular motion. In our case, it is the working fluid that will be pushed outwards upon entering the pump. Figure 2.17 shows a simple image of a centrifugal pump, where the circle in the middle represents the pump inlet. Inside the pump's casing is an *impeller* that has multiple curved veins that extend out from the center, as seen in the figure. The impeller rotates due to a force from an electrical motor mounted on the back of the pump, and requires the power consumption labelled P_{pump} in the image. Outside of the impeller is a chamber called the *volute*, that has an expanding shape towards the outlet of the pump (this can not be seen on the figure). Due to the centrifugal force, liquid that enters the pump is forced outwards and into the volute, thus creating a reduced pressure area at the inlet - drawing more working fluid into the pump. In addition, the working fluid will gain speed as it is forced outwards because it must move faster to keep up with the impeller when the travel distance is longer. When the liquid has spread out into the volute, the flow velocity decreases due to its expanding shape, thus increasing the pressure of the working fluid driving it out the outlet. Figure 2.8 shows how an industrial centrifugal pump provided by the company Amarinth looks like. One of the main disadvantages to the centrifugal pump is that it has almost no suction power, but that may prove itself as a non-issue with a subsea application. The isentropic efficiency of the pump is used in engineering considerations, and defined by Equation (2.51).

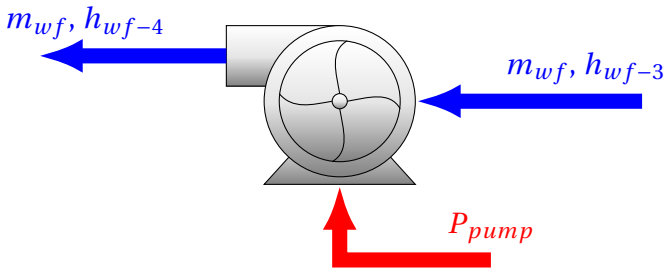

Figure 2.17: Simple illustration of a pump.

$$P_{pump} = m_{wf}(h_{wf-4} - h_{wf-3}) = m_{wf}(h_{4,ideal} - h_{wf-3})/\eta_{pump} \tag{2.50}$$

$$\eta_{pump} = \frac{h_{4,ideal} - h_{wf-3}}{h_{wf-4} - h_{wf-3}} \tag{2.51}$$

2.3.5 Boiling System Function and Analytic Thermodynamic Description

The main function of the boiling system is to heat the liquid working fluid until it reaches an evaporated state. In ORCs the evaporator can either consist of a single heat exchanger or it is built by a series of two shell and tube heat exchangers. On a conceptual level it is preferable to model it as two heat exchangers for the analytic thermodynamic description. The hot fluid cycles through both heat exchangers as seen in Figure 2.18, and transferring its thermal energy to the working fluid that is contained inside the pressurized shell. The high pressure working fluid coming from the pump passes into the preheater first, bringing its temperature up to saturation temperature. The evaporator is placed physically right next to the preheater, and in this stage the latent heat of evaporation is added. If possible, further superheating the working fluid after evaporation is beneficiary as it helps ensure the quality of gas that is directed to the turbine. If we assume a well-insulated system, Equation (2.52) can be used for thermodynamic analysis. In the case of the condenser, the equation was simplified by assuming a non-changing specific heat of the sea water. The same could be done here (see Equation (2.53)), but the average heat capacity of the produced hydrocarbon fluids may very well change over time, just as the composition does.

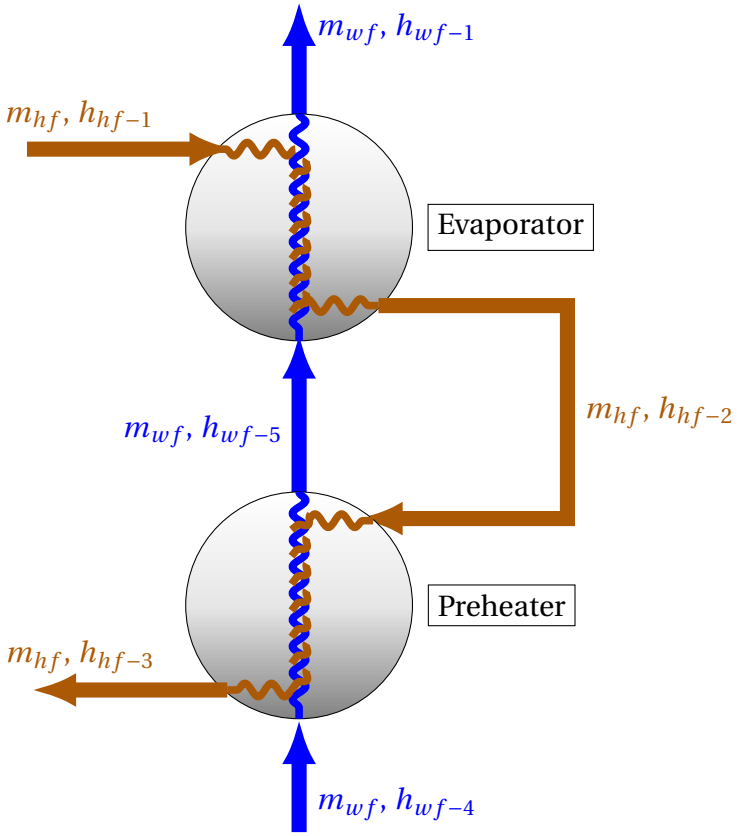

Figure 2.18: Simple sketch of heating process of the working fluid

$$Q_{heating} = m_{hf}(h_{hf-1} - h_{hf-3}) = m_{wf}(h_{wf-1} - h_{wf-4}) \tag{2.52}$$

$$Q_{heating} = m_{hf} \cdot c_{p,hf}(T_{hf-1} - T_{hf-3}) = m_{wf}(h_{wf-1} - h_{wf-4}) \tag{2.53}$$

Shell and Tube Boiler Design

The heat exchanger area can be expressed as by Equation (2.54). As previously in this thesis, the letter Q stands for heat load and ΔT is the temperature gradient. The letter U is the overall heat transfer coefficient, which is calculated from Equation (2.55) for shell and tube heat exchangers as shown in the Heat Exchanger Design Guide written by Nitsche and Gbadamosi (2016). f is here used for inner and outer fouling factor, s is the wall thickness of the tubes, κ is the thermal conductivity of the tube material and α is used for the heat transfer coefficient in the tubes and on shell side.

$$A = \frac{Q}{U\Delta T} \tag{2.54}$$

$$\frac{1}{U} = \frac{1}{\alpha_i} + \frac{1}{\alpha_o} + \frac{s}{\kappa} + f_i + f_o \tag{2.55}$$

The base data for heat exchanger design are the thermal properties and flow rates of the fluids that passes tubeside and shellside. It means that inlet and outlet temperatures, flow rates and fluid compositional properties are defined initially. Aspen HYSYS is a good tool when it comes to defining reasonable values for these properties for heat exchangers in an ORC and will be used for this purpose in this thesis. All the heat loads on shellside and tubeside are then calculated from the condensation and vaporization enthalpies for the condenser and the evaporator.

$$\Delta T_{LMTD} = \frac{(T_{ss,i} - T_{ts,o}) - (T_{ss,o} - T_{ts,i})}{\ln \frac{T_{ss,i} - T_{ts,o}}{T_{ss,o} - T_{ts,i}}} \tag{2.56}$$

Logarithmic mean temperature difference T_{LMTD} is calculated based on the temperature data as if the heat exchanger flows were ideal counter-currents, using Equation (2.56) with temperature values input as degrees Celsius. Since the heat exchangers in reality often have multiple passes it is common to account for it by using a factor F to determine a so-called corrected temperature difference. Equations (2.57) - (2.60) are valid for E-type heat exchangers and shows how it can be taken into account that multipass heat exchangers have both co-current and counter-current flows (Tubular Exchangers Manufacturers Association), where the letter N is the number of heat exchangers in series. Figure 2.19 shows a shell and tube heat exchanger with two passes. Note how the fluid tube side flows in the same direction as the shell side fluid on the bottom-most pass while counter-current flow takes place on the topmost passing.

$$R = \frac{T_{ss,i} - T_{ss,o}}{T_{ts,o} - T_{ts,i}} \tag{2.57}$$

$$P = \frac{T_{ts,o} - T_{ts,i}}{T_{ss,i} - T_{ts,i}} \tag{2.58}$$

$$P_z = \frac{1 - (\frac{RP-1}{P-1})^{1/N}}{R - (\frac{RP-1}{P-1})^{1/N}} \tag{2.59}$$

$$F = \frac{\sqrt{R^2+1}}{R-1} \frac{\ln[(1-P_z)/(1-RP_z)]}{\ln[\frac{(2/P_z)-1-R+\sqrt{R^2+1}}{(2/P_z)-1-R-\sqrt{R^2+1}}]} \tag{2.60}$$

Nitsche and Gbadamosi (2016) states that the temperature efficiency factor F should always be higher than 0.75 and it is simply multiplied with the logarithmic mean temperature difference to get a more realistic gradient, as shown in Equation (2.61). ΔT_{CMTD} can then be substituted into Equation (2.54) for calculation of the heat exchanger surface area based on assumed value for U. Once the required area is found one needs a data table like the one shown in Table 2.3 which is used to select a heat exchanger with sufficient size and volume flow rates. Once a specific configuration has been selected one calculates the real flow velocities in tubes and the shell, and use the result to determine the Reynolds number for the flow with Equation (2.62).

$$\Delta T_{CMTD} = F \Delta T_{LMTD} \tag{2.61}$$

$$Re = \frac{v \times D}{\nu} \tag{2.62}$$

$$Pr = \frac{3600 \nu C p \rho}{\kappa} \tag{2.63}$$

The heat transfer coefficients α_{ts} and α_{ss} for the tube- and shellside has to be determined, and as seen by Equations (2.69)-(2.70), it can be defined by the Nusselt number Nu, the pipe diameter D and the thermal conductivity of the fluid κ. A value for the diameter can be selected based on the heat exchanger under consideration, and finding the thermal conductivity of the hot fluid mixture can be done with the thermodynamic modeling software. The Nusselt number has to be calculated with empirical correlations, and there exists a number of Nu-correlations valid for a range of different applications. The definitions given by Equation (2.64), (2.65) and (2.66) are suitable for tube side heat transfer according to the Nitsche method and Equations (2.67) - (2.68) can be used for calculations shellside. The heat transfer coefficient for tubeside should always be converted to outer tube diameter because heat exchangers are specified based on outer area, and such conversion is easily done by multiplication with the fraction of inner to outer diameter, as shown in Equation (2.71).

$$Nu_{ts} = 1.86 \frac{Re \times Pr \times D}{l}, \quad Re < 2300 \tag{2.64}$$

Table 2.3: Geometric data of heat exchangers according to DIN 28,184, part 1, for 25 × 2 tubes with 32 mm triangular pitch. Data taken from Nitsche and Gbadamosi (2016).

Type nr.	DN [-]	Z [-]	Da [mm]	B [mm]	n [-]	AE [mm^2]	AR [mm^2]	AS [m^2/m]	fw [-]	VR [m^3/h]	VM [m^3/h]
1	150	2	168	30	14	1770	2425	1.1	0.251	8.73	6.37
2	200	2	219	40	26	2288	4503	2	0.366	16.21	8.24
3	250	2	273	50	44	5520	7620	3.5	0.259	27.43	19.87
4	300	2	324	60	66	5088	11,430	5.2	0.375	41.15	18.32
5	350	2	355	70	76	6230	13,162	6	0.397	47.38	22.43
6	350	4	355	70	68	6230	5888	5.3	0.381	21.20	22.43
7	400	2	406	80	106	11,072	18,357	8.3	0.319	66.09	39.86
8	400	4	406	80	88	9072	7620	6.9	0.382	27.43	32.66
9	500	2	508	100	180	14,600	31,172	14.1	0.360	112.22	52.56
10	500	4	508	100	164	12,100	14,201	12.9	0.430	51.12	43.56
11	600	2	600	120	258	19,560	44,681	20.3	0.389	160.85	70.42
12	600	8	600	120	232	22,560	10,044	18.2	0.348	36.16	81.22
13	700	2	700	140	364	22,260	63,038	28.6	0.456	226.94	80.14
14	700	8	700	140	324	25,760	14,028	25.4	0.395	50.50	92.74
15	800	2	800	160	484	29,440	83,819	38	0.454	301.75	105.98
16	800	8	800	160	432	37,440	18,703	33.9	0.367	67.33	134.78
17	900	2	900	180	622	41,400	107,718	48.9	0.407	387.79	149.04
18	900	8	900	180	556	41,400	24,072	43.7	0.416	86.66	149.04
19	1000	2	1000	200	776	46,000	134,388	61	0.452	483.80	165.60
20	1000	8	1000	200	712	56,000	30,826	55.9	0.373	110.97	201.60
21	1100	2	1100	220	934	55,220	161,750	73.4	0.460	582.30	198.79
22	1100	8	1100	220	860	60,720	37,234	67.5	0.420	134.05	218.59
23	1200	2	1200	240	1124	72,240	194,655	88.3	0.416	700.76	260.06
24	1200	8	1200	240	1048	78,240	45,373	82.3	0.390	163.34	281.66

DN = Nominal shell diameter; Z = number of tube passes; Da = shell diameter [mm]; B = baffle spacing [mm]; n = number of tubes; AE = shell-side flow cross section [mm^2]; AR = tube-side flow cross section [mm^2]; AS = Heat exchanger area per m tube length [m^2/m]; VR = Required flow rate for 1 m/s flow velocity on the tube side [m^3/h]; VM = Required flow rate for 1 m/s flow velocity at the shell side [m^3/h].

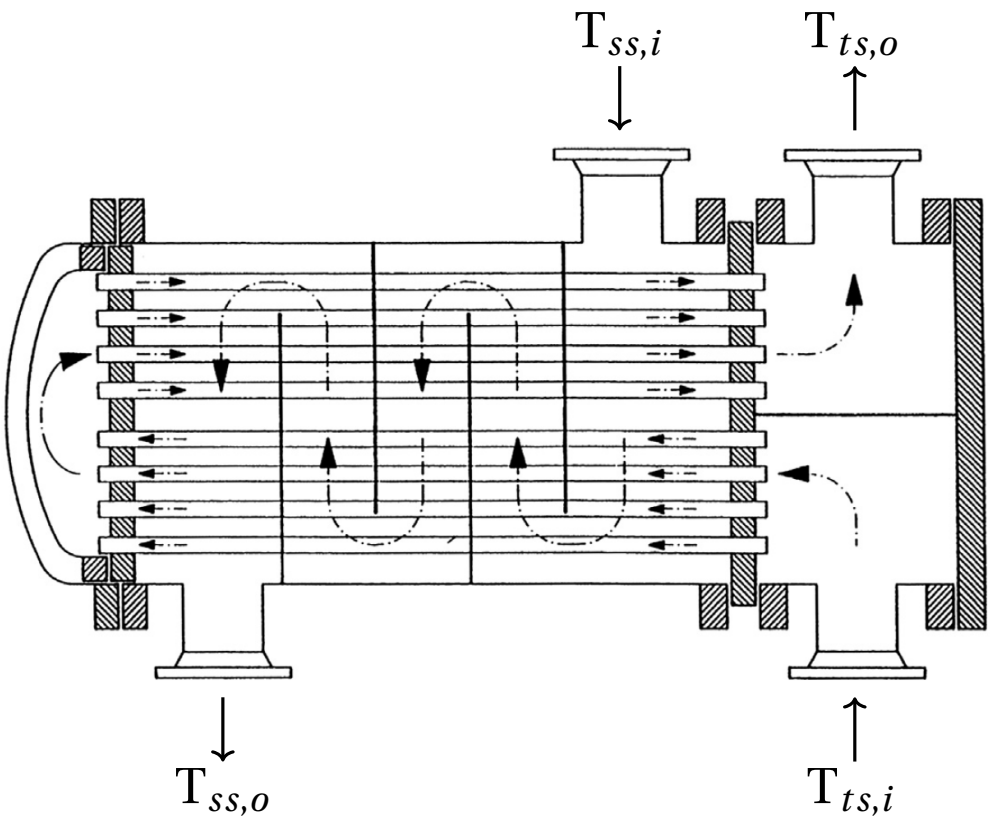

Figure 2.19: Shell and tube heat exchanger with two passes. Illustration taken from Nitsche and Gbadamosi (2016).

$$Nu_{ts} = [0.037Re^{0.75} - 6.66] \times Pr^{0.42}, \quad \begin{matrix} 2300 < Re < 8000 \\ 0.6 < Pr < 500 \end{matrix} \tag{2.65}$$

$$Nu_{ts} = 0.023Re^{0.8} \times Pr^{0.33}, \quad 8000 < Re \tag{2.66}$$

$$Nu_{ss,tri} = 0.196Re^{0.6} \times Pr^{0.33}, \quad 10 < Re \tag{2.67}$$

$$Nu_{ss,qua} = 0.156Re^{0.6} \times Pr^{0.33}, \quad 10 < Re \tag{2.68}$$

$$\alpha_{ts} = Nu_{ts}\frac{\kappa}{D_{ts}} \tag{2.69}$$

$$\alpha_{ss} = Nu_{ss}\frac{\kappa}{D_{ss}} \tag{2.70}$$

$$\alpha_{ts,o} = h_{ts,i}\frac{D_{ts,i}}{D_{ts,o}} \tag{2.71}$$

The natural next step in heat exchanger thermal design is now to calculate a new value for U using Equation (2.55). The actual heat load can then easily be calculated from Equation (2.54) based on actual heat exchanger area and the result from the U-calculation. It is also common to

see how much area your selected configuration has to spare and also check the excess fouling. These values can be estimated by application of Equation (2.72) and Equation (2.73).

$$A_{excess,[\%]} = (100\frac{U_{actual}}{U_{required}}) - 100 \tag{2.72}$$

$$f_{excess,[m^2K/W]} = \frac{U_{actual} - U_{required}}{U_{actual} \times U_{required}} \tag{2.73}$$

2.3.6 Exchanger Tube Patterns and Baffles

The engineers need to make some decisions of the geometry of the unit before the thermal performance of a shell and tube heat exchanger design can be estimated. The most important geometric consideration is deciding on what tube pattern will be used in the exchanger, a choice that has direct influence on the temperature profile which will be achieved. Performance-wise, using a triangular pattern as seen in Figure 2.20a is very good since the fluid shell side is forced "onto" the tubes when it flows towards the shell-side outlet. This means that the heat transfer coefficient when using a triangular pattern is higher than when a square pattern is used. Figure 2.20b shows how flow through a shell with tubing in a square pattern does not force the working fluid onto the tubes in the same way, hence performing worse. The positive side of using a square pattern is that it is much easier to clean, so in cases where deposits of wax, asphaltene or similar will occur then using square pattern tubing is convenient. It should be noted that in a ORC the working fluid is always run shell-side, so these types of flow assurance issues are not present except possibly inside the tubes where the heat source flows. In cases where square pattern has to be used in the exchanger, it is often opted to rotate the squares as seen in Figure 2.20c to improve the heat transfer coefficient.

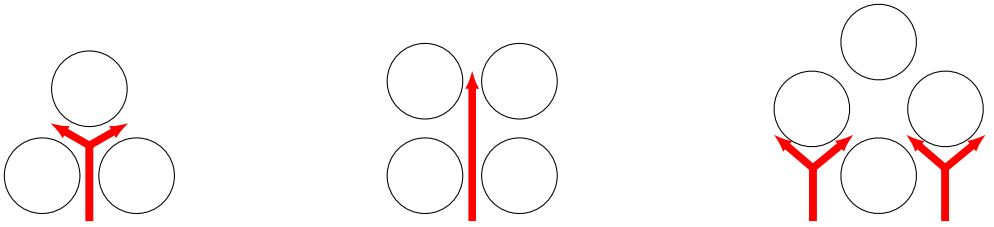

(a) Triangular tube pattern. **(b)** Square tube pattern. **(c)** Rotated square tube pattern.

Figure 2.20: Overview of common tube patterns geometry. Red arrow represents flow direction from shell-side inlet at the bottom towards shell-side outlet at the top.

A baffle is another physical object installed on the shell side of the S&T exchanger and it functions as an obstacle to the flow of the working fluid, effectively forcing it into a certain direction. In practice multiple baffles are usually installed, thus creating a sinusoidal flow pattern as seen

in Figure 2.19. The baffles have a big impact on the thermal performance of the unit and installing them horizontally helps avoid stratified flow in the heat exchanger. When it comes to volumetric considerations it is important to note that the spatial length between two baffles effectively determines the flow cross section, which means the baffle spacing and number should be calculated based on the expected operating conditions of the unit.

2.3.7 Binary Cycle Working Fluid Selection

The cycle configuration and component selection is not the only thing that matters when it comes to configuring an efficient thermal conversion cycle. Table 2.4 lists a summary of important characteristics that play a role when selecting a suitable working fluid, and the author chose to include information about these fluids only as examples of what the ORC engineers look for. The molecular weight and chemical formula is of great importance. If the molecular mass is high, the fluid will have a generally lower enthalpy drop when it expands. If the pressure ratio for the expansion is held fixed, a fluid with high molecular complexity will experience a higher volume ratio than a fluid with low complexity. The term molecular complexity is here referring directly to the molecular arrangement of the atoms. An example of a fluid with low molecular complexity would be water, which is a simple molecule of 3 atoms. An example of a fluid with higher molecular complexity is benzene, which consist of 12 atoms with a more complex molecular arrangement. If the reader is interested in extensive in-depth explanations for these effects, please see DiPippo (2016) or Astolfi and Macchi (2017).

In summary it means that the expander and turbine should be designed with the working fluid in mind. The working fluid has to undergo phase changes in a subcritical ORC, so it is important that the critical properties and boiling point are well suited such that the phase changes reflect optimal cycle behavior. This means that the temperature of the cooling media and the wellhead temperature of the thermal resource must be considered before selection. For a subsea application of ORC it is also very important that the working fluid used is environmentally friendly, as it would be very likely to experience some working fluid leakage to the sea from around the turbine shaft.

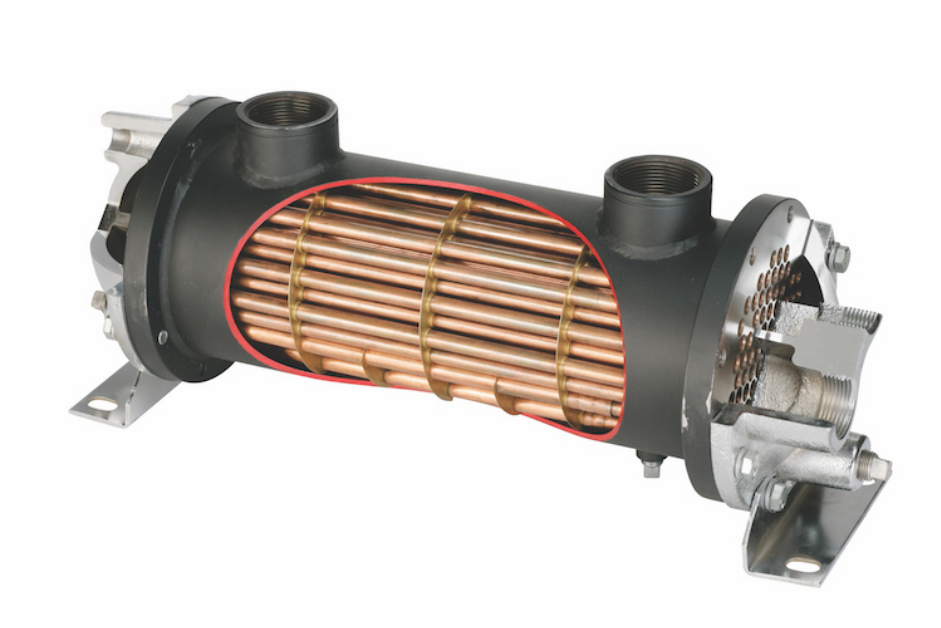

Figure 2.21: Thermal Products UC series shell and tube heat exchanger, 3/8" tubes. Image taken from thermalproducts.com

Table 2.4: Important properties for a selection of common working fluids Astolfi and Macchi (2017).

Name	Chemical formula	Molecular weight [kg/kgmol]	Critical temperature [°C]	Critical pressure [MPa]	Boiling point at 1.013 bar [°C]	Type of expansion
R134a	CH_2FCF_3	102.0	101.1	4.059	-26.1	Wet
R245fa	$CF_3CH_2CHF_2$	134.0	154.0	3.651	15.1	Dry
Isobutane	C_4H_{10}	58.1	134.7	3.629	-11.8	Dry
Butane	C_4H_{10}	58.1	152.0	3.796	-0.5	Dry
Isopentane	C_5H_{12}	72.1	187.2	3.378	27.8	Dry
Pentane	C_5H_{12}	72.1	196.6	3.370	36.1	Dry
Water	H_2O	18.0	373.9	22.064	100.0	Wet

2.4 Low Temperature Organic Rankine Cycle Working Fluids: An Annotated Bibliography

2.4.1 Introduction

Following this introduction two texts related to Low Temperature Organic Rankine Cycles Working Fluids are summarized with short evaluations to underpin their usefulness to this master's thesis. The main goal of this annotated bibliography is to give a brief overview of some of the literature that has been used and referenced in the report on the topic of working fluid selection, which is commonly considered as the most vital cycle parameter. It should be noted that work presented by other authors also serve as a basis for answering the thesis objective of evaluating thermodynamic feasibility of a power cycle at Tordis qualitatively, specifically by looking at results from using ORC technology at other application areas with similar thermodynamic traits as the Tordis wellstream. The summary also gives the reader better context on how other researchers analyze various ORC applications in regard to working fluid selection. As in any standard annotated bibliography, a reflection on the texts' relevance to the project has been included for each paper that has been reviewed, and the chapter is finalized with a conclusion.

2.4.2 Annotated Bibliography

Saleh, B. et al (2007). Working fluids for low-temperature organic Rankine cycles. In Energy 32 1210-1221. Elsevier.

Saleh, B. et al performed thermodynamic screening of 31 ORC eligible working fluids using BACKONE equation of state. Their screening process evaluated performance when the cycle operating conditions were varied from 30°C to 100°C. Supercritical pressures were used in a few cases, but usually the cycle pressure conditions were 20 bars or lower. For subcritical pressures the working fluid evaluation process proposed includes checking the curvature of the saturated vapor line in a temperature vs. specific entropy diagram and checking the state of the fluid going into the turbine inlet. The list of screened fluids includes alkanes and ethers, sometimes fluorinated. The authors have made an effort to match the different working fluids with the most optimal cycle configuration in order to maximize performance, which means that by example the cycle configuration used includes an internal heat exchanger when it is seen that the turbine outlet phase is superheated. The paper points out that the shape of the saturated vapor line in a Ts-diagram is one of the most important characteristics of an ORC. The operating pressures are pointed to as another important parameter when it comes to evaluating ORCs, and it is especially important to identify if the operation is subcritical or supercritical. When an ORC is operating in the supercritical pressure range it means that the working fluid does not undergo

phase changes from liquid to vapor, but instead stays in singular state throughout the cycle. Figure 2.22 shows what Saleh, B. et al calls a b1 cycle. The "b" is used because the curve is bell

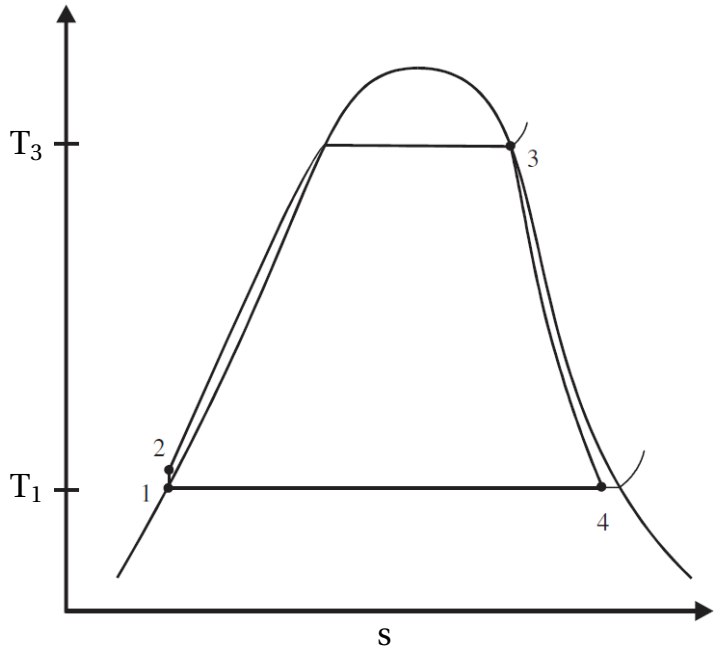

Figure 2.22: b1 configured ORC

shaped. The initial state shows a working fluid which is saturated at the condenser outlet. It is then brought from minimum to maximum cycle pressure using the cycle pump, here shown as state point 2. The working fluid is next heated by heat exchanging with a source fluid under constant pressure condition until gaseous state (3) is reached. The saturated gas is then expanded down to condenser pressure (4) which is in the liquid-gas region for this working fluid. The working fluid passes through the condenser at constant pressure, bringing it back to saturated liquid state at point 1. If a cycle like this has its state point 4 in the superheated vapor region while keeping everything else the same as before, the configuration is called a "b2"-cycle. A "b3"-cycle is shown in Figure 2.23. The initial points are at the same states as the previous configurations, but the working fluid is here superheated in the evaporator until state point 3 is reached. The expansion ends in the gaseous region, just as in cycle configuration b2. Figure 2.24 shows what Saleh, B. et al calls an "o2" cycle. The "o" is here used because the curve shape is overhanging. The states of the o2 cycle are generally the same as in b2, as seen in the figure. "o3" is a configuration not shown by figure here, and is an overhanging shaped curve with state points as in b3. Figure 2.25 shows a supercritical pressure cycle called "s1". Note that no phase change happens between state point 2 and 3 in this configuration. The end point (4) in Figure 2.25 is in the liquid-vapor region, and in cases where point 4 is in the superheated vapor region the cycle is called "s2". Equation (2.74) calculates cycle thermal efficiency unless an extra internal heat exchanger (IHE) is used in the configuration. IHE has been added in cases where the

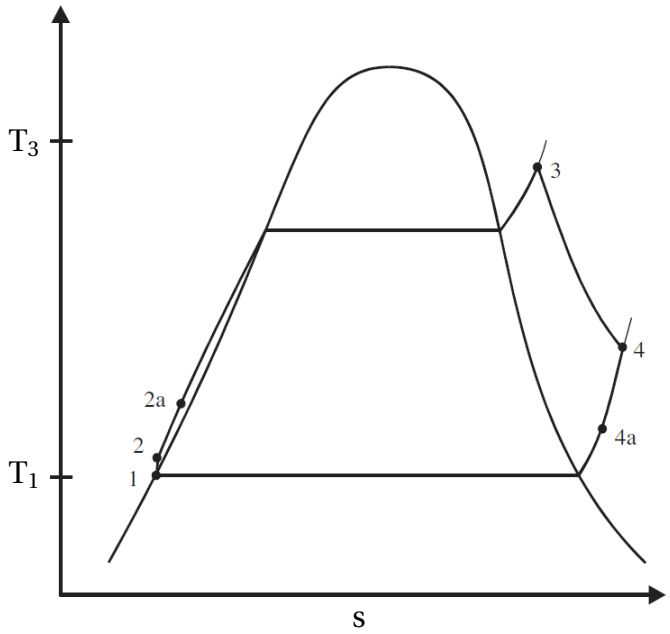

Figure 2.23: b3 configured ORC

temperature at state 4 is much higher than the temperature at initial state, and in these cases the thermal efficiencies are calculated with Equation (2.75). In the equations, the letter h stands for specific enthalpy, w stands for work, q stands for heat and the subscripts specifies the various cycle state points. Table 2.5 shows a summary of results for different working fluids when the ORC has been calculated using the BACKONE equation of state. The condensation temperature used was 30°C in all cases, and when IHE was used its outlet temperature was defined as 40°C. Isentropic efficiencies of pump and turbine were 0.65 and 0.85, respectively.

An observation of relevance in regard to this thesis is that efficiency increase by superheating the b-cycles are barely seen when no IHE is used. A significant thermal efficiency increase takes place when the cycle is modeled with IHE. For the o-cycles Saleh, B. et al found that the thermal efficiency went down when superheated. In addition, it was seen that fluids with higher critical temperature tend to fit o-cycles, and that b-cycle fluids have a generally lower critical temperature. From Table 2.5 it can also be seen that heavier hydrocarbons reach higher thermal efficiency while requiring lower mass flow rates, but the critical temperatures are very high. Examples of these are butanes, pentanes and n-hexane which all have higher than 12% thermal efficiency when modelled without IHE and higher than 13% with IHE.

$$\eta_{thermal} = -\frac{w_{34} + w_{12}}{q_{23}} - \frac{(h_4 - h_3) + (h_2 - h_1)}{(h_3 - h_2)} \tag{2.74}$$

$$\eta_{thermal} = -\frac{w_{34} + w_{12}}{q_{2a3}} - \frac{(h_4 - h_3) + (h_2 - h_1)}{(h_3 - h_{2a})} \tag{2.75}$$

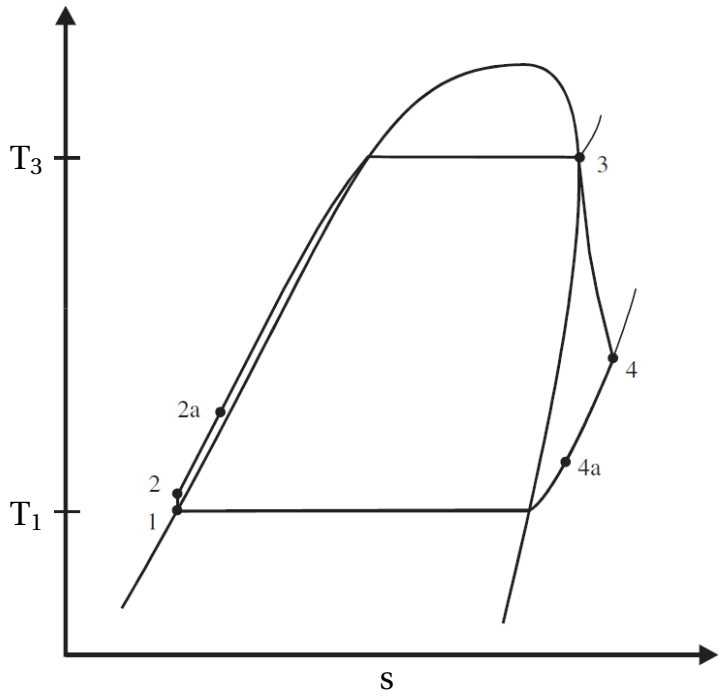

Figure 2.24: o2 configured ORC

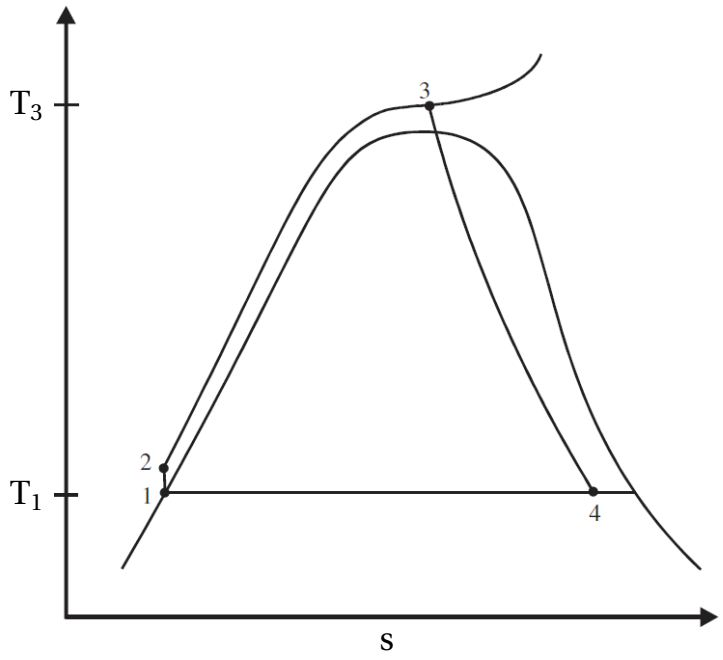

Figure 2.25: s1 configured ORC

Table 2.5: Selection of numerical results taken from Saleh et al. (2007) for different working fluid substances. Both basic ORC and ORC with IHE calculated using BACKONE EOS.

Substance	**Cycle type**	$\mathbf{T}_c$ [°C]	$\mathbf{p}_c$ [bar]	$\mathbf{T}_3$ [°C]	$\mathbf{T}_4$ [°C]	$\mathbf{p}_{min}$ [bar]	$\mathbf{p}_{max}$ [bar]	$\dot{m}$ [kg/s]	$\eta_{thermal}$ [%]	$\eta_{thermal}$ (IHE) [%]
R125	b1	66.18	36.30	40.06	30.0	15.64	20.0	400.37	2.32	—
R125	b3	66.18	36.30	100.0	91.92	15.64	20.0	246.30	2.36	3.36
R218	o2	71.89	26.80	58.99	33.68	10.04	20.0	238.23	5.22	—
R218	o3	71.89	26.80	100.0	82.86	10.04	20.0	151.55	5.15	7.50
R143a	b1	72.73	37.64	43.59	30.0	14.40	20.0	197.92	3.14	—
R143a	b3	72.73	37.64	100.0	87.37	14.40	20.0	127.89	3.31	4.36
R32	b1	78.11	57.83	31.36	30.0	19.31	20.0	1062.6	0.36	—
R32	b3	78.11	57.83	100.0	97.75	19.31	20.0	682.78	0.42	0.53
RE125	b2	81.34	33.51	57.67	31.50	10.11	20.0	145.17	5.67	—
RE125	b3	81.34	33.51	100.0	79.04	10.11	20.0	103.11	5.77	7.34
R1270	b1	92.42	46.65	48.54	30.0	13.09	20.0	69.334	4.28	—
R1270	b3	92.42	46.65	100.0	81.28	13.09	20.0	49.109	4.53	5.51
R290	b1	96.65	42.50	57.14	30.0	10.79	20.0	48.776	5.91	—
R290	b3	96.65	42.50	100.0	76.02	10.79	20.0	36.100	6.11	7.32
R134a	b1	101.03	40.56	67.75	30.0	7.722	20.0	68.55	7.74	—
R227ea	o2	101.74	29.29	83.88	44.19	5.331	20.0	81.523	9.20	—
R152a	b1	113.5	44.95	72.59	30.0	6.888	20.0	38.503	8.82	—
R152a	b3	113.5	44.95	100.0	53.84	6.888	20.0	31.987	9.22	9.71
RC318	o2	115.23	27.78	98.93	54.72	3.68	20.0	66.828	10.97	12.09
RC318	o3	115.23	27.78	100.0	56.38	3.68	20.0	68.694	10.55	11.75
CF3I	b1	123.29	39.53	85.24	30.0	5.652	20.0	97.043	10.63	—
CF3I	b3	123.29	39.53	100.0	39.60	5.652	20.0	86.917	10.93	—
RC270	b3	124.65	54.90	100.0	41.63	8.227	20.0	24.713	8.86	—
R236fa	o2	125.55	32.00	100.0	48.61	3.240	19.35	47.313	11.63	12.14
RE170	b1	126.85	52.40	75.10	30.00	6.733	20.0	63.068	9.38	—
RE170	b3	126.85	52.40	100.0	53.03	6.733	20.0	54.488	9.68	10.13
RE245mc	o2	133.68	28.87	100.0	54.50	2.416	14.88	42.549	11.84	12.72
R600a	o2	135.05	36.50	100.0	45.33	4.038	19.98	20.423	12.12	12.43
R236ea	o2	139.22	34.12	100.0	53.92	2.438	15.74	41.361	12.02	12.83
RE134	o2	147.1	42.28	100.0	41.04	2.501	16.66	32.149	12.56	—
C5F12	o2	148.85	20.40	100.0	72.76	1.037	7.66	67.15	10.49	13.10
R600	o2	152.05	38.00	100.0	48.43	2.850	15.29	17.746	12.58	13.04
R245fa	o2	154.05	36.40	100.0	50.70	1.801	12.67	33.424	12.52	13.07
R338mccq	o2	158.8	27.26	100.0	63.08	1.117	8.428	46.486	11.84	13.30
neo-C5 H12	o2	160.65	32.00	100.0	58.92	2.001	11.16	20.426	12.20	13.37
RE347mcc	o2	164.55	24.76	100.0	66.98	0.959	7.103	45.263	11.72	13.49
RE245	o2	170.88	30.48	100.0	58.47	1.040	8.198	42.549	12.59	13.59
R245ca	o2	174.42	39.25	100.0	53.75	1.230	9.343	30.548	12.79	13.47
R601a	o2	187.75	33.86	100.0	58.47	1.098	7.223	17.439	12.75	13.76
R601	o2	196.5	33.70	100.0	57.74	0.828	5.963	16.331	12.91	13.84
n-hexane	o2	234.67	30.10	100.0	61.89	0.250	2.481	15.853	13.00	14.14

Dong, B. et al (2017). Potential of Low Temperature Organic Rankine Cycle with Zeotropic Mixtures as Working Fluid. In Energy Procedia 105 1489-1494. Elsevier.

Dong et al. (2017) investigate how use of zeotropic mixtures as working fluids may increase thermodynamic efficiency of organic Rankine cycles, as compared to using pure fluids. A zeotropic mixture is when fluids with differing boiling points are blended, and the hypothesis was that such a working fluid may match with the working temperatures better than a regular fluid. In the paper, zeotropic mixtures are compared with pure fluids based on ORC performance and it is also checked what consequences using zeotropic mixtures have on the heat exchanger sizing.

Table 2.6: Main thermal properties related to the four substances selected by Dong et al. (2017) for investigation.

Fluid	**M [g/mol]**	**P_c [bar]**	**T_c [°C]**	**T_{bp} [°C]**
R245fa	134.05	36.51	154.01	15.14
R123	152.93	36.62	183.68	27.82
R365mfc	148.07	32.66	186.85	40.15
R113	187.38	33.92	214.06	47.59

Dong et al. (2017) presents a multi-objective optimization model made to compare ORC performance. The comparison criteria used is first law efficiency and net power per heat exchanger area. The cycle configuration used for calculations is a standard ORC with internal heat exchanger. The following parameters were specified in their model: The heat source is a water stream at 5 bars with inlet temperature 150°C and outlet temperature 130°C. The cooling fluid is also water at 5 bars, which has inlet temperature 25°C and outlet temperature 35°C. The pinch temperatures in the external heat exchangers are 20°C and 15°C pinch temperature was used for the internal heat exchanger. The pump operates at 80% isentropic efficiency, the expander at 75% isentropic efficiency and the generator at 95% efficiency.

Four fluids that are commonly used in ORCs was selected for analysis and these are listed in Table 2.6. The simulation was performed using MATLAB with fluid properties taken from REFPROP 9.0 database, and Dong et al. (2017) presents how all state points are formulated in the paper. Equations (2.76) and (2.77) show how the comparison criteria are defined, the letter W stands for power, Q stands for heat and A is area in these definitions.

Table 2.7 displays how the use of mixtures can improve cycle performance, note that the binary mixtures presented are the optimal mass fractions of each fluid combination. It is however apparent that because of a bigger portion of the heat transfer from the heat source happens during working fluid phase change, the required heat exchangers must be a lot larger and especially so for the IHE. Figure 2.26 shows the results from the heat exchanger calculations graphically, and looking to the rightmost plot it is clear that the most cost-effective performance is when pure fluids are used as working fluid. In other words it means that you cannot reach the highest cycle efficiency and cost-effective performance simultaneously.

$$\eta = \frac{W_{generator} - W_{pump}}{Q_{evaporator}} \tag{2.76}$$

$$\epsilon = \frac{W_{net}}{A_{total}} = \frac{W_{generator} - W_{pump}}{A_{evaporator} + A_{condenser} + A_{IHE}} \tag{2.77}$$

The findings are of significant interest to this master's thesis, because it shows that zeotropic mixtures could be used to get higher cycle efficiency if a certain output threshold can not be reached with pure fluids. On the other hand, it will be a bad idea if the threshold can already be met, since the heat exchangers will be more expensive. A practical example related to Tordis ORC would be if pure fluids used as working fluids made for lower net power output than required for a specific purpose, for example boosting. In such a scenario zeotropic mixtures can be considered as a substitute to meet the output requirement, despite the fact that the heat exchangers needs to be sized up.

Table 2.7: Results taken from Dong et al. (2017). Shows how cycle efficiency can be improved using zeotropic (binary) mixtures.

Fluid	**Mass fraction**	$\mathbf{P}_{evap}$ **[bar]**	$\mathbf{P}_{cond}$ **[bar]**	$\mathbf{P}_{ratio}$ **[-]**	$\mathbf{T}_{\frac{grad}{evap}}$ **[°C]**	$\mathbf{T}_{\frac{grad}{cond}}$ **[°C]**	$\mathbf{W}_{gen}$ **[W]**	$\mathbf{W}_{pump}$ **[W]**	η **[%]**
R245fa	1	19.0	3.9	4.9	0	0	210.1	15.3	9.10
R123	1	11.3	2.4	4.7	0	0	212.1	9.0	9.48
R365mfc	1	8.7	1.6	5.3	0	0	214.2	7.2	9.67
R113	1	6.3	1.3	5.0	0	0	214.4	5.2	9.77
R123/R365mfc	0.32/0.68	9.7	1.9	5.2	0.62	1.13	216.3	7.9	9.73
R245fa/R123	0.21/0.79	14.0	2.8	5.0	2.84	3.00	219.9	11.4	9.74
R365mfc/R113	0.40/0.60	7.2	1.4	5.2	0.81	0.47	216.2	6.0	9.82
R123/R113	0.26/0.74	8.2	1.6	5.3	3.75	4.19	225.5	6.9	10.21
R245fa/R365mfc	0.30/0.70	12.4	2.1	5.8	5.02	6.34	229.2	10.3	10.23
R245fa/R113	0.32/0.68	12.4	2.1	5.8	12.43	13.00	240.3	10.6	10.73

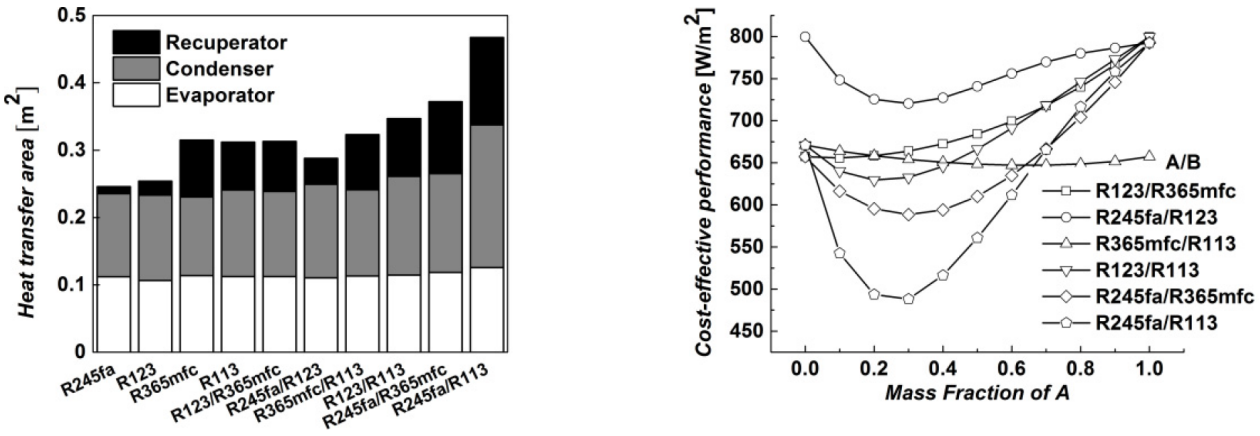

Figure 2.26: Effect of using binary working fluid on heat exchanger design. Taken from Dong et al. (2017).

2.4.3 Annotated Bibliography Result Summary and Conclusion

Saleh et al. (2007) investigated the thermal efficiencies of using various fluids as working fluids in low temperature ORCs with BACKONE EOS. The results varied from $\eta_{thermal} = 0.36\%$ for R32 to $\eta_{thermal} = 14.14\%$ for n-hexane. The model used the most fitting cycle configuration for every investigated fluid and added internal heat exchanger in cases where the gas at expander outlet was superheated. Comparing results with and without IHE it can be seen that the efficiency increase is usually less than a percent when IHE is added. Dong et al. (2017) showed that using multi-component working fluids may improve thermal efficiencies of low temperature Rankine cycles, proposing that the wide usage of singular component fluids in the present industry may be inefficient. The analysis focused on investigating possible issues with heat exchanger sizing when diverging from standard working fluids to see if it would pay off or not. It was shown that using binary mixtures as working fluids could increase the thermal efficiency of the cycles with around one percent, but the effective heat exchanger areas would be increased by significant margin. It was concluded that usage of pure fluids would be more cost effective in general, especially in cases when IHE is used.

The literature review of low temperature ORC working fluid screening showed that even for "bad" heat sources it is possible to get a reasonable thermal energy conversion efficiency. This is seen as a very promising find, as the Tordis wellstream poses a large energy potential due to the high mass rates, despite its low average temperature of around 75°C. The results from the other researchers showed that conversion efficiencies of 8-12% can be reasonably expected from low temperature sources, if the right fluid is chosen as working media. Covering the requirements for boosting is defined as a criterium for determining if use of ORC at Tordis is viable. If it is assumed that the wellstream cools from 75°C to 20°C by heat exchange with a working fluid, the

total energy transfer was shown earlier as 46.5 MW. If the ORC converts with 9% or better thermal efficiency it will be able to cover the Tordis boosting power consumption at 4MW, which means it is plausible that usage of ORC may be feasible, from a qualitative standpoint. Further on in this thesis it is investigated whether energy transfer of 46.5 MW would be realistically possible or not, by the use of more rigorous models.

Chapter 3

Methodology and Model Descriptions

3.1 Model for calculation of Raw Power Available

The model for the raw power estimation consists of multiple parts, all of which will be explained in detail in this section. Figure 3.2 is a picture taken of the Aspen HYSYS portion of the model, that is behind all the calculations and estimated results. In addition, Excel VBA code has been written to efficiently run the model with varying inputs for sensitivity analysis, see Appendix A. It should be noted that the VBA is a modified version of a script used in Gleditsch (2017) for sensitivity analysis of the phase effect on raw power available. The necessary inputs to run the model are hydrocarbon composition, flow rates, wellhead and surface process PT conditions. The surface process PT conditions are required to estimate GOR, WC and produced volume rates at standard conditions. Since Excel VBA can communicate with HYSYS, it was found convenient to limit all inputs to be made in a spreadsheet, keeping the manual work in HYSYS to a minimum.

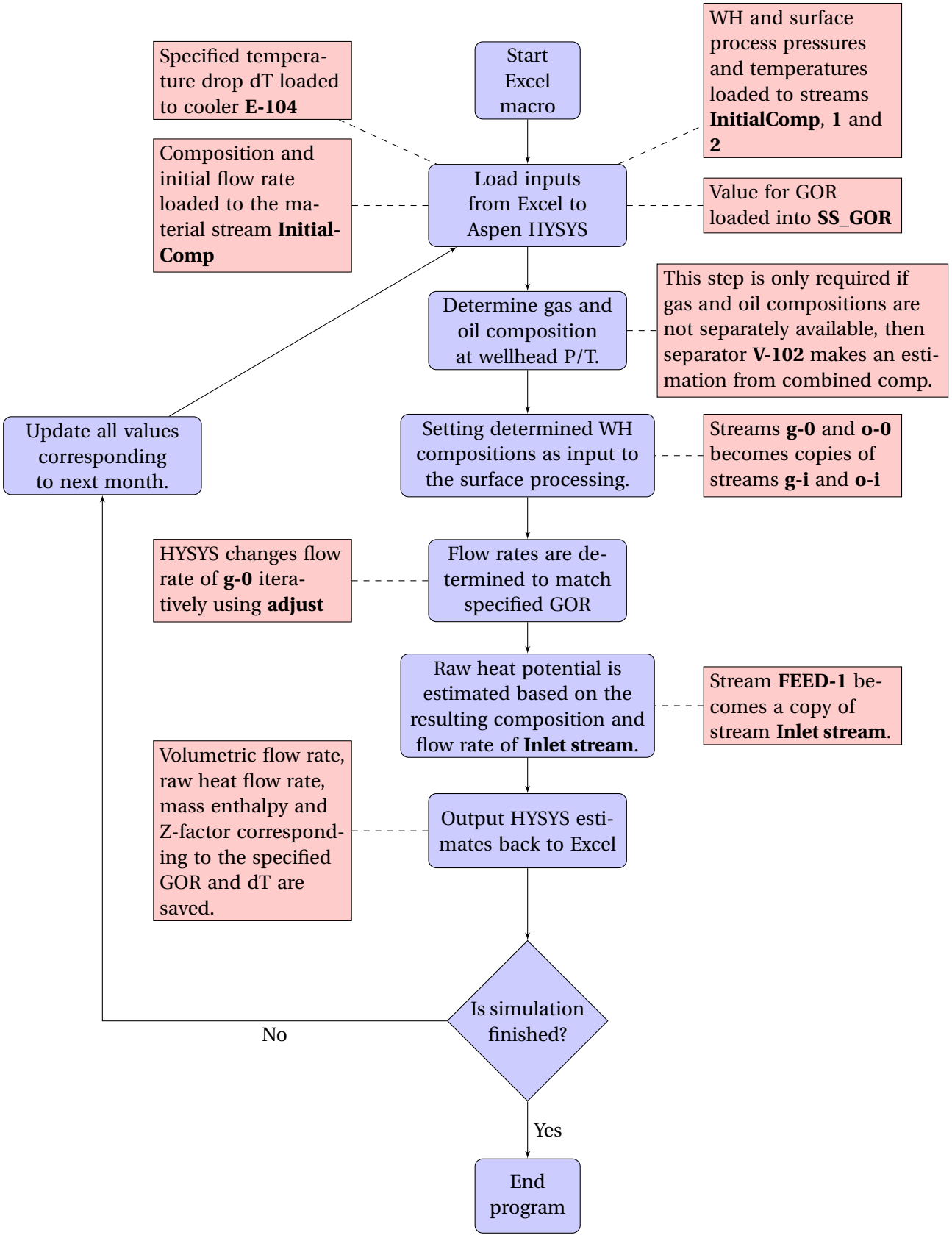

Figure 3.1: Flowchart for raw power model that estimates raw power potential over time based on a fields production history using monthly data.

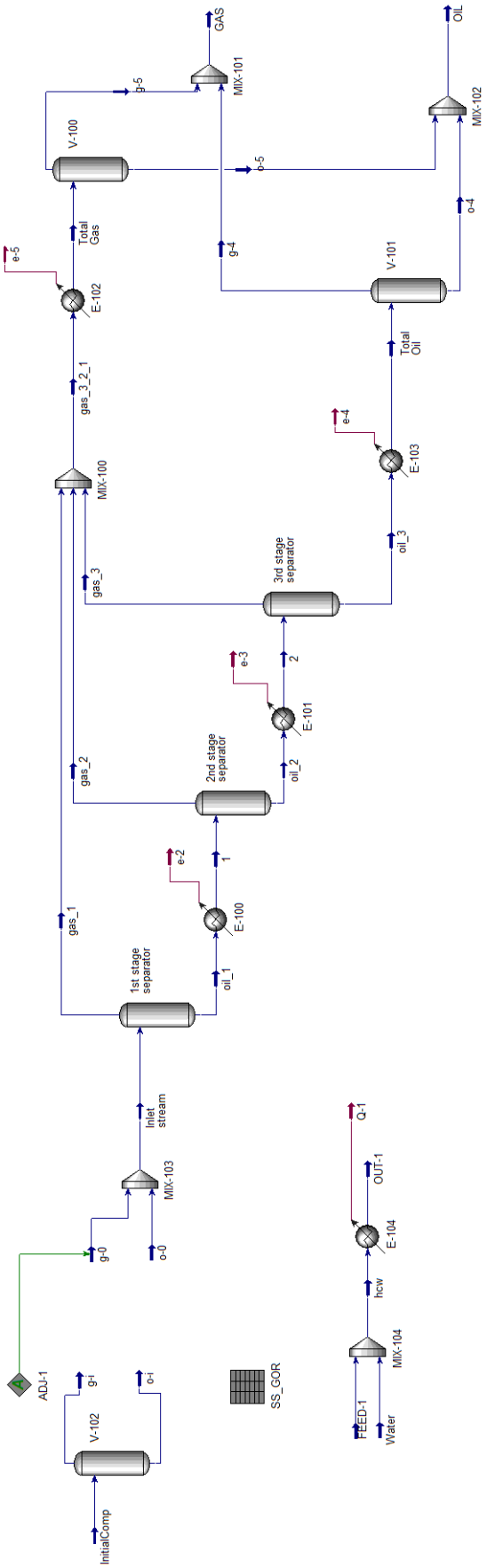

Figure 3.2: Raw power model. Snapshot from Aspen HYSYS.

Since specific gas and oil compositions of various wells producing on the NCS are not easily available, the model was simplified by only requiring a re-combined (or in-situ) composition. Using a seed composition, it is possible to estimate the composition of each phase at wellhead conditions, and use the results to determine mixture composition based on different GORs than the original. In Figure 3.2 the separator *V-102* takes in a combined composition and separates it into gas and oil streams using pressure and temperature values that are specified as equal to local wellhead conditions. In other words, the streams *g-i* and *o-i* represents the gas and oil compositions we expect to see at the wellhead and are used for further analysis. When *g-i* and *o-i* have been determined, their compositions are copied over into the material streams *g-0* and *o-0* automatically by the macro. For clarification, if gas and oil compositions are separately available to begin with, *g-0* and *o-0* could be defined directly without the need of separator *V-102*.

The flow rates of *g-0* and *o-0* can be adjusted in relation to each other, effectively changing the produced GOR/CGR. The produced GOR/CGR is calculated using rates from the material streams *OIL* and *GAS*, that are located after the third separator stage and at standard conditions. In Figure 3.2 there is a green arrow pointing at *g-0*, with a box labelled *ADJ-1*. Its function is simply to change the gas rate of *g-0* until the output of the system reaches a pre-defined value for the GOR/CGR, which it reads from the file *SS_GOR*. This means that the material stream *"Inlet stream"* located after the mixer *MIX-103* has composition and rate that corresponds to a pre-defined GOR/CGR, which is very convenient for sensitivity analysis purposes.

At the bottom, in the lower part of Figure 3.2 there is a material stream *"FEED-1"* that goes into cooler *E-104*, that outputs the energy stream *Q-1*. This cooler is where the raw power potential is calculated. $FEED-1$ is automatically set as identical to *"Inlet stream"*, and *Q-1* represents the thermal energy that has to be removed from the material stream in order to lower its temperature. In total the setup shown in Figure 3.2 allows the user to see how changes in GOR/CGR affects the raw thermal power available, see effects of changes in the temperature drop across the cooler *E-104* and to calculate raw thermal heat potential over a fields lifetime using NPD data. The actual script for the model is included in Appendix A, but the reader will get a better overview of the algorithm given on flowchart form in Figure 3.1.

3.2 The Subsea ORC Model for Tordis

A model has been made to determine the net output power potential of a subsea organic Rankine cycle based on the produced fluids from Tordis, and to get a rough overview of the equipment sizes necessary. The following constraints apply. Tordis is currently producing 31.5 kg/s of condensate and 161 kg/s of water. The wellhead temperature ranges between 50 - 75 °C, and the wellhead pressures are kept between 20 - 50 bara. The ambient sea water temperature ranges between 6 - 9 °C at the wellheads, which are located roughly 250 meters below the surface of the sea. Since specific details related to the cycle components are yet to be determined, typical values for the unknowns have to be assumed to get an approximate model that will give a larger understanding of which cycle components are necessary and their sizes. The basic ORC configuration consisting of an expander, turbine, pump, condenser and an evaporator has been presented earlier in this thesis, and is used as the starting point for this evaluation. The following common assumptions for ORC modelling has been taken from peer-reviewed literature and can be found at multiple sources. It is assumed that the cycle operates at steady state, that the isentropic efficiency of the expander is 85%, an isentropic efficiency of the pump of 80% and mechanical efficiency of the turbine is 98%-100%. In thermal analysis, the point where the temperature difference between hot and cold fluid is at its minimum is called a pinch point. It is common to model heat exchangers in ORCs with 5°C at pinch points, as it is assumed that the temperature difference between the streams needs to be at least 5°C to get meaningful heat transfer. When it comes to the cycle pressure it is always ensured that the expander outlet pressure is at a level where the vapor fraction of the working fluid is 100%, since having liquid droplets in the expander will erode the turbine blades. The pressure and temperature at the condenser outlet are adjusted to a level where the vapor fraction of the working fluid is zero, so that no gas passes through the pump and also to ensure that the cycle operates below the critical point. This means that the pump duty will be adjusted accordingly and have direct effect on the cycle net power output.

The most important part for any ORC model is to select a fitting working fluid to run in the cycle. The methodology for selecting a proper working fluid for the model is explained in Section 3.3, and the fluid screening process is based upon the restraints of the model presented here. Since the Tordis wellhead temperatures are reported as ranging between 50 - 75°C, it would make sense to at least include the entire interval in the analysis as a minimum. It is also interesting to look into the effects of higher cycle inlet temperatures since other fields produce fluids with higher enthalpy than Tordis, so the temperature interval from 50 to 115 °C is therefore examined for the working fluid selection. As mentioned, the sea water temperature in the area is reported as ranging between 6 - 9 °C, so the ORC is modeled with a fixed value of 9 °C ambient temperature for cooling purposes.

3.3 Evaluation of Potential Working Fluids

The working fluids used for comparison are chosen from the Aspen HYSYS components list in the Basis Environment, which contains in total 37 fluids that are suitable for removing heat by evaporation close to the normal boiling point. To make the initial working fluid comparison efficient, an Excel VBA that interacts with Aspen HYSYS was written to help with the process. The VBA makes it possible to choose a working fluid substance and run a Rankine cycle simulation using HYSYS while saving data to an Excel spreadsheet, working only from the Excel interface. As an example, the author could select n-Butane as a working fluid and by the press of a button HYSYS would calculate Rankine cycle solutions for the temperature pre-defined range 50 to 115 °C and save the parameters of interest for each iteration. The VBA can be found in Appendix B, and was used to get data points for several of the trend plots contained in the results section.

For a low temperature organic Rankine cycle, it is possible to either use a hydrocarbon or refrigerant substance as the working fluid. Refrigerants are sometimes chosen due to being non-flammable, but the potential environmental impact is much larger than for hydrocarbon working fluids. The working fluid selection has been performed based on two primary criteria, being performance and level of environmental risk. The HYSYS model is based on the constraints listed in Section 3.2 and was used to vet the heat transfer fluids contained in the HYSYS basis environment component list, computing net power output and thermal efficiency over the heat source temperature interval 50-115°C. After seeing the performance of each fluid ranked from best to worst, the environmentally harmful ones have been removed until we have a ranking with less environmental risk. Table 3.1 contains an overview over candidate refrigerant fluids that have low boiling points and could possibly work in the ORC. Additional fluids proposed by the paper *Working fluids for low-temperature Rankine cycles* by Saleh et al. (2007) were added to the list of potential candidates, here listed in Table 3.2. Note that some of the fluids in Table 3.2 could not be found in the Aspen HYSYS component list, and was therefore simulated using a basic ORC model in Aspen Plus V9 instead.

Some of the boundary conditions for the fluid selection model affect the various working fluids differently. Since the model assumes heat exchangers with 5°C pinch, some fluids may be at the point of saturation and others may be completely dry or wet depending on the critical points of the fluid. In practice this will for example mean that the working fluid leaving the condenser will be at 14 °C when the sea water temperature is 9 °Celsius, no matter what the working fluid is. The working fluid gas leaving the evaporator is defined in the same way, being 5 °Celsius lower than wellhead temperature. Because of these specifications it should be noted that some potential fluids will be superheated when passing through the expander and some will be subcooled when passing through the pump, since all the fluids have different phase curves. The pressure

changes across the heat exchangers on the working fluid side were defined as fixed values of 1 bara shell side in this analysis and the isentropic efficiencies of pump and turbine are equal to unity for the fluid screening only. The wellstream supplying the raw thermal energy has the composition shown in Table 4.1 and the tube side pressure drop in the evaporator was defined as 3 bara.

Table 3.1: Possible heat transfer fluids contained in the HYSYS database.

Full Name	**Formula**	**Norm. T_{BP}[°C]**
Refrig-11	CCl3F	24
Refrig-12	CCl2F2	-30
Refrig-13	CClF3	-81
Refrig-14	CF4	-128
Refrig-22	CHClF2	-41
Refrig-23	CHF3	-82
Refrig-50	CH4	-162
Refrig-113	C2Cl3F3	48
Refrig-114	C2Cl2F4	4
Refrig-170	C2H6	-89
Refrig-290	C3H8	-42
Refrig-500	-	-34
Refrig-502	-	-45
Refrig-503	-	-88
Refrig-600	C4H10	-1
Refrig-702	H2	-253
Refrig-704	He	-269
Refrig-717	NH3	-33
Refrig-718	H2O	100
Refrig-720	Ne	-246
Refrig-728	N2	-196
Refrig-729	-	-195
Refrig-732	O2	-183
Refrig-740	Ar	-186
Refrig-744	CO2	-79
Refrig-1150	C2H4	-104
Refrig-1270	C3H6	-48
Refrig-13B1	CBrF3	-58
Refrig-142b	C2H3ClF2	-10
Refrig-152a	C2H4F2	-25
Refrig-600a	C4H10	-12
Refrig-702a	H2	-253
Refrigerant_113	C2Cl3F3	48
Refrigerant_125	C2HF5	-48
Refrigerant_152	C2H4F2	11
Refrigerant_133a	C2H2ClF3	6
Refrigerant_134a	C2H2F4	-26
Refrigerant_216ca	C3Cl2F6	36

Table 3.2: Possible working fluids especially suited for low-temperature ORCs, presented in Saleh et al. (2007).

Full Name	Formula
R32	CH2F2
R41	CH3F
R125	C2HF5
R134a	C2H2F4
R143a	C2H3F3
R152a	C2H4F2
R218	C3F8
R227ea	C3HF7
R236ea	C3H2F6
R245ca	C3H3F5
R245fa	C3H3F5
RC-270	Cyclo-Propane
R290	Propane
RC318	Cyclo-C4F8
R338mccq	C4H2F8
R600	n-butane
R600a	Iso-butane
R1270	C3H6
CF3I	CF3I
C5F12	C5F12
R601	n-pentane
R601a	Iso-pentane
neo-C5H12	Neo-pentane
n-C6H14	n-hexane
RE125	C2HF5O
RE134	C2H2F4O
RE170	C2H6O
RE245	C3H3F5O
RE245mc	C3H3F5O
RE347mcc	C4H3F7O

3.4 Shell and Tube Evaporator Model

Calculating the heat exchanger properties should be performed using an iterative process. This is mainly because the heat transfer coefficients are a function of the Reynolds numbers, which means the flow velocities and hence the cross sectional areas have to be specified initially. Figure 3.3 shows the algorithm that is used for thermal design of a shell and tube evaporator.

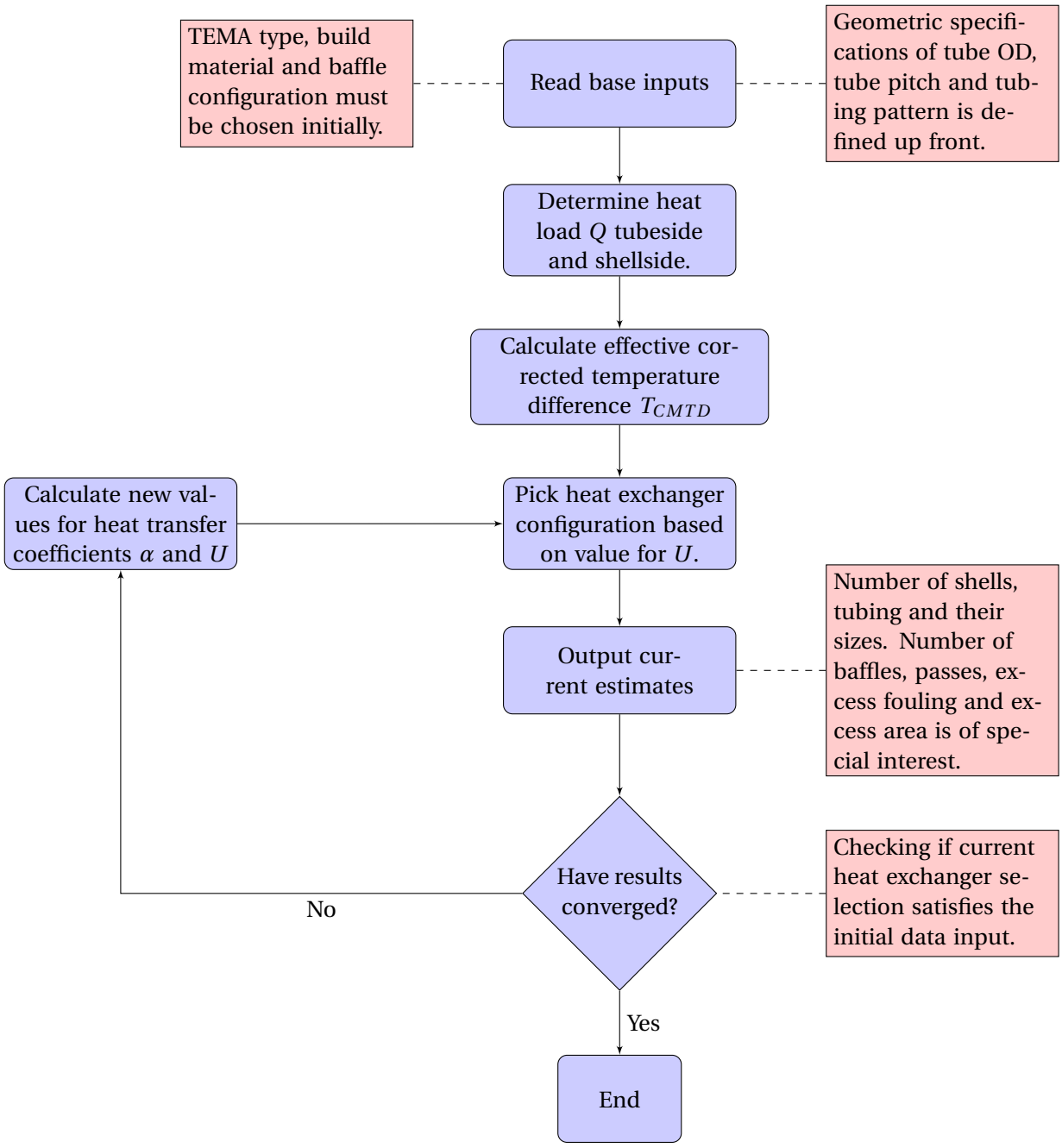

Figure 3.3: Flowchart for thermal modeling of S&T heat exchangers. Based on the algorithm shown in Nitsche and Gbadamosi (2016).

3.5 Passive Cooling Manifold Model

In order to estimate an approximate size of a passive cooling system, a simple model for calculating the natural convection effect between the sea and cycle working fluid has been developed. The aim is to see how much piping would be needed to get the required cooling duty, and note that pipe bends are not accounted for in this model. Figure 3.4 illustrates the expected thermal resistance for single wall-section of tubing when it is made of super duplex with no coating.

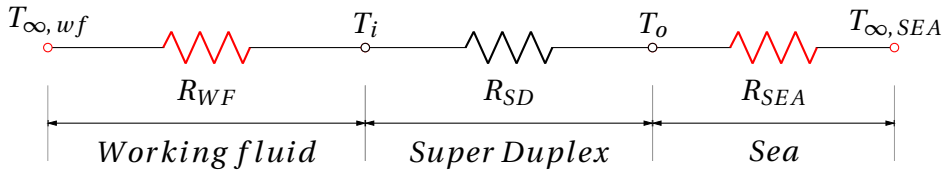

Figure 3.4: Illustration of equivalent thermal resistance for the modeled system. Red color points to convective thermal resistance of the fluid-solid interfaces. Thermal resistance of the solid tube material Super Duplex is shown in black.

3.5.1 Forced Convective Heat Transfer

Forced convective heat transfer from the working fluid can be expressed with Newton's Law of Cooling, here formulated in Equation (3.1). Figure 3.5 illustrates convection happening at the contact surface between the working fluid and the super duplex tube. The convection coefficient α_1 is a function of surface geometry, fluid properties and velocity. A term for the convective thermal resistance is shown in Equation (3.2), which can be used to express the heat flow in terms of temperature difference and thermal resistance as in Equation (3.3).

$$Q = \alpha_1 A_1 (T_{\infty, wf} - T_i) \tag{3.1}$$

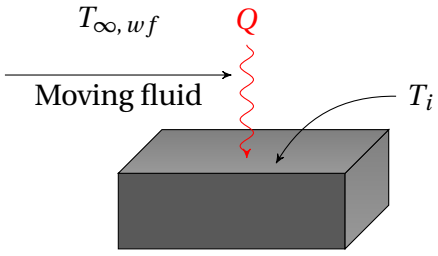

Figure 3.5: Convection on interface between the working fluid and inner side of pipe wall.

$$R_{WF} = \frac{1}{\alpha_1 A_1} \tag{3.2}$$

$$Q = \frac{T_{\infty,wf} - T_i}{R_{WF}} \tag{3.3}$$

The heat transfer coefficient α_1 has to be determined, and as seen by Equation (3.4), it can be defined by the Nusselt number Nu_1, the pipe diameter D and the thermal conductivity of the fluid κ_1. A value for the pipe diameter can be selected based on available process drawings or assumed, and finding the thermal conductivity of the working fluid can be done with Aspen HYSYS. The Nusselt number has to be calculated with empirical correlations, and as mentioned earlier in the thesis, there exists a number of Nu-correlations valid for a range of different applications. The definitions given by Equation (3.5) and Equation (3.6) are suitable for laminar flow within a circular tube with constant wall temperature according to the publication *Subsea Pipeline Design, Analysis, and Installation* by Bai and Bai (2014). If the internal pipe flow conditions are turbulent, the Gnielski empirical formula given in Equation (3.7) can be used.

$$\alpha_1 = Nu_1 \frac{\kappa_1}{D} \tag{3.4}$$

$$Nu_1 = 3.66 + \frac{0.0668RePr(D/L)}{1 + 0.04[RePr(D/L)]^{2/3}}, \quad \begin{matrix} Re < 2300 \\ Pr \geq 5 \end{matrix} \tag{3.5}$$

$$Nu_1 = 1.86(\frac{RePr}{L/D})^{1/3}(\frac{\mu_b}{\mu_w})^{0.14}, \quad \begin{matrix} Re < 2300 \\ 0.6 < Pr < 5 \\ 0.0044 < \frac{\mu_b}{\mu_w} < 9.75 \end{matrix} \tag{3.6}$$

$$Nu_1 = \frac{(f/8)(Re - 1000)Pr}{1 + 12.7(f/8)^{1/2}(Pr^{2/3} - 1)}, \quad \begin{matrix} 3000 \leq Re \leq 5 \cdot 10^6 \\ 0.5 \leq Pr \leq 2000 \end{matrix} \tag{3.7}$$

$$f = (0.79ln(Re) - 1.64)^{-2} \tag{3.8}$$

Nomenclature for Chapter 3.5.1

Q	Rate of heat flow (W)	Nu_1	Nusselt number, forced convection [−]
α_1	Heat transfer coefficient (W/m^2·K)	D	Pipe diameter (m)
A_1	Pipe internal surface contact area (m^2)	L	Pipe length (m)
$T_{\infty,wf}$	Working fluid temperature (K)	Re	Reynolds number [−]
T_i	Temperature on pipe internal surface (K)	Pr	Prandtl number [−]
R_{WF}	Working fl. thermal resistance (K/W)	μ_b	Viscosity at fluid temperature (Pa·s)
κ_1	Working fl. thermal conductivity (W/m·K)	μ_w	Viscosity at wall temperature (Pa·s)
		f	Friction factor [−]

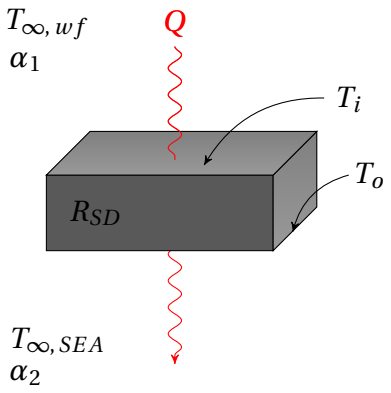

Figure 3.6: Illustration of complete heat transfer process through super duplex pipe wall.

3.5.2 Natural Convective Heat Transfer

The thermal energy is then conducted through the solid pipe wall and is eventually transferred to the surrounding sea water via natural convection, as illustrated in Figure 3.6. The expression for the resistance to convective heat transfer on the interface between super duplex and water on the outside of the pipe, R_{SEA}, can be formulated in the same way as for the inner side, here given by Equations (3.9)-(3.11).

$$Q = \alpha_2 A_2 (T_o - T_{\infty, SEA}) \tag{3.9}$$

$$R_{SEA} = \frac{1}{\alpha_2 A_2} \tag{3.10}$$

$$Q = \frac{T_o - T_{\infty, SEA}}{R_{SEA}} \tag{3.11}$$

The convection on the interface between outer pipe and the sea happens naturally, which means the expression for the Nusselt number is different from the equations given in Section 3.5.1. It is also important to distinguish between horizontal and vertical systems when analyzing natural convection, Equation (3.12) defines the heat transfer coefficient for vertical systems and Equation (3.13) defines it for horizontal systems. The Nusselt number correlation given in Equation (3.14) is suitable for horizontal cylinders (Churchill and Chu (1975a)). For reference it can be noted that for vertical systems a more accurate expression is given by Equation (3.15) (Churchill and Chu (1975b)), but since we are modeling without bends this final correlation is not used in our model.

$$\alpha_2 = Nu_2 \frac{\kappa_2}{L} \tag{3.12}$$

$$\alpha_2 = Nu_2 \frac{\kappa_2}{D} \tag{3.13}$$

$$Nu_2 = \sqrt{0.60 + 0.387(\frac{Ra}{[1+(0.559/Pr)^{9/16}]^{16/9}})^{1/6}} \tag{3.14}$$

$$Nu_2 = \sqrt{0.825 + 0.387(\frac{Ra}{[1+(0.437/Pr)^{9/16}]^{16/9}})^{1/6}} \tag{3.15}$$

Nomenclature for Chapter 3.5.2

Q	Rate of heat flow (W)
α_2	Heat transfer coefficient (W/m$^2\cdot$K)
A_2	Pipe external surface contact area (m^2)
$T_{\infty,SEA}$	Average temperature of sea (K)
T_o	Temperature on pipe external surface (K)
R_{SEA}	Brine thermal resistance (K/W)
κ_2	Brine thermal conductivity (W/m$\cdot$K)
Nu_2	Nusselt number, natural convection [−]
D	Pipe diameter (m)
L	Pipe length (m)
Pr	Prandtl number [−]

3.5.3 Equivalent Thermal Resistance

To determine the equivalent thermal resistance of the system, we use the fact that the heat energy is conserved. Note that we look at the system as a whole, thus the expressions for heat flow via conduction takes into account the cylindrical geometry of pipes, which is somewhat different from when heat flow through flat plates is considered. In this regard note that the parameter inside the natural log is the fraction between outer and inner pipe radius.

$$\begin{aligned} Q &= \alpha_1 A_1 (T_{\infty,wf} - T_i) \\ &= 2\pi L k_{SD} \frac{(T_i - T_o)}{ln(\frac{r_o}{r_i})} \\ &= \alpha_2 A_2 (T_o - T_{\infty,SEA}) \end{aligned} \tag{3.16}$$

With two steps, we formulate the expressions in Equation (3.16) into terms of thermal resistance as shown by Equations (3.17)-(3.18). Since the resistances act as a series, we can calculate the equivalent thermal resistance simply by adding each individual contribution, as in Equation (3.19). Figure 3.4 visualizes how the different thermal resistances relate to each other as a series, but the figure does not illustrate how significant the different resistances are in relation to each other. For example, the resistance related to convection is often negligible in comparison to the resistance to conduction. If one decides to ignore the resistance to convection when setting up the equations, they become much easier to solve and knowledge of the temperature on the

convection interface is no longer required.

$$\begin{aligned} Q &= \frac{(T_{\infty,wf} - T_i)}{1/(\alpha_1 A_1)} \\ &= \frac{(T_i - T_o)}{ln(\frac{r_o}{r_i})/(2\pi L k_{SD})} \\ &= \frac{(T_o - T_{\infty,SEA})}{1/(\alpha_2 A_2)} \end{aligned} \tag{3.17}$$

$$\begin{aligned} Q &= \frac{T_{\infty,wf} - T_i}{R_{WF}} \\ &= \frac{T_i - T_o}{R_{SD}} \\ &= \frac{T_o - T_{\infty,SEA}}{R_{SEA}} \end{aligned} \tag{3.18}$$

$$R_{Total} = R_{WF} + R_{SD} + R_{SEA} \tag{3.19}$$

$$Q = \frac{T_{\infty,WF} - T_{\infty,SEA}}{R_{Total}} \tag{3.20}$$

Chapter 4

Numerical Results

4.1 Tordis Raw Power Potential Variation with Time

The estimates from the raw power potential simulation over time have been made as realistic as possible by using the Excel sheet 20170402_NCS_Production_Data.xls as prepared by Prof. Milan Stanko, which summarizes production data from fields on the NCS. Table 4.1 contain the mol percentages used to represent the composition of the fluid produced from Tordis and compositional changes over time has been accounted for with a recombinational procedure to match the field GOR and WC for each iteration of the simulation. Aspen HYSYS estimated the properties of the hypotheticals based on molecular weight and density as specified in Table 4.2. It should be noted that a big disadvantage of using hypotheticals estimated this way by equation of state is that one can not be 100% certain that the PVT properties are reproduced properly unless laboratory measurements are performed. Higher accuracy would be achieved by performing a fluid characterization study to estimate binary interaction parameters that reproduce the experimental data.

As the excel sheet 20170402_NCS_Production_Data.xls contains information about monthly average GOR, WC and oil production, it was possible to perform the simulation with correct averaged monthly fluid volumes. However, HYSYS struggled to reach convergence when adjusting multiple parameters at once and in this case it was necessary to adjust both the GOR to be correct for each monthly input (one iteration) and the total amount of oil produced to match a value. Therefore, it was opted to have the volume matching done by iterating through Excel VBA in the form of two *while*-loops, and leaving GOR matching to HYSYS. Script is found in Appendix A.1.1. Once the model reaches match for both GOR and oil rate, the amount of water was calculated based on the value for average WC for that month and the actual liquid volume flow from HYSYS. The estimated amount of water was then added to and mixed with the hydrocarbon rates at wellhead conditions, before a heat energy calculation was run with $\Delta T = 50°C$

across the cooler. Note that the composition used for water was simply H_2O, and not brine.

Table 4.1: Tordis hydrocarbon composition. Data supplied by Equinor ASA.

$Nitrogen$	0.60	$mol-\%$
CO_2	0.27	$mol-\%$
$Methane$	36.61	$mol-\%$
$Ethane$	7.07	$mol-\%$
$Propane$	6.89	$mol-\%$
$i-Butane$	1.19	$mol-\%$
$n-Butane$	3.49	$mol-\%$
$i-Pentane$	1.28	$mol-\%$
$n-Pentane$	1.79	$mol-\%$
$n-Hexane$	2.46	$mol-\%$
$n-Heptane$	3.65	$mol-\%$
$n-Octane$	4.27	$mol-\%$
$n-Nonane$	2.73	$mol-\%$
$C10-C12$	6.46	$mol-\%$
$C13-C15$	4.95	$mol-\%$
$C16-C18$	3.80	$mol-\%$
$C19-C22$	3.73	$mol-\%$
$C23-C25$	2.05	$mol-\%$
$C26-C30$	2.41	$mol-\%$
$C31-C36$	1.79	$mol-\%$
$C37-C46$	1.50	$mol-\%$
$C47-C80$	1.01	$mol-\%$

Table 4.2: Tordis hypothetical components properties estimated in Aspen HYSYS based on molecular weight and density.

				Critical Properties			
Hypothetical	**Molecular Weight**	**Density [kg/m^3]**	**Normal Boiling Pt [°C]**	**Temperature [°C]**	**Pressure [kPa]**	**Volume [m^3/kgmole]**	**Acentricity**
C10-C12	146.56	799.40	181.78	373.60	2442.35	0.557	0.406
C13-C15	189.44	825.30	231.65	423.42	2106.41	0.675	0.495
C16-C18	235.83	846.00	286.52	473.90	1766.39	0.832	0.608
C19-C22	281.98	865.80	334.87	517.69	1535.98	0.978	0.713
C23-C25	330.56	882.90	380.80	557.86	1346.96	1.128	0.822
C26-C30	385.36	899.00	428.48	598.32	1175.94	1.295	0.943
C31-C36	461.50	917.90	489.96	649.20	988.25	1.524	1.111
C37-C46	567.19	939.80	569.59	713.69	788.60	1.839	1.344
C47-C80	783.00	974.50	721.35	834.86	500.50	2.485	1.770

Table 4.3: Processing modelled as a simple three stage separator train

Wellhead Temperature	75	[°C]
Wellhead Pressure	40	[bar]
1st Stage Temperature	75	[°C]
1st Stage Pressure	40	[bar]
2nd Stage Temperature	74	[°C]
2nd Stage Pressure	31	[bar]
3rd Stage Temperature	73	[°C]
3rd Stage Pressure	10	[bar]

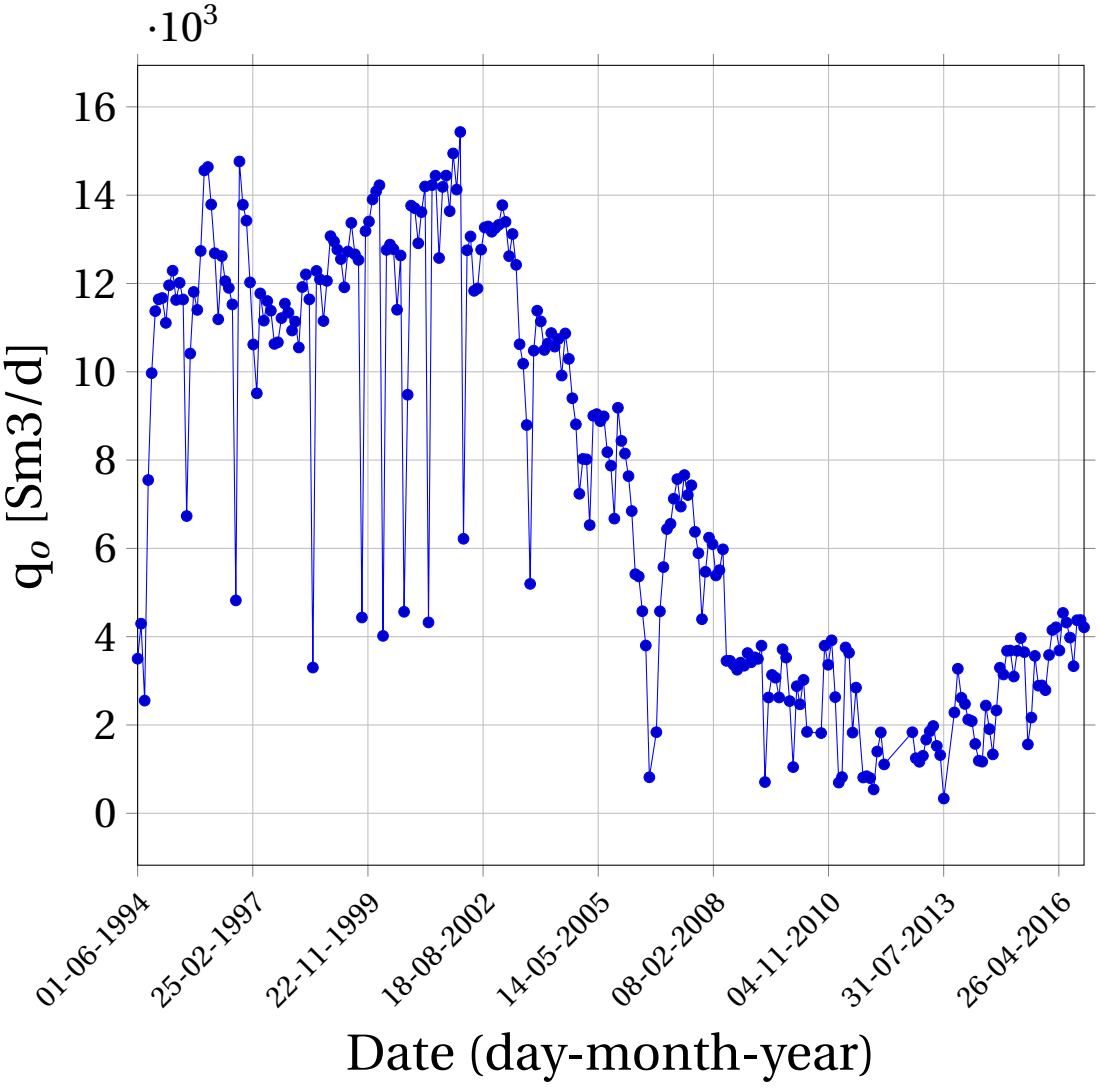

Figure 4.1: Tordis production data used as input in the raw power model.

Tordis production history plots

Figure 4.1 is a graphical representation of the rates of oil q_o that were produced from the Tordis field between start-up in 1994 and 2017. It can be seen that production was ramped up fairly quickly and plateau rates were held until approximately mid-2003. Post 2003 the oil production decreased until 2011, then slightly enhanced since 2011. Figure 4.2 displays the gas oil ratio development over the same period. It can be seen that the field gradually produced relatively larger volumes of gas as it grew older. Post 2014 the average GOR decreased slightly, from a level of around 120 Sm^3/Sm^3 to around 105 Sm^3/Sm^3. All data points are monthly averages from the public NPD database, and the reasoning behind the various outliers has not been investigated.

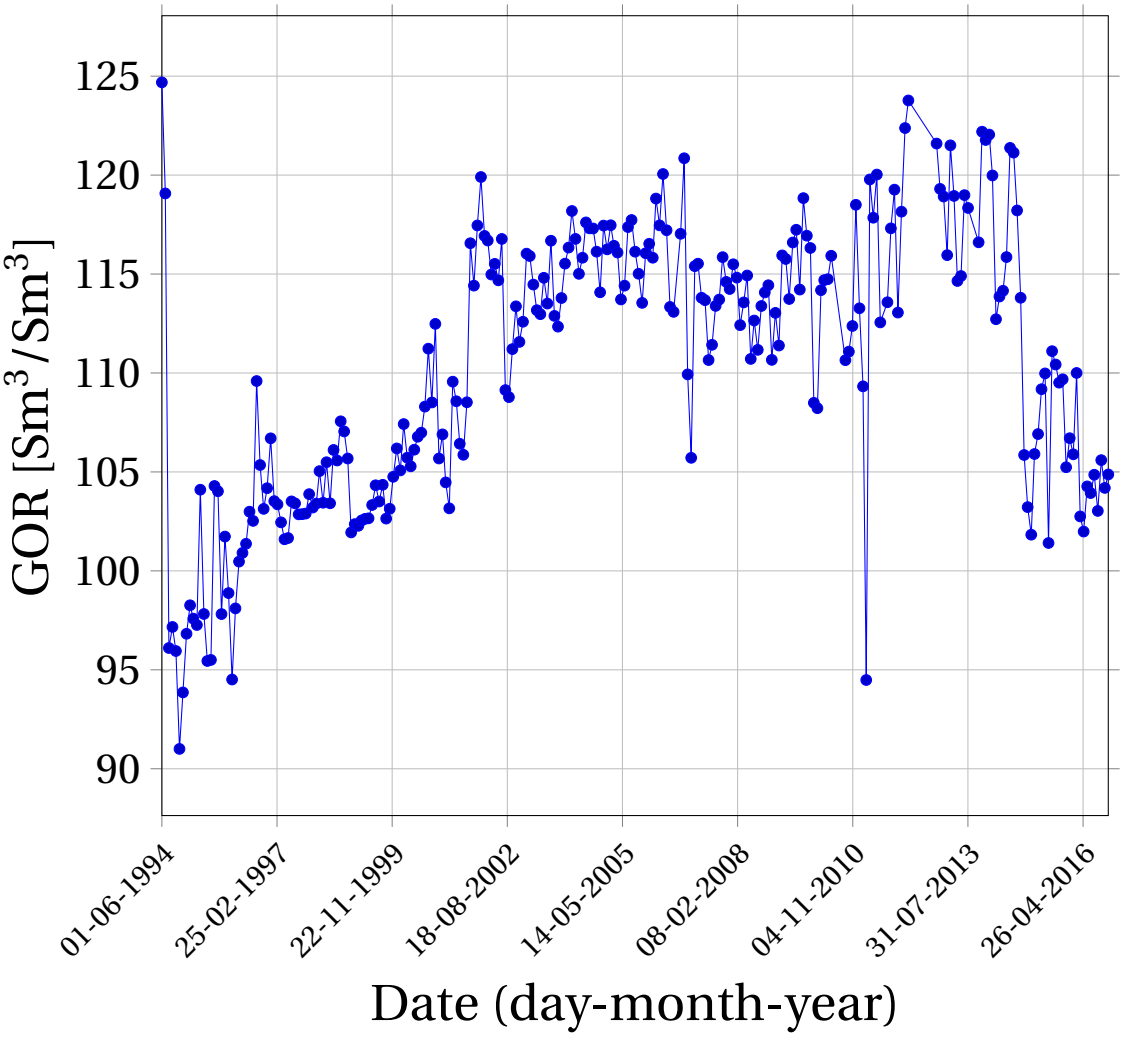

Figure 4.2: Tordis GOR data used as input in the raw power model.

Tordis water production history plot

Figure 4.3 show the water cut of the fluids produced from the Tordis reservoir from 1994 to 2017. It is clearly seen that water influx started at the end of 1999, around 5 years after initial opening of the wells at the field for production. The water cut has generally shown to be increasing over time, but some months have had lower water production. As in the previous plots, the data is monthly averages of the field production as a whole from the public available database. The (few) WC anomalies have not been investigated, and are likely an effect of varying the rates from available wells due to the reservoir production strategy. From the plot it can be seen that the field produced with around 70% WC early 2017, which is lower than some other fields at NCS that are in a similar post plateau-tail production decline stage.

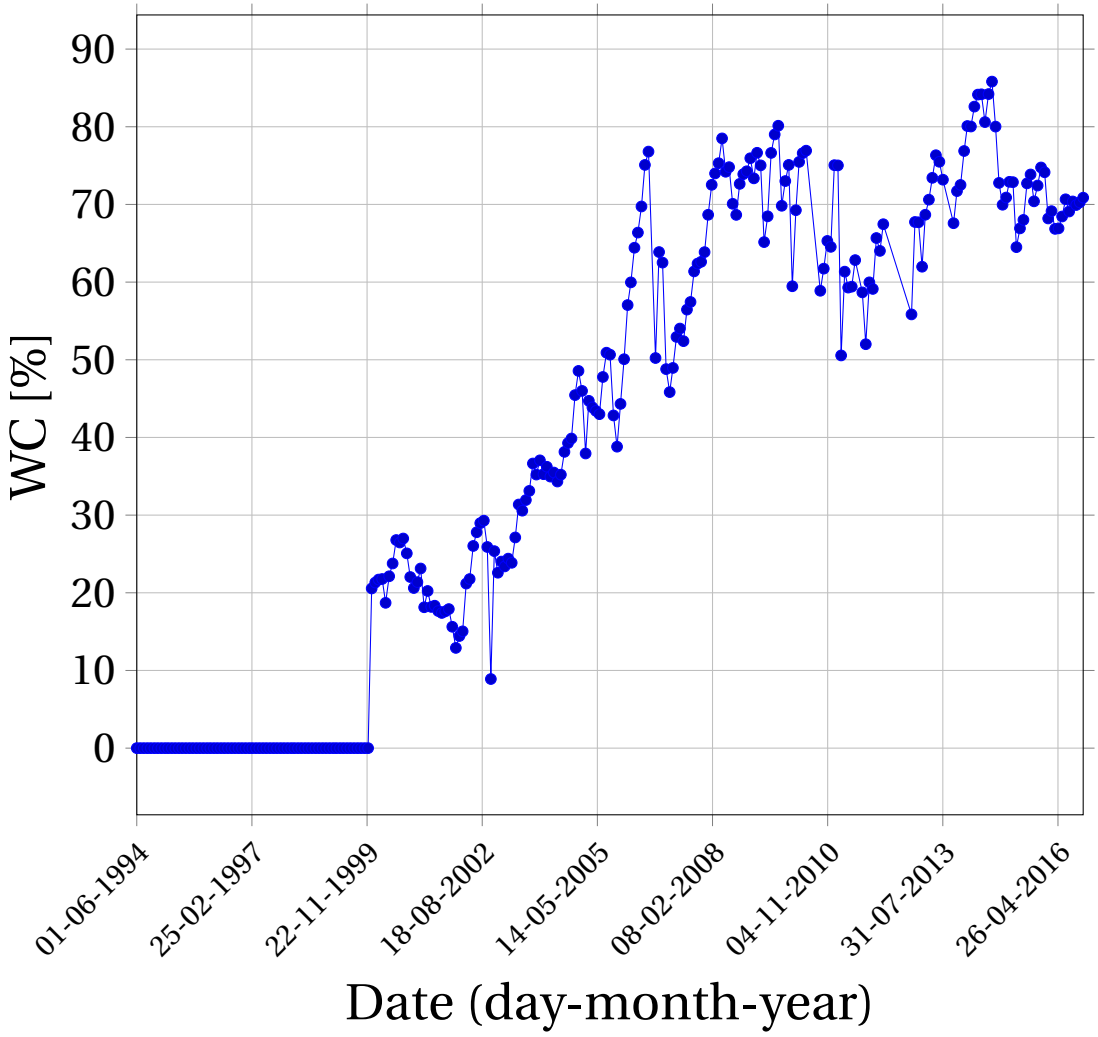

Figure 4.3: Tordis WC data used as input in the raw power model.

Tordis raw power potential plotted as function of time

In Figure 4.4 the Tordis raw power potential from June-1994 to December-2016 with $\Delta T = 50°C$ has been plotted. It is evident that the resulting data set has very scattered points, which is an implication of the production history taken from NPD (and used as model input) being scattered as well, as seen in Figure 4.1. After November-1999 a big increase in thermal potential is seen, this is not surprising as influx of brine into the production stream happens at that time, as shown in Figure 4.3.

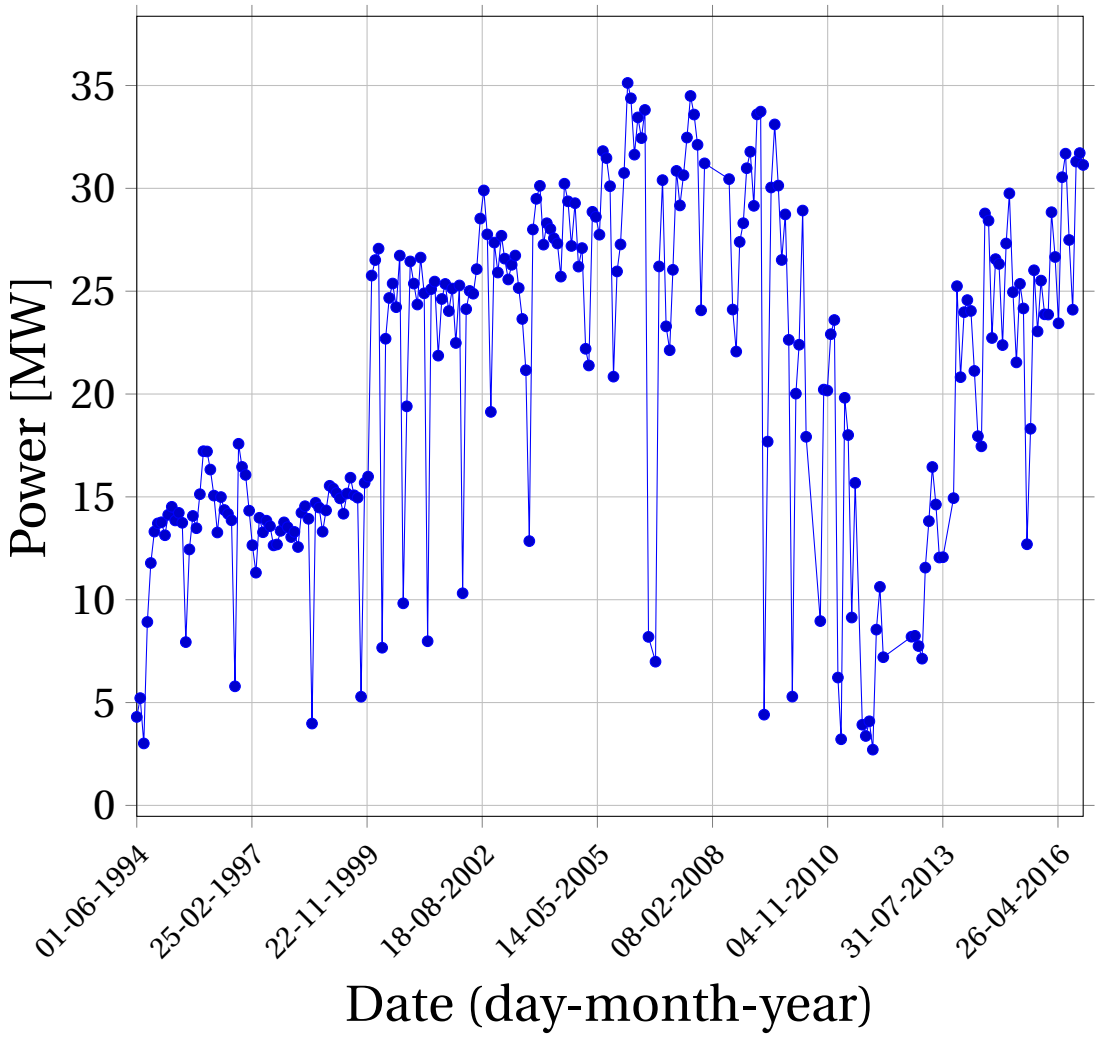

Figure 4.4: Raw heat potential of Tordis field, taking into account actual composition, WC, GOR and production. Assumed temperature drop of $\Delta T = 50°C$ of the produced fluids, $P_{WH} = 40$ bar, $T_{WH} = 75°C$ and the separation processing shown in Table 4.3.

4.2 Comparing Oil and Gas Producers

Since the enthalpy is a function of temperature in any fluid stream, a good way to compare liquid and gas based systems is simply to estimate the heat potential at different temperatures and check the trends. In present time Midgard and Tordis produce at very similar mass rates, both being around 200 kg/s. Therefore, it is opted to perform a sensitivity analysis on how the raw power relate to the wellhead temperatures when the mass rates are equalized. In Table 4.4 the saturated Midgard composition is found, with the estimates for the corresponding hypotheticals listed in Table 4.5.

Table 4.4: Midgard saturated hydrocarbon composition. Data supplied by Equinor ASA

$Water$	0.690	$mol-\%$
$Nitrogen$	0.676	$mol-\%$
CO_2	0.790	$mol-\%$
$Methane$	82.497	$mol-\%$
$Ethane$	8.662	$mol-\%$
$Propane$	3.189	$mol-\%$
$i-Butane$	0.540	$mol-\%$
$n-Butane$	0.927	$mol-\%$
$i-Pentane$	0.287	$mol-\%$
$n-Pentane$	0.311	$mol-\%$
$n-Hexane$	0.325	$mol-\%$
$n-Heptane$	0.395	$mol-\%$
$n-Octane$	0.390	$mol-\%$
$n-Nonane$	0.166	$mol-\%$
$C10-C12$	0.095	$mol-\%$
$C13-C14$	0.028	$mol-\%$
$C15-C16$	0.015	$mol-\%$
$C17-C19$	0.010	$mol-\%$
$C20-C22$	0.004	$mol-\%$
$C23-C25$	0.002	$mol-\%$
$C26-C30$	0.001	$mol-\%$
$C31-C38$	0.000	$mol-\%$
$C39-C80$	0.000	$mol-\%$

Table 4.5: Midgard hypothetical components properties estimated in Aspen HYSYS based on molecular weight and density.

				Critical Properties			
Hypothetical	**Molecular Weight**	**Density [kg/m3]**	**Normal Boiling Pt [°C]**	**Temperature [°C]**	**Pressure [kPa]**	**Volume [m3/kgmole]**	**Acentricity**
C10-C12	178.97	145.81	804.81	372.84	25.17	0.542	0.394
C13-C14	221.77	181.33	825.07	415.27	22.03	0.643	0.472
C15-C16	259.99	212.28	837.70	450.32	19.32	0.750	0.550
C17-C19	299.66	248.14	849.90	485.35	16.90	0.874	0.638
C20-C22	341.08	289.22	863.84	521.48	14.82	1.010	0.733
C23-C25	379.05	330.34	875.51	553.55	13.14	1.145	0.827
C26-C30	425.45	384.70	888.61	591.66	11.35	1.323	0.950
C31-C38	493.29	471.16	906.10	645.88	9.164	1.604	1.144
C39-C80	628.75	662.46	936.20	751.22	5.947	2.223	1.566

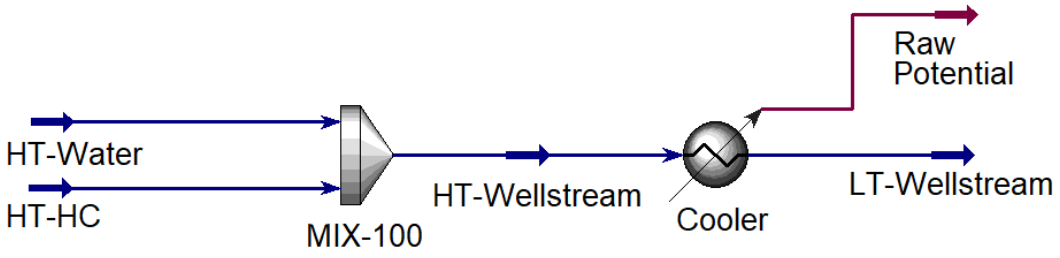

Figure 4.5: HYSYS snapshot of simple cooler model used to calculate raw power potential.

Raw Power Potential dependence of WHT

Figure 4.6 show how the raw potential from Tordis wellstream and regular water increases linearly with increased wellhead temperature. The Midgard discovery at the Åsgard field produces with very high vapor fraction and it is seen that its raw potential is not directly proportional to WHT. The data is generated from simulating the wellstreams in Aspen HYSYS as a simple cooling system with 3 bara pressure drop tube side, and show that the Tordis raw thermal potential is around 44 MW at 75°C WHT (at the specified outlet temperature) while Midgard only has around 30 MW. A snapshot of the HYSYS portion of the model used to generate the curves is shown in Figure 4.5

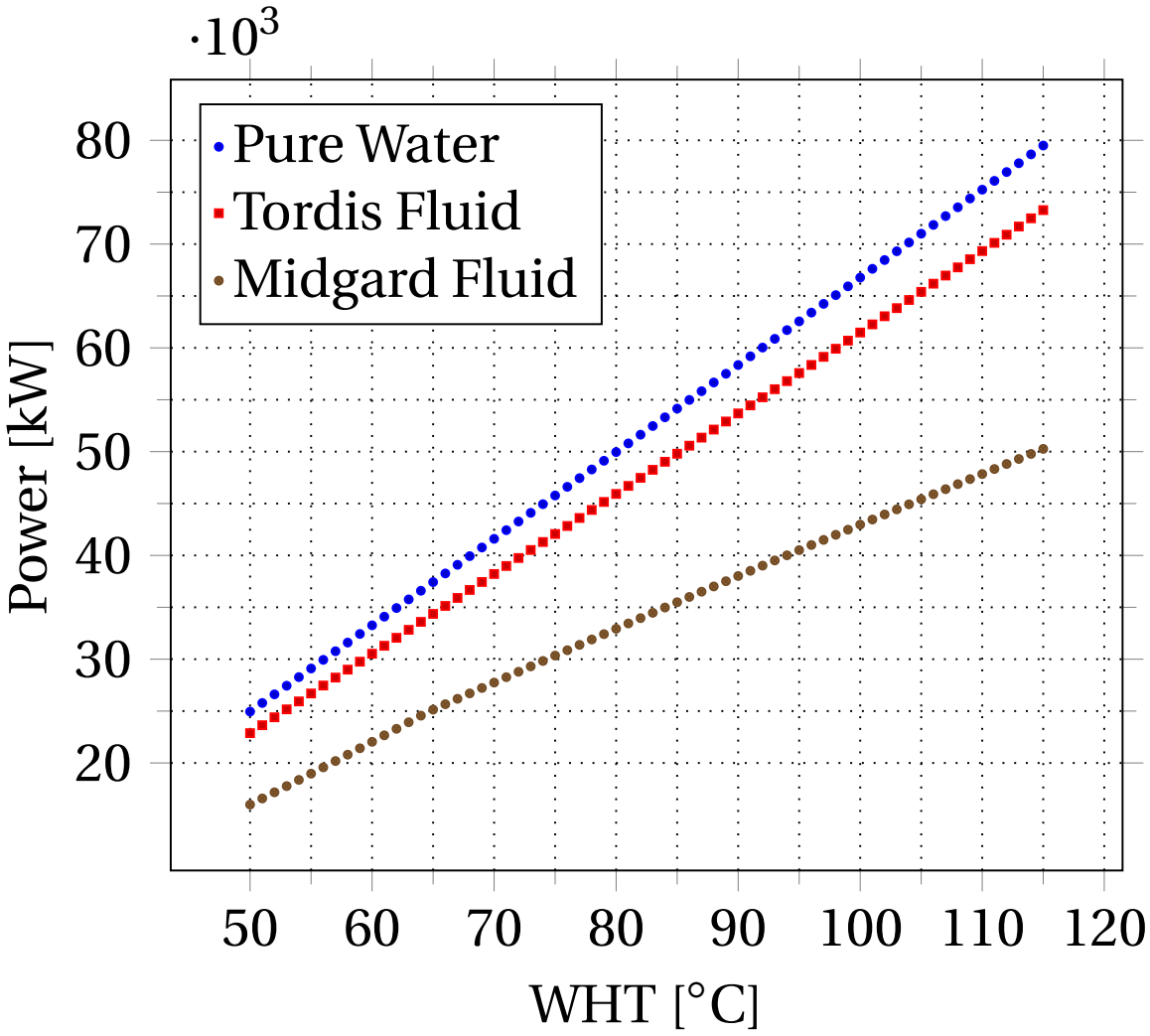

Figure 4.6: Raw power potential versus cycle inlet temperature when outlet temperature is fixed at 20°C and total production kept at 192.5 kg/s for all cases.

4.3 General ORC Working Fluid Screening

Figure 4.7 shows how R134a, butane, pentane and hexane performs as working fluids based on the assumptions mentioned in Section 3.3 and the thermal efficiencies of the corresponding cycles are plotted in Figure 4.8. Butane and R134a performs best but also requires higher cycle pressures in order to work, as can be seen in Figure 4.9. Potential working fluids that would only converge with net power output towards the end of the evaluated temperature range or not at all, as for example R245fa, was removed from the screening process.

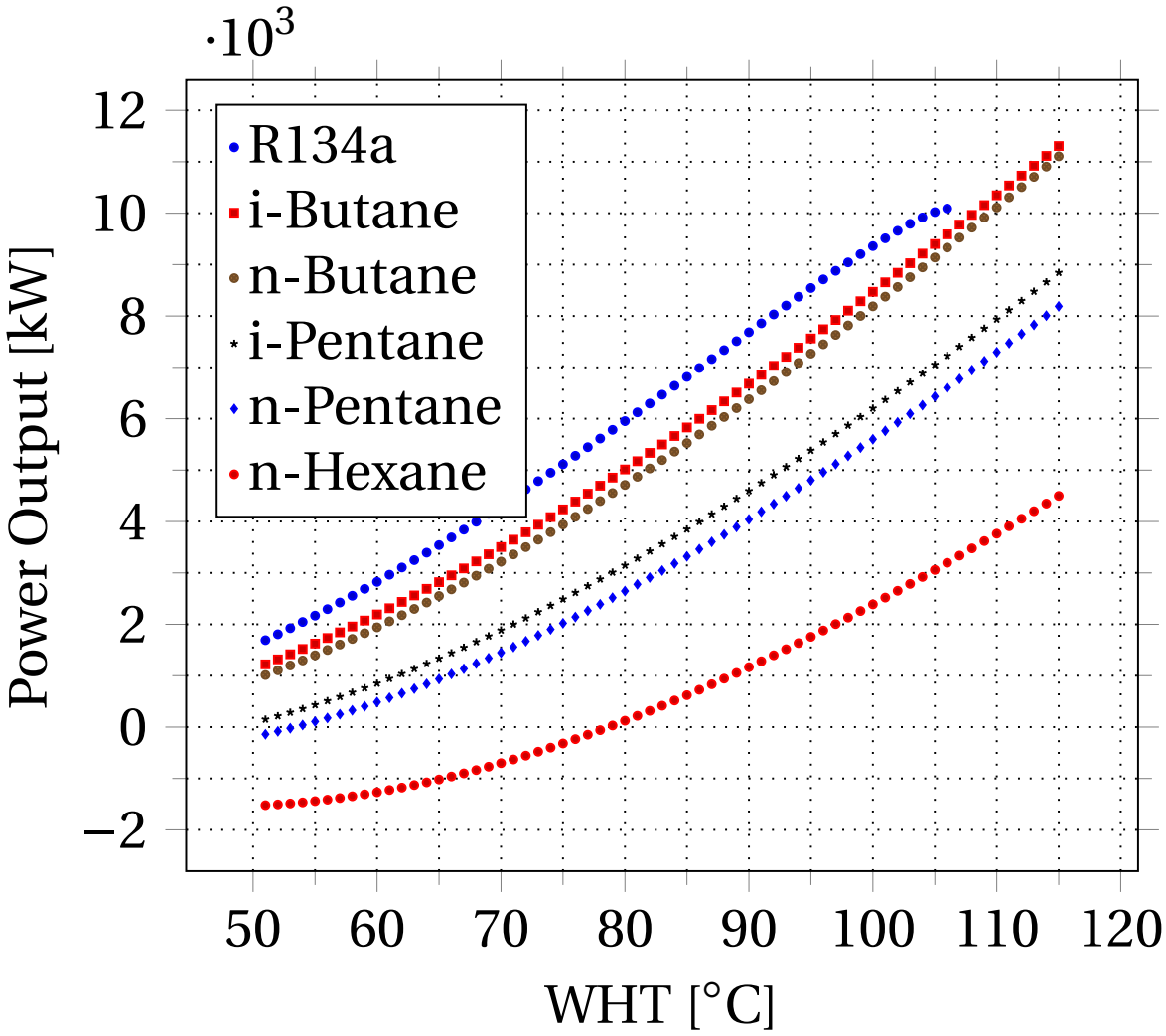

Figure 4.7: Net power output versus wellhead temperature, data produced in Aspen. R134a experienced turbine exhaust vapor fraction drop after 105°C.

Thermal efficiency plotted as function of wellhead temperature

The thermal efficiency of using R134a as cycle working fluid was very good at low wellhead temperatures but showed to drop once the temperature got higher, as seen in Figure 4.8. The butanes performed with high thermal efficiency for the entire examined temperature interval compared to the other fluids.

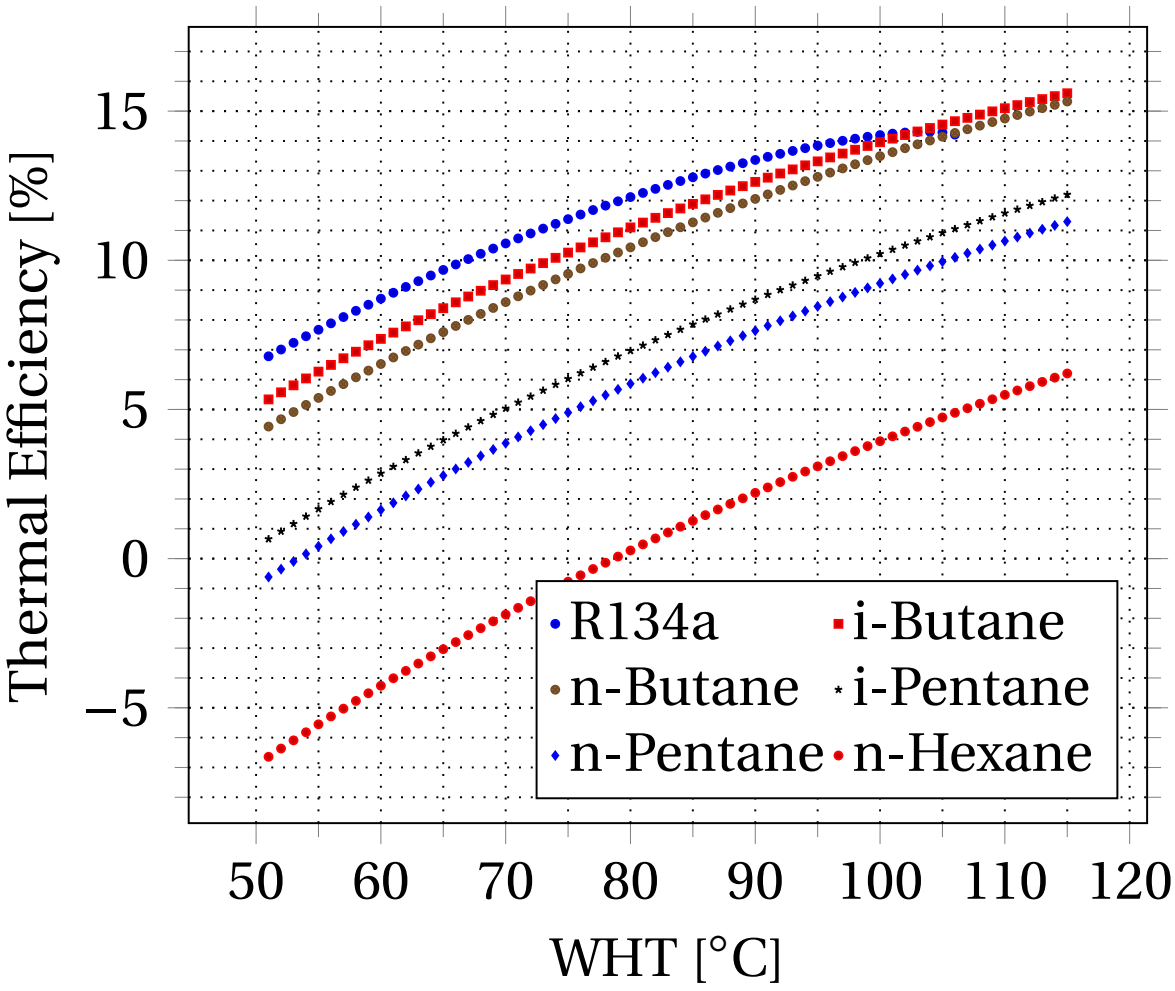

Figure 4.8: Cycle thermal efficiency versus wellhead temperature, data produced in Aspen.

Expander inlet pressure plotted as function of wellhead temperature

When simulating cycles using heavier working fluids it was found that for these fluids less pressure at expander inlet is possible since a large pressure ratio across the turbine would eventually lead to condensation inside the expander. The effect is clearly seen in Figure 4.9 with butanes and pentanes pressures being hugely different when reacting to the same cycle constraints.

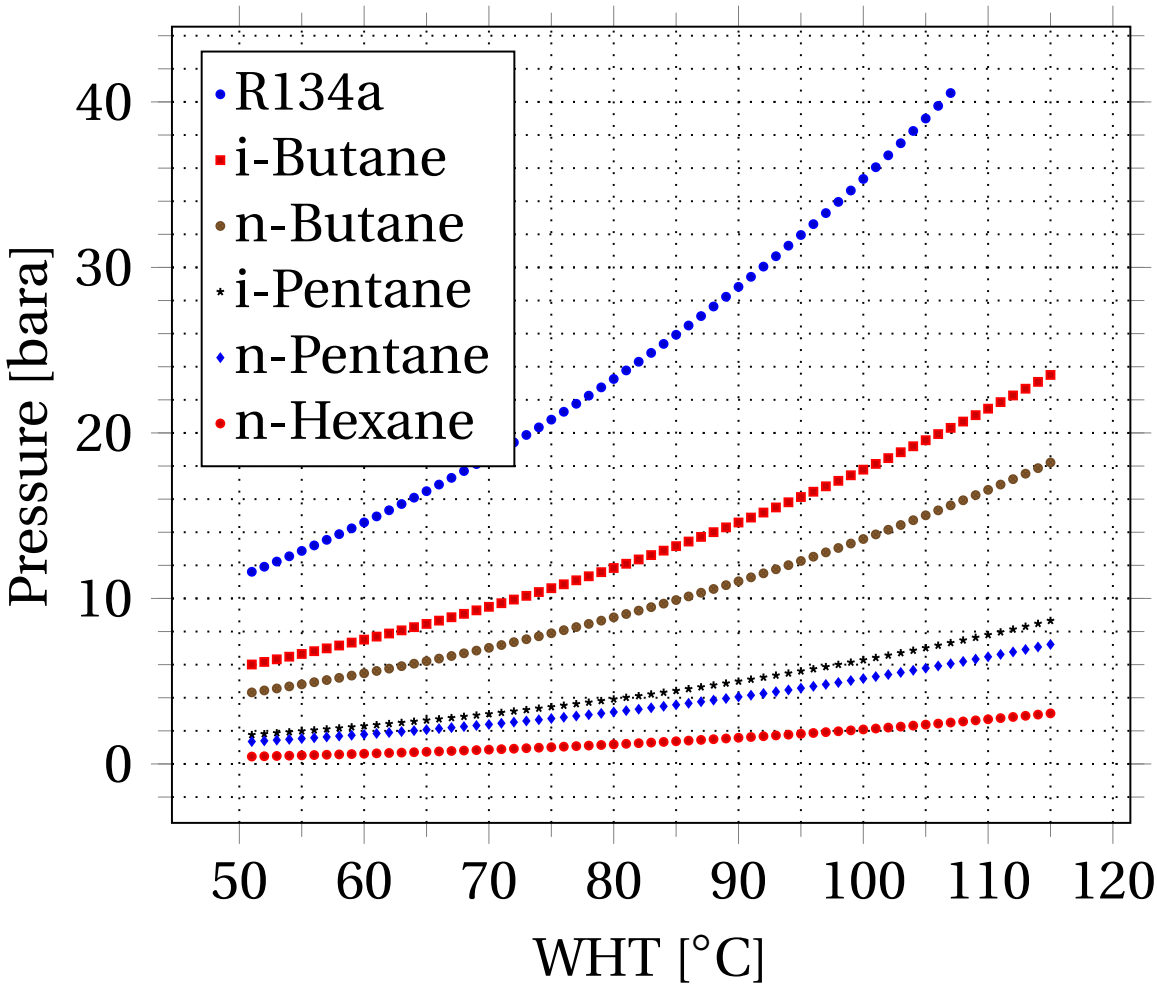

Figure 4.9: Expander inlet pressure versus wellhead temperature, data produced in Aspen.

4.4 Subsea ORC Working Fluid Screening

A subsea cycle operates under higher natural pressure than other cycles due to the sea water level. This means that the working fluids that are usually proposed for low temperature organic Rankine cycles may not be suitable for operation, and that the potential for using lighter fluids should be evaluated. It is also clear that selecting a fluid with low environmental risk is very important, since a leak of the working fluid would directly pollute the ocean. Therefore, we opt to evaluate light natural gases that are naturally present in the Tordis reservoir composition as working fluids, since they are most easily accessible and involve less environmental harm potential. Figure 4.10 shows phase curves for the fluids methane, ethane, propane, iso-butane and CO_2. Extra tick marks has been added to show where the cycle is expected to operate, especially important since a subsea design is more constrained pressure wise than one topside. The natural pressure at 250 meters depth is around 26 bars. The first observation from Figure 4.10 is that methane tends to stay in gaseous state for the entire operating range, and is therefore not well suited for application in a sub-critical cycle. CO_2 and ethane are in gaseous state at natural pressure and 14°C, but can be compressed into liquid state by adding relatively few bars of pressure. Propane is in liquid state at this temperature with a large pressure margin and stays liquid when heated to 70°C at natural pressure. Iso-butane is even less suited for operation than propane because of its tendency to stay liquid for the entire operating range.

Since it is observed that CO_2 and ethane are plausible choices as working fluids which both require a highly pressurized system, a simulation has been run to see the effect of changing the expander inlet pressure on net output potential. Figure 4.11 shows the simulation results and it should be noted that a basic ORC system model was used for this analysis as well. From the curves it is evident that while CO_2 has a slightly higher net power output peak, it requires 40 bar higher expander inlet pressure to achieve it. Ethane is therefore determined as the fluid with the best suited properties for ORC application in this pressure and temperature range, but since it is not perfectly suited a slight adaption of the working fluid is proposed. Figure 4.13 show phase curves of ethane, propane and a binary mix of these two hydrocarbons. By experimenting in Aspen it was found that adding 18 mol-% of propane to ethane would yield a binary fluid that requires much less added pressure to condense compared to pure ethane. In addition, the resulting fluid has its critical point only at a slightly higher temperature and would still allow the binary mixture to stay in gaseous state at very high pressures when the working temperature is 70°C.

Phase diagram of potential working fluids subsea

Figure 4.10 show the phase curves of the five lightest fluids naturally occurring in the Tordis wellstream. Fluids with such low density is often considered as non-condensable gases because they require very high pressures to go into liquid state, which means fluids like Methane or CO_2 are generally not considered as potential working fluids in sub-critical ORCs. The one advantage with a *subsea* ORC application is that the seabed ambient pressures are very high, potentially making it possible to run a thermodynamic cycle using light weight working fluids, such as these. The subsea ambient at the Tordis wellheads is around 26 bars of pressure and around 5-9°C temperature. With red dotted lines the operating condition restrictions are shown in the figure, the minimum cycle pressure should be above 26 bars and the working fluid will cycle between minimum 14°C to a maximum temperature of approximately 70°C. The diagram was made to get an overview over how the gases react to the operating conditions to see which are better suited.

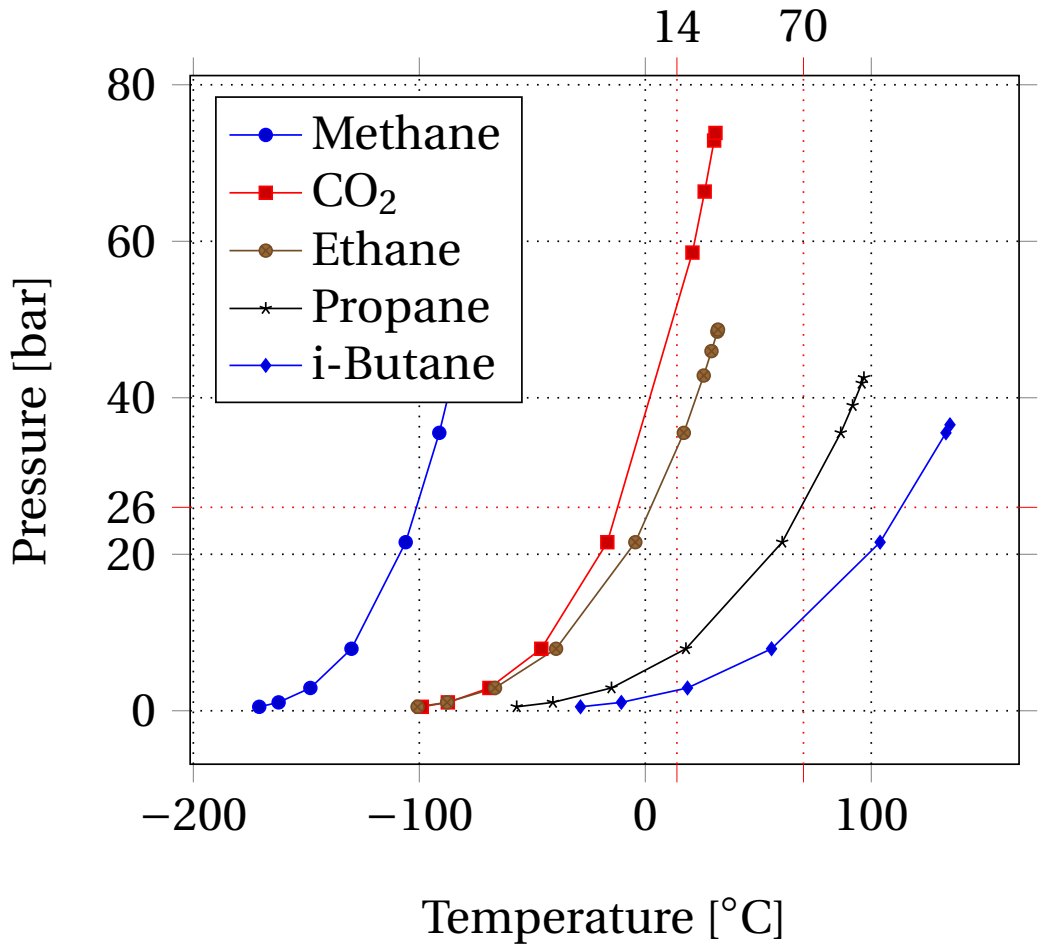

Figure 4.10: Phase diagram. Natural pressure is around 26 bar where the subsea ORC operates inside temperature interval 14 - 70°C.

Expander inlet pressure effect on performance sensitivity plot

Figure 4.11 show how increasing the cycle maximum pressure, which correspond to the expander inlet pressure, affects the calculation of net power output from the unit. The analysis was performed for two different working fluids, ethane and CO_2, and the script given in Appendix B.1.4 was used to iterate through all the pressure states. Both fluids peak at around 3 MW net power output, with CO_2 giving a slightly higher output at the expense of requiring 40 bars higher cycle maximum pressure. The figure underpins how the choice of working fluid directly affects the selection of other ORC components. For example, using CO_2 will require a more powerful pump that can boost the working fluid from the ambient to 111 bars, while using ethane would require a lesser rated pump for boosting to 71 bars.

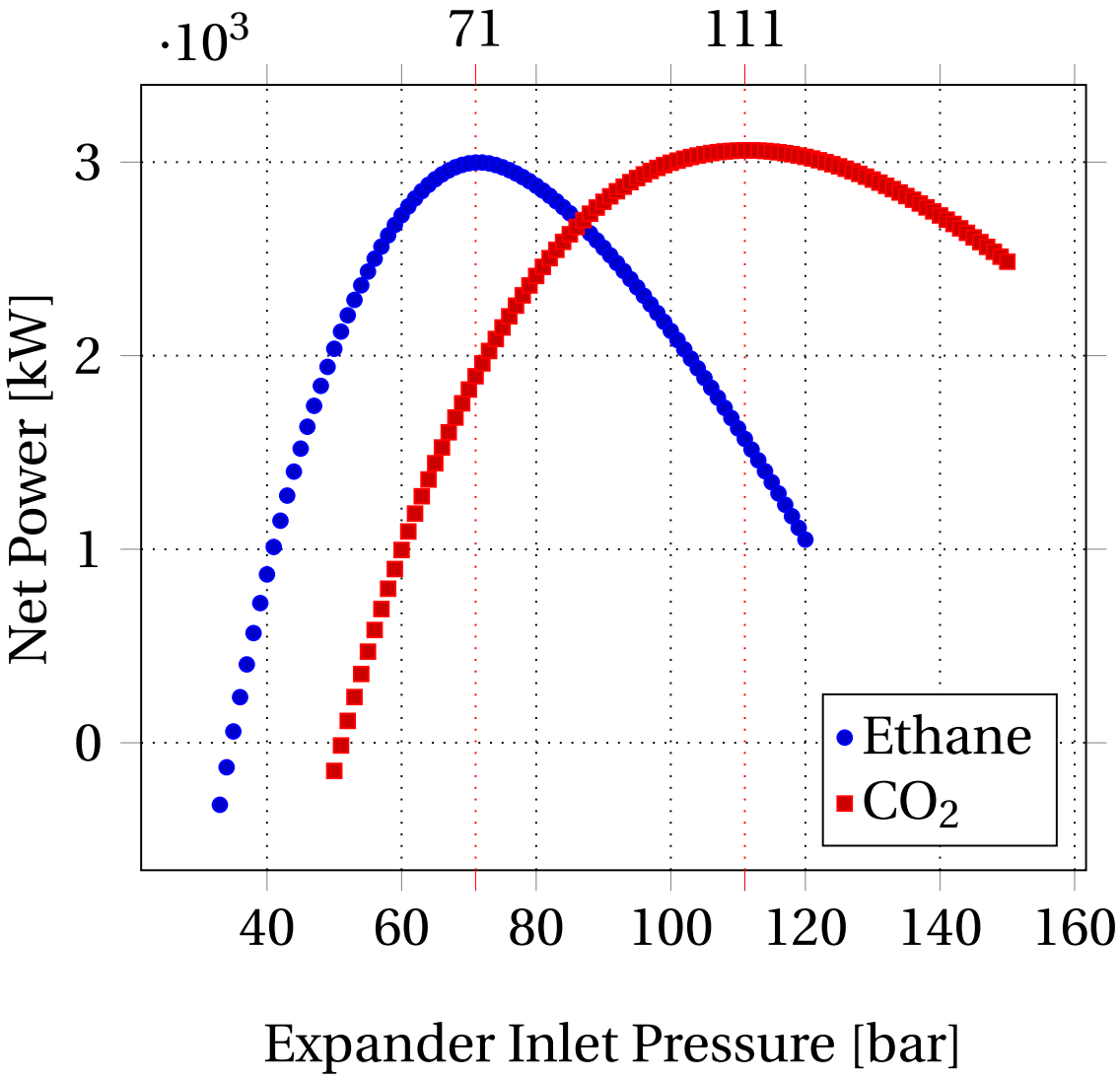

Figure 4.11: Effect of increasing the highest cycle pressure point. After peak liquid droplets are seen in the expander outlet.

Expander inlet pressure effect on performance plotted for binary mixtures

Figure 4.12 show a similar sensitivity analysis as the previous, in this case use of two binary mixes based on ethane as working fluids. In red color the results from blending ethane with 10 mol-% of CO_2 is shown, and by comparing it with the results for pure ethane in blue it is seen that the net output is decreased by a small amount and the maximum pressure is increased. When propane is used instead of CO_2 as a component of the binary working fluid (brown curve) it is seen that the maximum net output is lowered in this case as well, but the pressure maximum is also decreased. It was seen that increasing the mol-% of propane in the binary fluid will lower the required pump duty and continuously decrease the cycle potential. In this sensitivity no special bound was defined for the cycle minimum pressure and before final selection of working fluid such a restriction must be imposed.

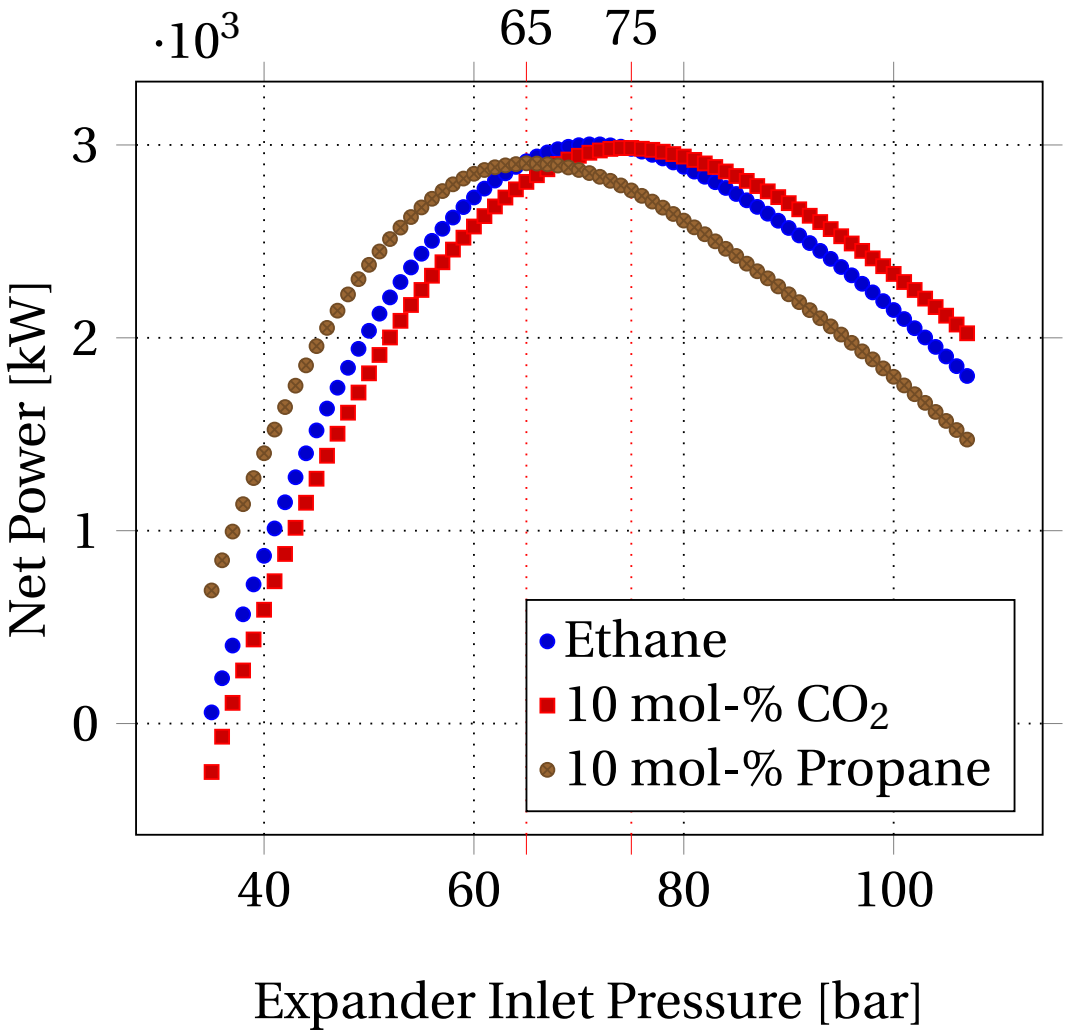

Figure 4.12: Effect on net power output of blending 10 mol-% CO2 and propane with ethane, plotted versus expander inlet pressure.

Bubble- and dew point lines of binary working fluid mixture

Figure 4.13 is a PT-phase diagram where the phase curves of ethane, propane and a binary mix of the two is plotted. The composition of the binary fluid is 82 mol-% ethane and 18 mol-% propane, and it can be seen that this composition has the bubble point line cross through the point of 26 bar and 14°C. This means that if the cycle minimum pressure at condenser outlet has these conditions, the working fluid will be in a saturated liquid state. When selecting the final working fluid for the subsea cycle it is therefore recommended to use a binary mix with maximum 18 mol-% propane, as any higher amount would inconvenience the condensation and evaporation processes. For example, look to the phase curve for pure propane. Here it is seen that at 14°C the fluid is in liquid state at subsea ambient pressures and it barely starts to evaporate when the temperature is increased to 70°C. Considering that the pressure level is boosted at evaporator outlet, the fluid needs to display a steeper curve within the cycle operating interval. It should be noted that using less than 18 mol-% propane will imply a higher minimum pressure in the cycle in order to condense the working fluid to zero vapor fraction before it is boosted through the centrifugal pump.

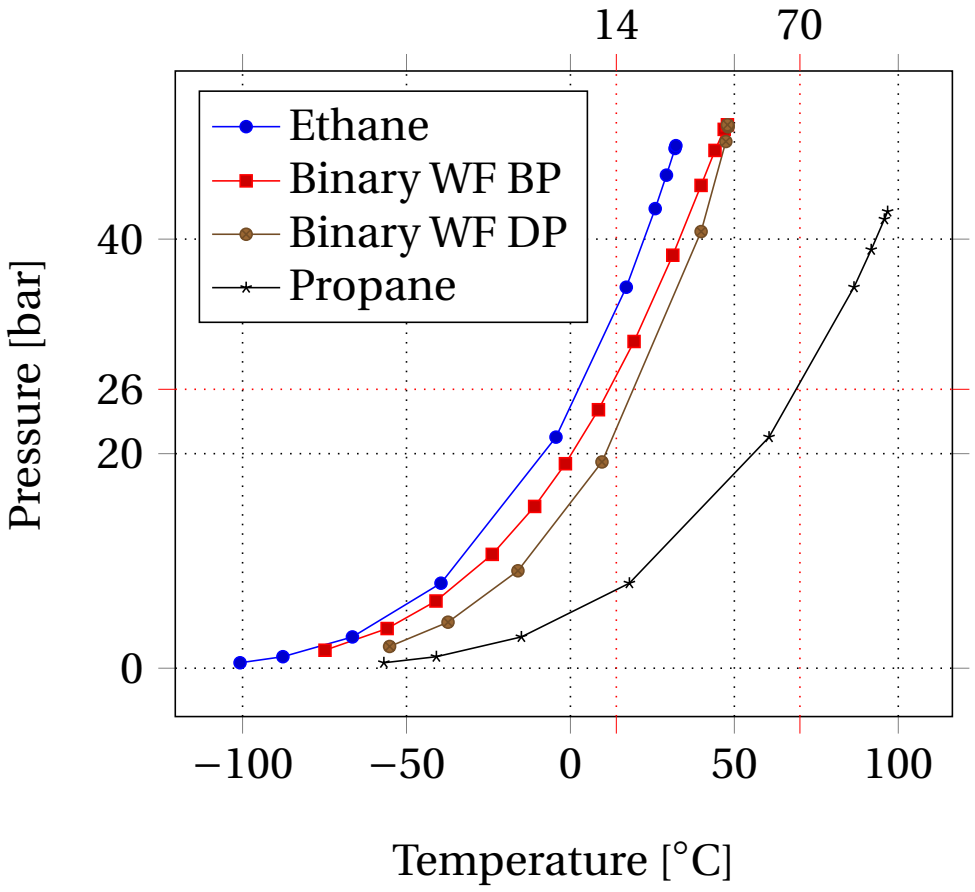

Figure 4.13: Phase diagram. 18 mol-% propane mixed with ethane.

4.5 Subsea ORC Operating Conditions

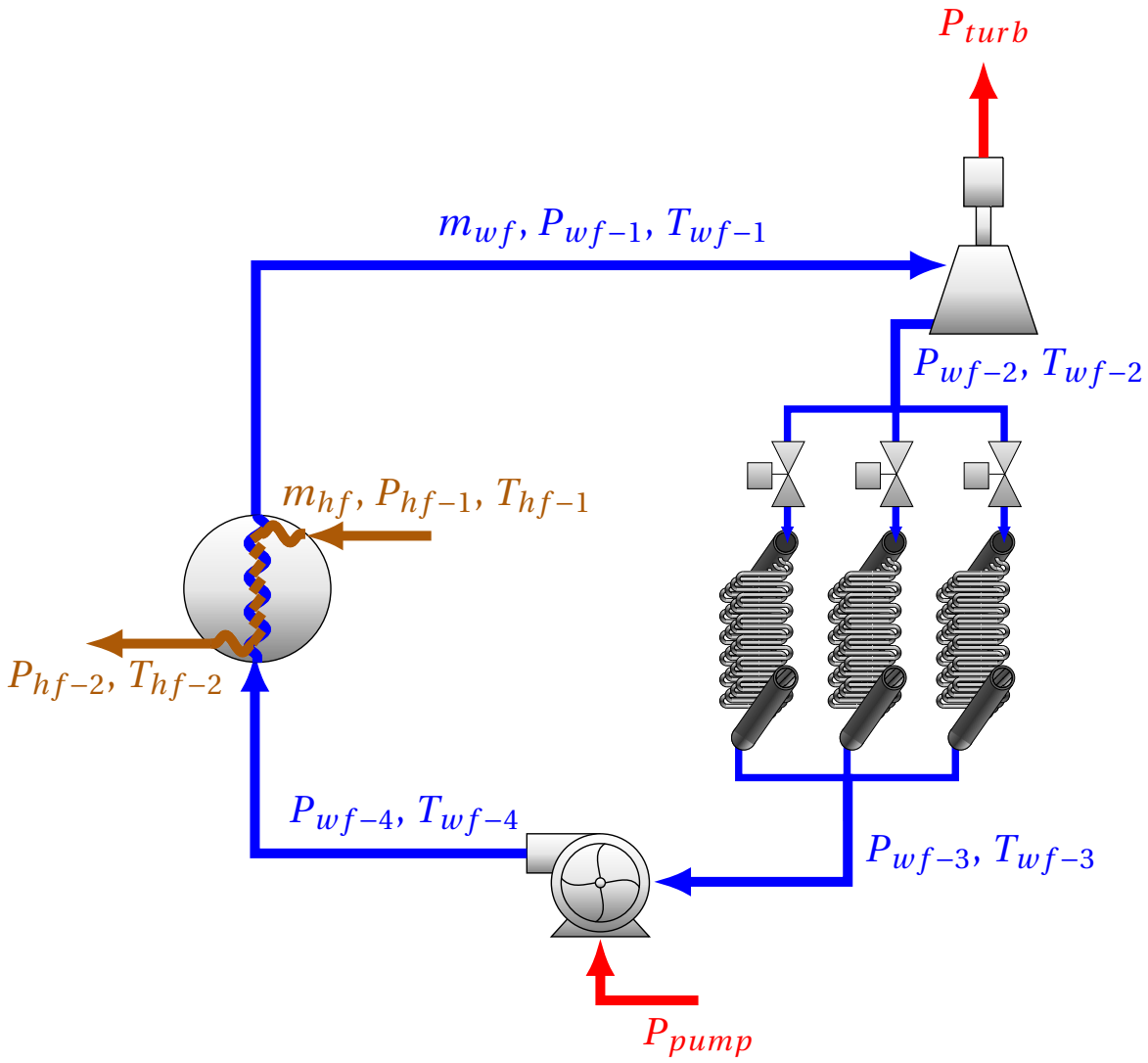

Figure 4.14: The operating conditions of the evaluated subsea binary cycle are listed in Table 4.6.

According to Toffolo et al. (2014) an ORC should be modeled based on the following four key decision parameters. The maximum pressure of the cycle, the flow rate of the working fluid, degree of superheat and condensation pressure. An ORC placed subsea will however be even more restricted in many ways, the cycle minimum pressure would for example be especially important. It were necessary to perform the design of an optimal cycle working condition based on the literal bounds of the Tordis wellstream in combination with some realistic assumptions and limitations. The design has to address the following two main concerns. The first concern is that the wellstream represents a low enthalpy heat source due to its relatively low WH temperature and mass rate, meaning heat has to be efficiently transferred to the cycle working fluid

Table 4.6: Operating conditions for a ORC configuration as shown in Figure 4.14 based on the selected binary working fluid and subsea pressure and temperature conditions.

Parameter	**Operating condition**	**[Unit]**
Working fluid mass flowrate, m_{wf}	81.0	[kg/s]
Expander inlet pressure, P_{wf-1}	63.8	[bar]
Expander inlet temperature, T_{wf-1}	70.8	[°C]
Expander outlet pressure, P_{wf-2}	31.0	[bar]
Expander outlet temperature, T_{wf-2}	22.0	[°C]
Cooling manifold outlet pressure, P_{wf-3}	30.0	[bar]
Cooling manifold outlet temperature, T_{wf-3}	14.4	[°C]
Pump outlet pressure, P_{wf-4}	65.0	[bar]
Pump outlet temperature, T_{wf-4}	21.7	[°C]
Wellstream mass flowrate, m_{hf}	192.5	[kg/s]
Wellstream inlet pressure, P_{hf-1}	40.0	[bar]
Wellstream inlet temperature, T_{hf-1}	75.0	[°C]
Wellstream outlet pressure, P_{hf-2}	37.4	[bar]
Wellstream outlet temperature, T_{hf-1}	44.7	[°C]

unless production is significantly increased. The second big concern that limits the cycle design freedom of choice is that the pressures subsea are very high, effectively limiting the amount of attractive working fluid substances. As mentioned in the annotated bibliography section of this thesis, Saleh et al. (2007) calculated thermal efficiency for a large range of working fluids suited for low temperature cycles and it was shown that the benefit of having an internal heat exchanger was usually 1% or less. For this reason, it were not opted to use IHE for this cycle evaluation as the added benefit is relatively modest. Earlier in this thesis the wellstream heat potential has been evaluated using an arbitrary value of $\Delta T = 50$°C, but at this point it were necessary to calculate the potential heat transfer using a real shell and tube heat exchanger and the chosen working fluid. In the PT-diagram in Figure 4.13 it were shown how the bubble point line of a ethane and 18 mol% propane crosses the 26 bar and 14 °C point, meaning this blend could run a cycle with natural pressure as minimum pressure and 5°C cooling pitch. It is not optimal to be restrained to having natural pressure as minimum pressure, therefore a binary working fluid of ethane and 10 mol% propane were used for actual cycle calculation, because it allows for a higher cycle pressure minimum by a slight shift of the fluid mix phase curve. The binary fluid composition and the Tordis wellstream conditions were used as input for the evaporator shell and tube heat exchanger calculation, and a realistic heat transfer of 23.3 MW were estimated. This heat exchange put the wellstream outlet temperature to 44.78 °C, meaning a real $\Delta T = 75 - 44.78 = 30.22$°C. The evaporator heat exchanger calculation is summarized with results in Section 4.7. In order to maximize the thermal efficiency of the cycle it were opted to

use a passive cooling manifold to avoid the duty that having an extra pump for a S&T cooler would require. The passive cooling system would be required to transfer 21.8 MW worth of heat, effectively condensing working fluid gas at 22°C to sub-cooled liquid at 14.45 °C. The efficiencies related to individual equipment were defined based on common assumptions used when ORCs are modeled. It is common to use a turbine with 85% isentropic efficiency, and a pump operating at 80% isentropic efficiency. The mechanical efficiency of turbine is expected to be very high and is therefore kept at 100% in this analysis. Additional common assumptions are also to model the ORC with superheating, subcooling and pinch point approximately equal to 5°C and less than 1 bar shell-side pressure drops in the heat exchangers, and these premises are true also for the model presented here. Table 4.6 lists a summary of the chosen operating conditions, but it should be noted that a slightly more efficient cycle is possible by reducing the minimum pressure level from 30 bars towards natural pressure because a lesser duty would be required from the pump.

4.6 Design Standards and Cycle Control Requirements

In a real application of a subsea ORC the operating conditions will not be steady state, which means that the cycle has to have a system for both supervision and control, which as a main purpose is used to ensure that the production of electricity is maximized at all times. This section lists the main controllers in addition to PT-gauges which are necessary from an output optimization perspective and also informs on relevant physical requirements based on the *Process system design* NORSOK standard. This review over the different necessary control elements is split into two subsections, shell and tube heat exchangers in the first and rotating equipment in the other.

4.6.1 Subsea Heat Exchangers

The content in that follows will be based on the NORSOK P-002 (2014) requirements for heaters and coolers operating on the NCS. The shell and tube heat exchangers should be designed so that both sides can withstand the maximum design temperature, it should also be ensured that the temperature is kept at a level where hydrates and wax does not deposit. As an example, this means that the tube side of the cooler in a subsea ORC should at least be rated for the temperature of the working fluid at shell-side inlet and vice versa. If the heat exchanger is in an oil train, such as the evaporator in the ORC is, it is required that it is designed with all realistic flow rates and temperatures in mind. Once the heat exchanger area is determined it should be added excess area to the design to account for fouling, which is referred to as *design margin*. The requirement for the design margin is different in every case, and recommendations can be found

at The Tubular Exchanger Manufacturers Association, Inc. (TEMA) for specific applications. In cases where it is opted to use a different type of heat exchanger the engineers are referred to NORSOK R-002 for recommendations. It is also required that nozzles are installed onto or in close proximity to the heat exchanger, so that it can be flushed with chemicals for cleaning purposes. A check valve or shut down valve can be installed upstream the S&T exchanger in case of leakage or some kind of internal rupture, this is to minimize chances for contamination through back flow into the side of lowest pressure. In cases where the shell side fluid is cycled with a very high rate it is a possibility for vibration of the tubes inside the shell, therefore it must be taken into account in the exchanger design that such vibrations shall not occur to the extent where the apparatus may be damaged. When it comes to thermal optimization, a main actuator of the cycle is a bypass valve that will be used to control the vapor fraction entering the evaporator. The Tordis field produces a small amount of gas which is contained in the wellstream that is channelled tube side with the oil in the evaporator. The bypass valve can then be used to let a certain amount of gas and possibly condensate to be routed past the evaporator system, and that way the engineers can control the evaporator pressure with high accuracy.

4.6.2 Subsea Pump and Turbine

The NORSOK standard does not include many special requirements for submerged pumps or turbines in general, it is mainly the engineers job to select units that are rated for the realistic operating conditions. For sub-cooled liquids and in relation to the discharge flow lines it is stated that the pipe dimension should be designed with the centrifugal pump in mind, such that the pressure drop will be a maximum of 0.25 bar per 100 meters of line. If a reciprocating pump is used, the flow line sizing should be determined based on recommendations by ISO 13703. When it comes to the thermal optimization of the ORC, the pump functions as another main actuator because working fluid mass rate entering the evaporator can be directly controlled through the pump speed. In practice this means that the pump is key for controlling the temperature (degree of superheat) at evaporator outlet and expander inlet. A thing to think about when doing the turbine design is to consider if the produced electricity from the ORC should match the Norwegian power socket. Since the standard voltage in Norway is 230 V and the standard frequency is 50 Hz this means that the rotational speed of the rotor has to be 3000 rounds per minute. It might therefore be necessary to use a gear box to equalize the speed of the generator with grid frequency. The turbine speed also has a direct effect on the energy contained in the fluid at expander outlet, and can therefore serve as another control element for cycle optimization. A final main actuator for the subsea ORC is made by installation of a by-pass valve around the turbine, which is mainly there as a safety measure. During normal cycle operation this by-pass will be closed for flow, and it is only opened in the event where working fluid condensate is registered in the expander. The by-pass valves were added to the illustration of the subsea ORC which now

shows all the main cycle control elements, as seen in Figure 4.15.

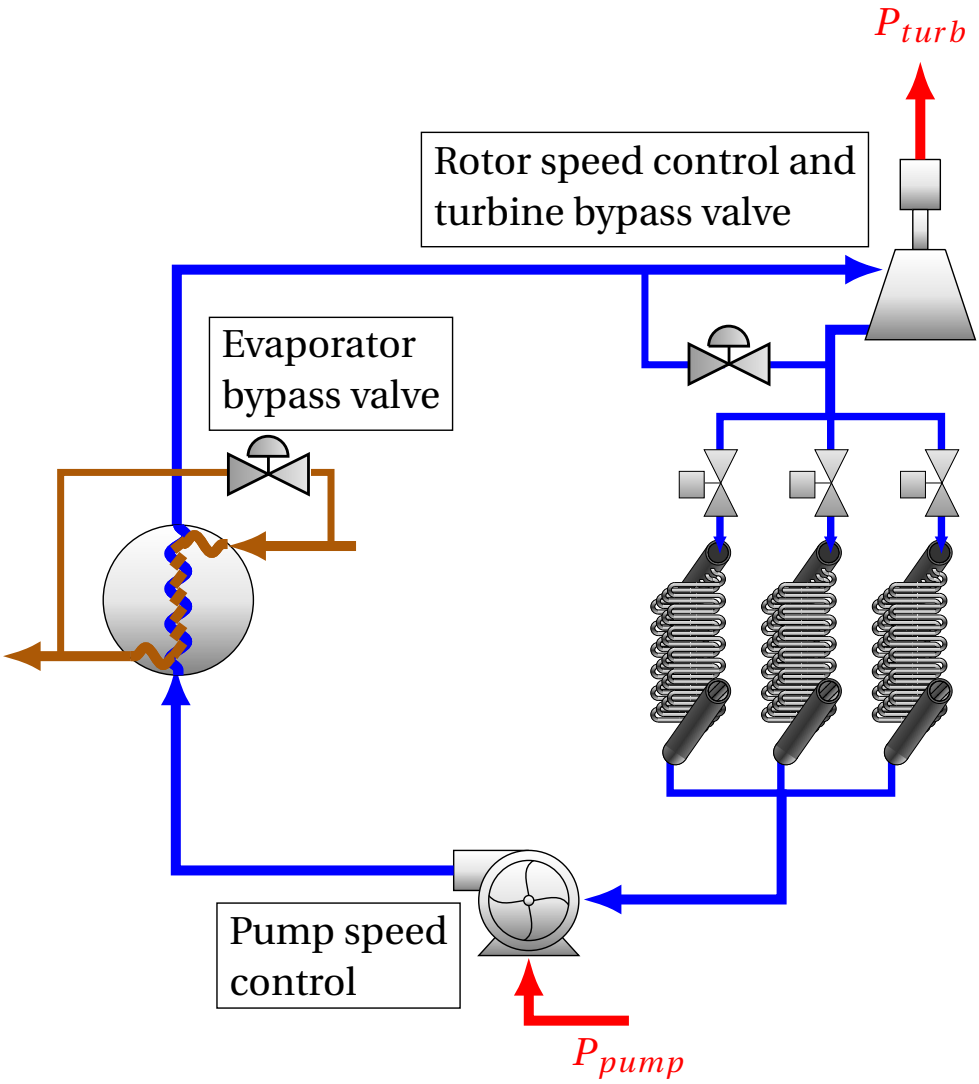

Figure 4.15: Overview over the main actuators for subsea ORC control.

4.7 Approximate Component Sizes

In order to get an idea of the necessary sizing for an ORC installed at Tordis, a rough pre-design has been made based on a subsea model. Special emphasis has been made on the design of the heating system. Note that the numbers presented for evaporator cost should be regarded as ballpark numbers which are mostly suited for financial comparison of different design options.

4.7.1 Subsea ORC Component Sizing

Results from the early evaluation of component sizes for the Tordis subsea ORC model are summarized below. Calculations have been performed based on a binary working fluid consisting of 10 mol-% propane blended with ethane. Table 4.7 show input data for the calculations based on using basic a ORC configuration without internal heat exchanger which has been fitted to have as high net power output as possible while operating as a subcritical cycle.

Table 4.7: Input data used for component size calculations made in Section 4.7.1 with a binary blend of ethane and propane as working fluid using a basic ORC configuration.

Parameter	**Simulated Value**	**[Unit]**
Working fluid type	Binary	[-]
Working fluid mass flowrate	81.0	[kg/s]
Expander inlet pressure	63.8	[bar]
Expander outlet pressure	31.0	[bar]
Expander effciency	85.0	[%]
Expander mechanical efficiency	100.0	[%]
Gross power output	2384.0	[kW]
Pump duty	283.1	[kW]
Pump efficiency	80.0	[%]
Geothermal fluid mass flowrate	192.5	[kg/s]
Geothermal fluid temperature	75.0	[°C]
Geothermal fl. exit temperature	44.78	[°C]
Net plant power	2100.9	[kW]
Thermal efficiency	9.034	[%]

The Shell and Tube Evaporator Design

For this analysis it were convenient to start by looking into a heat exchanger configuration that is not very complex to see how a simple evaporator could perform under the specified operating conditions. Therefore, all front and rear heads of the apparatus are assumed to be bolted integral covers. The shell types under main consideration are of E and F type of which E is a one-pass shell and F is a two-pass shell with a longer baffle. The tube size selected is 25.00mm outer diameter with 31.25mm pitch, which is the same size as was presented in Table 2.3 in the theory section of this thesis. It is opted to run the calculations for only a triangular tube pattern since using a square pattern mainly changes the temperature profile and not the thermal performance. It is assumed that the baffles are of the single segmental type with horizontal cut

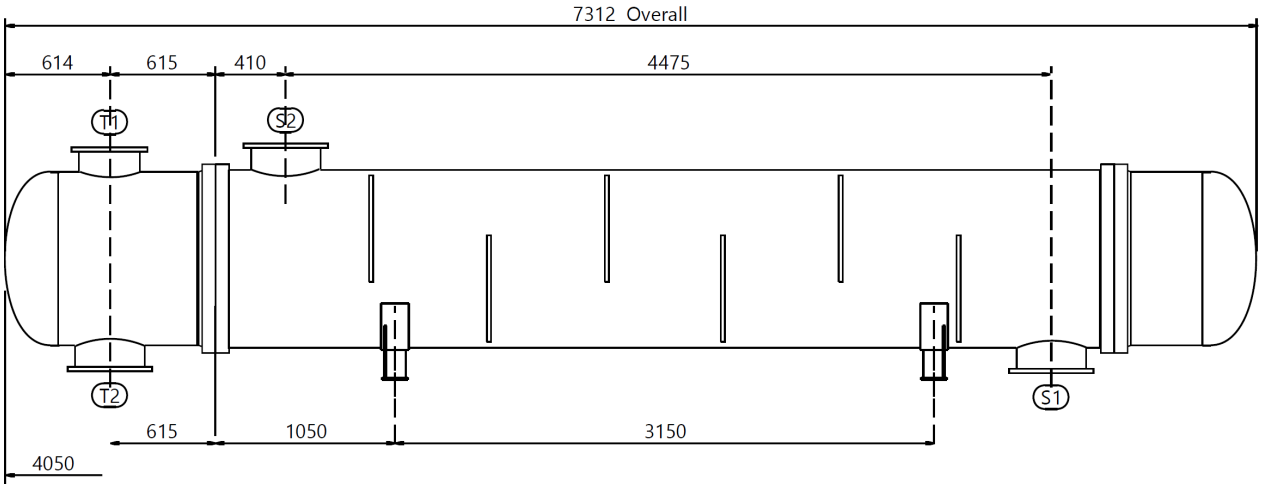

Figure 4.16: Single pass evaporator with 6 baffles seen in profile. Tubing inlet and outlet have the same spatial placement while shell side inlet and outlet are on separate sides of the exchanger. Illustration generated using Aspen EDR.

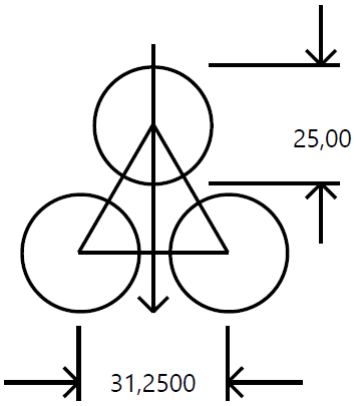

Figure 4.17: 25mm tubes with 31.25mm pitch in triangular tube pattern. Illustration generated using Aspen EDR.

Table 4.8: Assumptions made as the evaporator design basis.

Parameter	Assumption	[Unit]
TEMA Type:	BEM	
Tube OD:	25.00	[mm]
Tube pitch:	31.25	[mm]
Tube Pattern:	30-Triangular	
Tubes in baffle window:	Yes	
Baffle Type:	Single semental	
Baffle cut orientation:	Horizontal	
Exchanger material:	Carbon Steel	

Table 4.9: Proposed design based on assumptions made in Table 4.8 and thermal requirements.

Parameter	Proposed size:	[Unit]
Shell ID:	975.0	[mm]
Shell OD:	1045.0	[mm]
Tube length:	5250.0	[mm]
Baffle spacing center:	685.0	[mm]
Number of baffles:	6	[-]
Number of tubes:	700	[-]
Number of passes	2	[-]
Shells in Series	5	[-]
Shells in parallel	1	[-]
Excess surface:	0	[%]

orientation, that the fouling resistance is zero as design margin can be added at later on, and that the heat exchanger material used is carbon steel. An evaporator with E type shell is proposed as seen in Figure 4.16. The tubes are installed using the triangular tube pattern shown in Figure 4.17 and the full crossectional geometry can be seen in Appendix C.1. All the main technical assumptions made for the design is listed in Table 4.8 and Table 4.9 contain a summary of key results for the proposed exchanger geometry. Using five shells of approximately 6-meter length in series will cover the required heat transfer by installing a calculated number of 700 tubes and 6 baffles in each. This evaporator design has no estimated excess surface, which means any fouling will affect the thermal efficiency of the system. The temperature development spatially can be seen graphically from the temperature profiles plotted in Figure 4.18. As previously mentioned, the front and rear heads are assumed to be very simple in order to get the cheapest possible solution. Table 4.10 show expected prices based on the Aspen cost correlation along with a system mass estimate. The thermal performance of this design is listed in Table 4.11 and the total heat exchange were shown to be 23260.7 kW with an effective area of 1397.8 m^2.

Table 4.10: Approximate evaporator weight and cost using carbon steel as building material.

Weights	**[kg]**	**Cost approximation**	**[USD]**
Shell	5816.2	Labor	343 734
Front head	1814.3	Tube material	59 655
Rear head	1288.5	Other material	143 404
Bundle	5764.2		
Total weight - Empty	14683.0	Total (one shell)	109 359
Total weight - Water filled	19149.9	Total (all shells)	546 795

Table 4.11: Summary of thermal performance related to the proposed evaporator using a binary working fluid.

	Shell Side		**Tube Side**		
Parameter	**In**	**Out**	**In**	**Out**	**[Unit]**
Vapor mass flow rate	0	81.0	2.49	2.10	[kg/s]
Liquid mass flow rate	81.0	0	190.01	190.4	[kg/s]
Vapor mass quallity	0	1	0.01	0.01	[-]
Temperature	21.67	70.73	75.00	44.78	[°C]
Pressure	65.0	63.76	40.0	37.40	[bar]
Film coefficient	3722.2		3936.4		[W/(m²-K)]
Fouling resistance	0		0		[m²-K/W]
Pressure drop	1.237		2.601		[bar]
Total heat exchanged	23260.7				[kW]
Effective area	1397.8				[m²]
Effective mean temp. difference	9.45				[°C]

Temperature plotted as function of evaporator axial length

The expected temperature development of the working fluid and the Tordis wellstream in the heating system can be seen in Figure 4.18. The reason behind the "bend" on each wellstream segment in red is that the tube side inlets and outlets are on the same side of the shells, because the heaters are designed as dual pass exchangers.

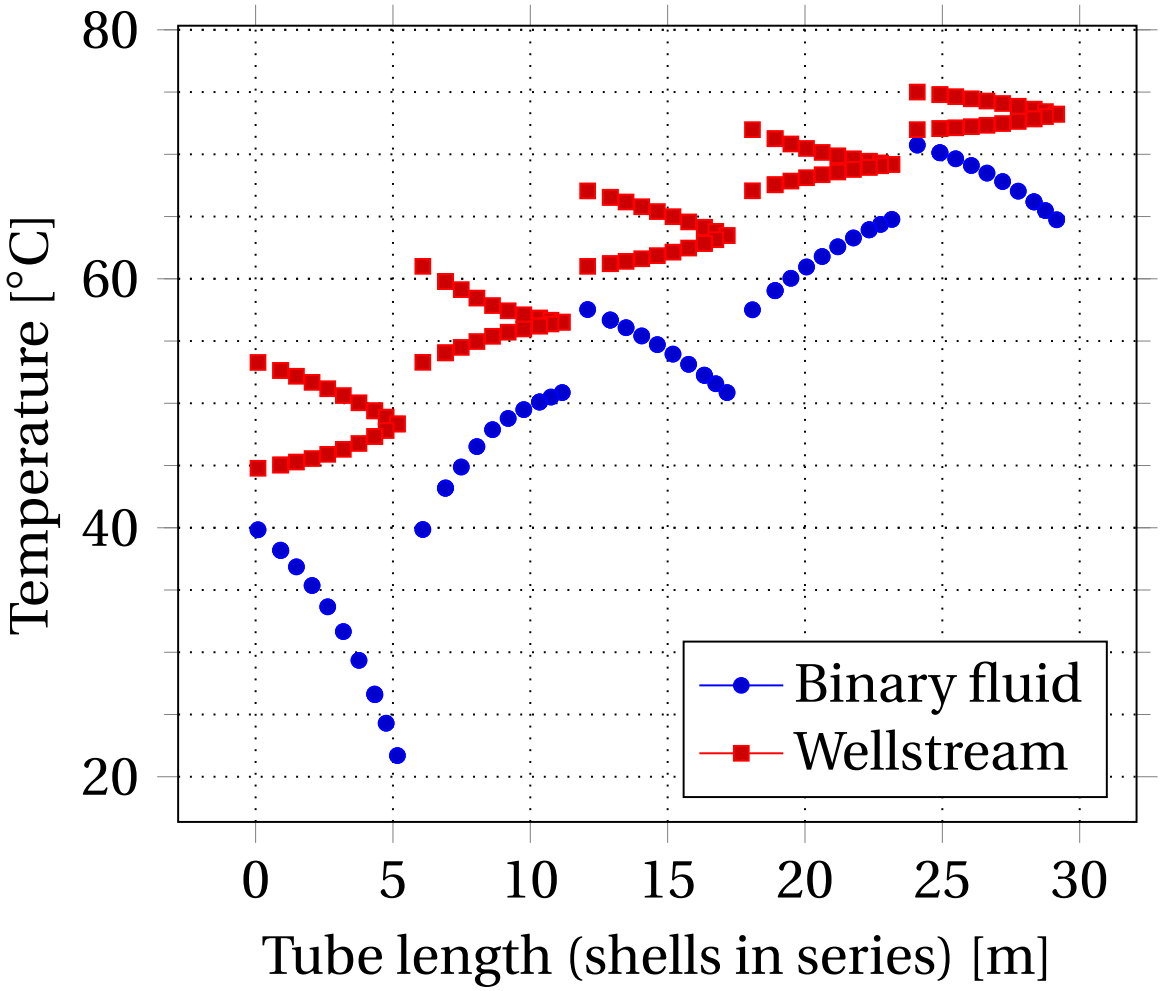

Figure 4.18: Temperature profile inside the evaporator system with shells as shown in Figure 4.16 with triangular tube pattern. Tubing inlet and outlet have the same spatial placement while shell side inlet and outlet are on separate sides of the exchanger.

Cooling System Selection

The working fluid is in gaseous state at 21.99°C and 31 bars at the expander outlet. Cooling the working fluid down to a condensed state at this pressure level and current rate requires a heat transfer of 21826.37 kW, effectively putting the working fluid down to 14.45°C at the cooling system outlet. Using an active cooling system such as a shell and tube heat exchanger is an option, but it would imply an extra duty on the system due to pumping of the coolant brine. To maximize the power output, it would seem convenient to use a passive subsea cooling system instead that utilizes the natural convection effect seen subsea.

In Section 2.3.3 the concept of using a sectioned passive cooler manifold was introduced with a short description. One of the companies providing this technology is Future Technology AS and they use their in-house software SIMCOOL as a design tool to scale their exchangers to proper sizing. Table 4.12 show the technical specification and limitations of the design and judging from the list it is clear that the passive sectioned exchanger would cover the needs of the proposed cycle. The size of the structure can not be estimated precisely at this point, but it is known that sectioned passive heat exchangers are roughly four times the size of a tube and heat exchanger with the same inlet and outlet conditions.

It is possible to make rough size approximations based on the passive cooler model presented in Section 3.5. Since the required amount of heat transfer is known in this case, the calculations can be simplified greatly if it is assumed that the inner and outer pipe walls have the same temperature as their respective mediums. The biggest reason for making the simplification is the fact that our passive cooler condenses the working fluid, which means the Kern heat transfer equations for condensation processes would have to be used in addition to the standard modelling of the sub-cooling of liquid. Because of this effect, it is opted to only calculate the amount of outer pipe area required for the super duplex solid to conduct the 21826.37 kW of heat and completely disregard the natural and forced convection that takes place in reality, effectively calculating the minimum value for required area. Using the thermal properties of the duplex alloy 2507 UNS S32750 and assuming outer pipe radius of 0.025m with 0.005m thickness for the coils, it was found that necessary outer pipe surface area is 949.9 m^2. This was done by calculating the pipe length with Equation (4.1) then multiplication with the pipe circumference based on the assumed pipe radius as in Equation (4.2). Approximate minimum cooler weight is calculated in similar manner, using Equation (4.3) for empty system and Equation (4.4) for system filled with condensate. The density of the super duplex and the working fluid condensate is respectively 7750 kg/m^3 and 385.1 kg/m^3, which means the weight of an empty system is 33.12 tonnes and condensate filled system is 36 tonnes.

Table 4.12: Technical specification of available passive cooler compared with thermal requirements of the proposed subsea thermodynamic cycle.

Technical specification	**Limitations**	**Subsea cycle**
Process inlet temperature	Up to 150°C	21.99°C
Cooling rate	Up to 50 MW	22 MW
Pressure drop	In accordance to client request	1 bar
Operating depth	Down to 2000m	250m
Scalability	High	
Controllability	5%-100%	
Material	Pipes are super duplex	
Dimensions and weight	Depends on req. cooling rate	
Control valve	Axial	
Sensors	3 Dual P&T sensors	
Design life	>25 years	

$$L_{pipe} = \frac{Q \ln(r_o/r_i)}{2\pi\kappa_{SD}(T_i - T_o)} \tag{4.1}$$

$$A_{pipe} = 2\pi r_o \times L_{pipe} \tag{4.2}$$

$$m_{pipe,e} = \rho_{SD}\pi(r_o^2 - r_i^2) \times L_{pipe} \tag{4.3}$$

$$m_{pipe,f} = m_{pipe,e} + \rho_{wf}\pi r_i^2 \times L_{pipe} \tag{4.4}$$

Basic design features of the turbine

Since thermodynamic software has been used in the ORC modeling, the energy analysis consideration is done using the computer. However, the resulting parameters from the Aspen HYSYS estimation can be used to get an idea of the basic design features of the rotating equipment. By basic design features of a turbine it is pointed to physical dimensions of the unit, required blade angles and velocity ratios of all its stages. The gas turbine can be of radial or axial type, and in this assessment it is assumed that a turbine of the axial type is selected for the subsea ORC. Referring back to the theory related to the velocity diagrams of a two-stage turbine shown in Figure 2.10, the ideal design features of an unit can be determined using the mass rate and energy state of the ORC cycle working fluid along with well-known geometric relationships.

Figure 4.19 represents the control volume used for the assessment, where mass rate and enthalpy states of the working fluid at turbine inlet and outlet is known. In this case the numerical value for enthalpy is taken directly from the thermodynamic modelling software, but it could also have been determined using a Mollier diagram and the PT conditions on either side of the unit, if the working fluid were not of binary type. It were mentioned earlier in this thesis that it is possible to design a turbine using a *velocity compounding* technique where the entire pressure drop happens in the inlet nozzle of the turbine, and assuming the turbine is of such type makes the thermodynamic analysis easier as only one working fluid expansion stage needs to be considered. Note that P_{turb} is gross power and not the cycle net power output. It is opted to perform the analysis by assuming that the working fluid expansion in the nozzle is an isentropic process and that the gross power output requirement corresponds to a isentropic efficiency at 85%. When the nozzle expansion is isentropic it essentially means that there is no friction and the working fluid entropy will be unchanged. The enthalpy after isentropic expansion of the binary working fluid (at nozzle outlet) is estimated to $h_{wf-2} = -2855$ kJ/kg by the software. This makes calculating the necessary inlet diameter of the turbine a trivial task, and we assume velocity compounding using two stages, just as was derived in the theory section of this thesis.

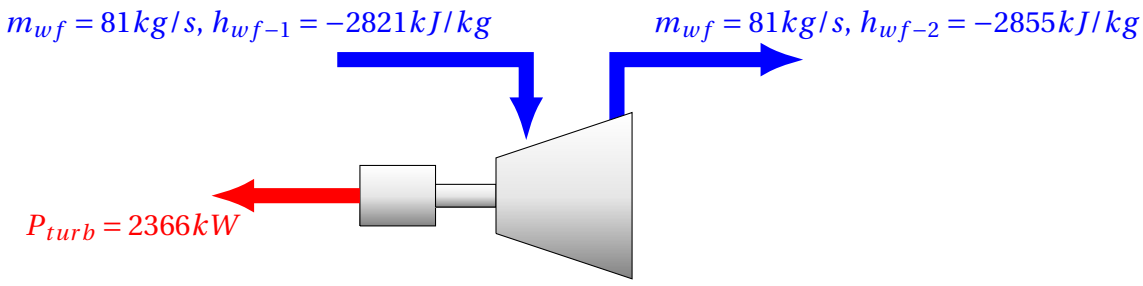

Figure 4.19: Control volume for thermodynamic analysis of the proposed subsea ORC turbine with isentropic pressure expansion.

Finding the inlet velocity of the working fluid can be done by using the energy equilibrium across the nozzle. It were explained in Section 2.3.1 that a certain amount of the energy potential exits the turbine outlet as kinetic energy proportional to $V_{out}^2/2$, and the same line of thinking can be used here to solve for the inlet velocity. Since energy is conserved, the balance can be expressed as with Equation (4.5) which states that the amount of energy before and after expansion is the same.

$$h_{wf-1} = h_{wf-2} + \frac{V_1^2}{2} \tag{4.5}$$

The equation can be solved for the working fluid velocity at the inlet V_1 by rearranging the terms as shown in Equation (4.6), please note that 1 kJ/kg = 1000 m^2/s^2 and that the V_1 label corresponds to the vector in the first stage velocity triangle diagram in Figure 4.20.

$$\begin{aligned} V_1 &= \sqrt{2h_{wf-1} - 2h_{wf-2}} \\ &= \sqrt{2(h_{wf-1} - h_{wf-2})} \\ &= \sqrt{2(-2821 \times 1000\, m^2/s^2 - -2855 \times 1000\, m^2/s^2)} \\ &= 20\sqrt{170}\, m/s \\ &= 260.8\, m/s \end{aligned} \tag{4.6}$$

It was derived earlier (see Equation (2.37)) that the highest possible gross power output for a two-stage turbine of this type would be $E = 8u^2$, where u is the blade velocity. This result is very useful because it allows for calculating the required radial size of the turbine at the nozzle. Equation (4.7) relates blade velocity to turbine gross power and working fluid mass rate, and by solving for u it is found that the blades will rotate at tip speed 65.5 m/s in the calculation shown by Equation (4.8). After determining tip speed at the nozzle, it is possible to find the length of the blades at the inlet. This is done in Equation (4.9), and it uses the fact that the standard electrical grid frequency in Norway is 50 Hz, which means the rotor should revolve at 3000 rounds per minute. It is easily shown that 3000 rounds per minute equals 314.16 radians per second, and with that figure input in the equation it were found that the optimum radius r_i at the turbine inlet to match grid frequency is 0.19 meters.

$$\begin{aligned} E_{Total} &= \frac{P_{turb}}{m_{wf}} \\ 8u^2 &= \frac{P_{turb}}{m_{wf}} \end{aligned} \tag{4.7}$$

$$
\begin{aligned}
u &= \sqrt{\frac{P_{turb}}{8 \times m_{wf}}} \\
&= \sqrt{\frac{2366 \times 1000\, W}{8 \times 81\, kg/s}} \\
&= \sqrt{\frac{2366 \times 1000\, kgm^2/s^3}{8 \times 81\, kg/s}} \\
&= \sqrt{\frac{2366 \times 1000\, kgm^2/s^3}{8 \times 81\, kg/s}} \\
&= \frac{65\sqrt{70}}{9}\, m/s \\
&= 60.4\, m/s
\end{aligned}
\tag{4.8}
$$

$$
\begin{aligned}
D_i &= 2 \times r_i = 2 \times \frac{u}{revolutions} \\
&= 2 \times \frac{60.4\, m/s}{314.16\, rad/s} \\
&= 2 \times 0.19 m
\end{aligned}
\tag{4.9}
$$

The velocity triangle method presented in Murty (2018) can be put to use for help calculating the rest of the unknowns for both stages of the turbine. The working fluid exit velocity out the turbine outlet can be determined using geometrical considerations of Figure 4.20, along with figuring out what angles are most suitable for the turbine blades. The relation shown in Equation (4.10) was derived in the theory section, and is used for solving for optimum inlet nozzle angle for maximum turbine efficiency, α_1, as seen in Equation (4.11). Note that to simplify the calculations in velocity compounding it is often assumed constant axial velocity through the turbine stages, and that assumption is true for the calculations made here as well.

$$
\frac{u}{V_1} = \frac{\sin(\alpha_1)}{4} \tag{4.10}
$$

$$
\begin{aligned}
\alpha_1 &= \arcsin \frac{4 \times u}{V_1} \\
&= \arcsin \left(\frac{4 \times 60.4\, m/s}{260.8\, m/s}\right) \\
&= 67.9^\circ
\end{aligned}
\tag{4.11}
$$

Earlier in this thesis it was shown that the maximum utilization factor for a two-stage setup such as this could be simplified to the expression $\epsilon_{Max} = \sin^2 \alpha_1$, which in this case would translate to

$\epsilon_{Max} = 0.858$. This means that 14.2% of the kinetic energy potential entering the turbine will be lost to friction, turbulence and other factors. Determining more of the required physical traits of a unit before final turbine selection could potentially prove useful. The calculated maximum utilization factor is of a typical order for an industrial turbine, and it is opted to determine the rest of the related unknowns such as optimum positioning of the blades (blade angles), fluid relative velocities and the remaining nozzle angles. Referring to Figure 4.20, the assessment starts with decomposing the first stage vectors into x- and y components in Cartesian coordinates as seen in Equations (4.12)-(4.14). In Equation (4.15) the Pythagorean theorem is used to calculate the absolute length of the relative velocity vector w, which is the relative velocity of the working fluid after contact with rotor. The value is then used to calculate the blade angle β for the first stage inlet in Equation (4.16), and it was shown that these blades should have 61.6° tilt.

$$\begin{aligned} V_{y1} &= V_1 \times \sin(\alpha_1) \\ &= 260.8\, m/s \times \sin(67.9^\circ) \\ &= 241.6\, m/s \end{aligned} \tag{4.12}$$

$$\begin{aligned} V_{x1} &= V_1 \times \cos(\alpha_1) \\ &= 260.8\, m/s \times \cos(67.9^\circ) \\ &= 98.1\, m/s = V_{x2} \end{aligned} \tag{4.13}$$

$$\begin{aligned} w_{y1} &= V_{y1} - u \\ &= 241.6\, m/s - 60.4\, m/s \\ &= 181.4\, m/s = w_{y2} \end{aligned} \tag{4.14}$$

$$\begin{aligned} w_1 &= \sqrt{w_{y1}^2 + V_{x1}^2} \\ &= \sqrt{181.4^2 + 98.1^2}\, m/s \\ &= 206.2\, m/s \end{aligned} \tag{4.15}$$

$$\begin{aligned} |\beta_1| &= \arctan\left(\frac{w_{y1}}{V_{x1}}\right) \\ &= \arctan\left(\frac{181.4\, m/s}{98.1\, m/s}\right) \\ &= 61.6^\circ = |\beta_2| \end{aligned} \tag{4.16}$$

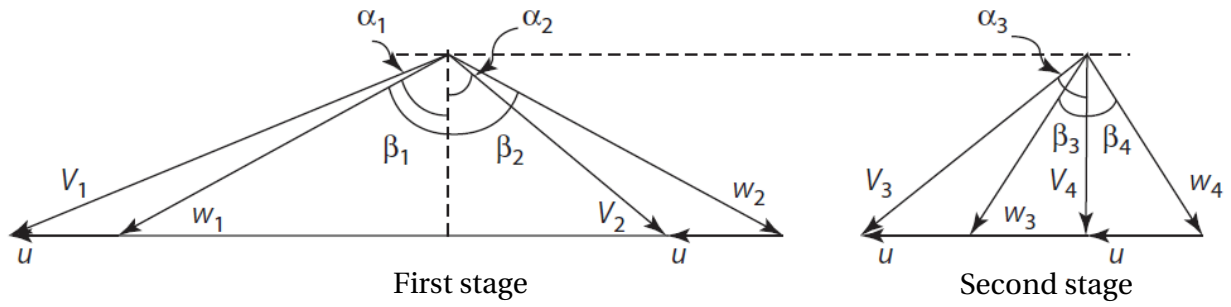

Figure 4.20: Velocity triangles for first and second stages, used for explanation of the thermodynamic analysis of the subsea ORC turbine. Figure taken from Murty (2018).

The same type of assessment is performed for the exit velocity triangle of the first stage. Using the fact that the relative velocity vectors w_1 and w_2 are of same length, it is possible to determine the y-component of the exit velocity vector V_{y2} as shown by Equation (4.17). Since the axial velocity is assumed constant through all the turbine stages, finding the exit velocity V_2 is a trivial task as seen in Equation (4.18). It should be stated that even though the velocities inside the turbine that have been calculated so far are not of particular interest by themselves, they are still direct consequences of using a geometrical design that give the most optimum utilization factor to minimize the energy state of the working fluid at turbine outlet. The most favorable exit nozzle angle of stage one α_2 was shown to be 51° by Equation (4.19).

$$\begin{aligned} V_{y2} &= w_{y2} - u \\ &= 181.4\,m/s - 60.4\,m/s \\ &= 121\,m/s \end{aligned} \tag{4.17}$$

$$\begin{aligned} V_2 &= \sqrt{V_{y2}^2 + V_{x2}^2} \\ &= \sqrt{121^2 + 98.1^2}\,m/s \\ &= 155.8\,m/s \end{aligned} \tag{4.18}$$

$$\begin{aligned} |\alpha_2| &= \arctan\left(\frac{V_{y2}}{V_{x2}}\right) \\ &= \arctan\left(\frac{121\,m/s}{98.1\,m/s}\right) \\ &= 51^\circ \end{aligned} \tag{4.19}$$

The analysis for the second stage velocity triangles is shown below, and it is solvable once the parameters related to the first stage is known. Equations (4.21)-(4.23) lists variables that has the same numeric value between the stages, and the relationship is used as shown by Equations (4.24)-(4.26) to calculate the optimum blade angles for the second stage of the turbine, which was shown to be $\beta = 31.7°$. The calculation for working fluid outlet velocity is shown in Equation (4.28) and it can be seen that the movement is almost purely in the axial direction, as it should. The flow velocity is approximated to 98.1 m/s when it is exhausted from the turbine. Equation (4.29) calculates the utilization factor as the ratio between ideal energy transfer to the rotor and the rotor drive energy plus kinetic energy (which is not utilized), and as it results to same number as before, $\epsilon_{Max} = 0.858$, it indicates that the performed calculations check out.

$$V_3 = V_2 \tag{4.20}$$

$$V_{y3} = V_{y2} \tag{4.21}$$

$$V_{x3} = V_{x2} \tag{4.22}$$

$$|\alpha_2| = |\alpha_3| \tag{4.23}$$

$$\begin{aligned} w_{y3} &= V_{y3} - u \\ &= 121\ m/s - 60.4\ m/s \\ &= 60.6\ m/s = w_{y4} \end{aligned} \tag{4.24}$$

$$\begin{aligned} w_1 &= \sqrt{V_{x3}^2 + w_{y3}^2} \\ &= \sqrt{98.1^2 + 60.6^2}\ m/s \\ &= 115.3\ m/s \end{aligned} \tag{4.25}$$

$$\begin{aligned} |\beta_3| &= \arctan\left(\frac{w_{y3}}{V_{x3}}\right) \\ &= \arctan\left(\frac{60.6\ m/s}{98.1\ m/s}\right) \\ &= 31.7° = |\beta_4| \end{aligned} \tag{4.26}$$

$$\begin{aligned} V_{y4} &= w_{y4} - u \\ &= 60.6\, m/s - 60.4\, m/s \\ &= 0.2\, m/s \approx 0 \end{aligned} \tag{4.27}$$

$$\begin{aligned} V_4 &= \sqrt{V_{y4}^2 + V_{x4}^2} \\ &= \sqrt{0.2^2 + 98.1^2}\, m/s \\ &= 98.1\, m/s \end{aligned} \tag{4.28}$$

$$\begin{aligned} \epsilon &= \frac{E_{Total}}{E_{Total} + V_4^2/2} \\ &= \frac{8u^2}{8u^2 + V_4^2/2} \\ &= \frac{8 \times 60.4^2}{8 \times 60.4^2 + 98.1^2/2} \\ &= 0.858 \end{aligned} \tag{4.29}$$

The turbine selected for the subsea ORC at Tordis needs to be tailored to maximize the utilization factor, and if it is opted to use a two-stage turbine with velocity compounding design then the final design parameters will be of similar values to what has been estimated in this section. Referring to SIEMENS (2014), an industrial ORC turbine that has standard design traits very similar to the subsea cycle requirements is the Siemens SST-060. It is known for its high reliability under tough working conditions and can produce up to 6 MW gross power. The base design is pressure rated for up to 131 bara at the inlet side and 29 bara at the outlet, so the custom unit for the Tordis ORC would have to be rated for slightly higher outlet pressure than the standard design since it will be operating subsea. A summary of the SST-060 specifications is listed in Table 4.13, and Figure 4.21 shows how the unit looks.

Table 4.13: Siemens SST-060 technical data, dimensions and general features. Information taken from SIEMENS (2014)

Power Output	<6 MW
Inlet Pressure	<131 bara
Outlet Pressure	<29 bara
Inlet Temperature	<530° C
Length	1.5 m
Width	2.5 m
Height	2.5 m
Customizable	Yes
Control valves	Yes
Suitable for ORC	Yes
Suitable for gas expansion	Yes

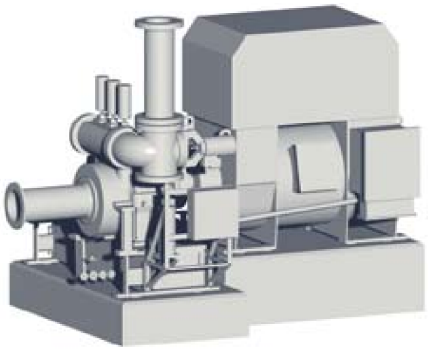

Figure 4.21: Animated illustration of the Siemens SST-060. Figure taken from SIEMENS (2014).

Chapter 5

Conclusions, Discussion, and Recommendations for Further Work

5.1 Summary and Conclusions

The raw thermal power potential of a well producing from an oil reservoir has been compared to a well producing from a gas reservoir. Mol fractions from the Tordis field were used as composition for the oil and Midgard fluid composition were used for the gas producer. Both cases were simulated using a production mass rate of 192.5 kg/s with wellhead temperatures ranging between 50-115°C. The results were plotted in Figure 4.6 and showed that the Tordis wellstream, consisting of 31.5 kg/s of oil and 161 kg/s of water, has considerably higher raw thermal potential than Midgard saturated gas for the entire wellhead temperature range. In fact, as WHT increases it is increasingly more beneficiary to exploit heat from Tordis compared to Midgard.

In Section 4.1 it were investigated how the raw power potential of the Tordis field varies over time, using monthly average NPD field data as input for the calculations. The results are shown in Figure 4.4 and it can be seen that the raw thermal potential was around 14 MW between the years 1994-1999, when the wells were still producing at zero water cut. After water influx the potential were essentially doubled from year 2000 to year 2010, then followed the same trend as the oil production as it decreased towards year 2012. Production increase were seen from year 2013 to 2017 and the calculated values for the raw thermal power potential have increased over that period as well.

A literature review of general thermodynamic phenomena and on low temperature organic Rankine cycles (LTORC) were performed to support a qualitative thermal feasibility assessment of using ORC technology subsea at the Tordis field on the Norwegian continental shelf, to convert geothermal waste heat to usable electricity. Several research articles involving LTORC were re-

viewed, but none involving a subsea application specifically. The Tordis field is producing 31.5 kg/s of oil and 161 kg/s of water at approximately 75°C wellhead temperature. Based on the literature review, the thermal efficiency of a system working with a heat source bounded by these constraints is realistically 9-14% at the highest. The most efficient systems have easy access to an effective coolant and use a cycle working fluid perfectly suited to operate between heat sink and heat source. Dong et al. (2017) found that use of a suited zeotropic mixture as cycle working fluid would increase the thermal efficiency compared to using a pure substance, but it would require a larger heat exchanger area because a bigger portion of the heat transfer happens during working fluid phase change. The author of this thesis received a data set containing thermal properties of the Tordis wellstream from Equinor ASA, and as seen in Section 2.2.1 a PVTsim flash showed a raw thermal heat potential at 46.5 MW. Under the assumption that 46.5 MW of heat could be transferred from the wellstream to the cycle working fluid, 9% thermal efficiency would mean a net power output of 4.19 MW from the generator which would be enough to cover the fields boosting requirements at around 4 MW. In conclusion the qualitative thermal feasibility assessment showed that using ORC power generation for boosting can be viable, but would require no thermal efficiency loss of subsea cycle application as compared to onshore, and that 46.5 MW of heat can be transferred by heat exchanger at these conditions.

A quantitative thermal feasibility assessment were performed to numerically determine the viability of a subsea ORC plant at Tordis. In order to get information on what heat transfer from wellstream to cycle that can realistically achieved and to learn the consequence on thermal efficiency of placing the ORC subsea, a series of thermodynamic models have been used. Aspen HYSYS were used to represent the Tordis ORC, using a basic cycle configuration consisting of a pump, an evaporator, a turbine and a condenser. The condenser coolant were modelled as an isothermal heat sink of water at 9°C and the evaporator heat source were modeled using the Tordis composition and rates, at wellhead temperatures ranging between 50-115°C. In total 37 substances were evaluated as working fluids for the cycle. The fluids R134a and butane performed with high thermal efficiency at onshore ambient pressures, respectively at 11.3% and 10%. When the potential working fluids were tested reacting to a subsea environment at 250m depth, it were shown that the previously best performing substances could not be evaporated efficiently at the present temperature and pressure level. The highest thermal efficiency were achieved using a zeotropic mixture between ethane and propane, with up to 18 mol-% of the blend being propane. A mixture of 10 mol-% propane and 90 mol-% ethane were chosen as final composition for the subsea ORC working fluid, because it were opted to go for a slightly lighter fluid to enable cycle operation at a higher minimum pressure than 250m subsea ambient.

With the selected working fluid, it were possible to make a realistic subsea model of the ORC. To take advantage of the isothermal heat sink which is the North Sea, a passive cooling manifold were proposed as replacement for the shell and tube condenser that is generally used in ORCs onshore. The cooling manifold effective area was estimated to be at least 950 m^2 and weigh 36 tonnes when filled with working fluid condensate. The cooling manifold outlet pressure were modelled as being 30 bars, a few bars higher than natural pressure at 26 bars. The working fluid is modelled as being at 14.4°C upon leaving the cooling system, and will be a sub-cooled liquid at this level of pressure and temperature. The working fluid flows with a mass rate of 81.0 kg/s through the pump working at 80% isentropic efficiency, which boosts the cycle pressure to 65.0 bars at 21.7°C.

The heating system is modelled as a series of five dual pass shell and tube heat exchangers with 700 5.25-meter tubes in each. The effective area of the heating train is estimated to 1397.8 m^2 before design margin is added to account for fouling. The total heat transferred from wellstream to cycle with such configuration is 23.2 MW, effectively bringing the temperature of the working fluid to 70.73°C at 63.76 bars at evaporator outlet. As the reader may have noticed, this figure for realistic heat transfer is only approximately half of the ideal heat transfer of 46.5 MW estimated earlier. The working fluid is at a superheated state at these conditions and it is assumed no energy loss until it flows into the expander inlet. The turbine is modelled as working at 85% isentropic efficiency and a net total power output from the generator is calculated to 2.1 MW corresponding to a cycle thermal efficiency of 9%. The chosen working fluid undergoes a relatively high pressure and temperature drop across the expander while still being in gaseous phase at expander outlet, this being respectively 31 bars and 22°C. The required basic features of the turbine were determined when it were assumed a two-stage unit of the axial type, designed using the velocity compounding technique. It was shown that the working fluid velocity at turbine inlet should be 260.8 m/s for maximum utilization, which means the pipe leading from evaporator to turbine should be sized appropriately to suit this requirement. The rotor blades will rotate at 60.4 m/s tip speeds and installing blade lengths of 0.19 meters at the turbine inlet side will tune the production frequency to 50 Hz, in order to correspond with the Norwegian electrical grid frequency. The nozzle angles for both turbine stages were determined to be 67.95° and 51°, and the matching rotor blade angles should be designed as 61.6° for stage one and 31.7° for stage two. The axial working fluid velocity leaving the turbine was calculated to 98.1 m/s, which corresponds to an overall maximum energy utilization efficiency of 85.8%. An industrial turbine that has basic design features rated similar to the subsea ORC requirements is the Siemens SST-060, which can be customized by Siemens before delivery to adequately cover the needs. In this case, the custom SST-060 has to be tailored with slightly higher exhaust pressure rating than

the base design. The basic SST-060 is rated for 29 bara exhaust pressures, while the subsea ORC application would require it to be rated to 31 bara before design margin is added.

Since the model assumes steady state conditions and this is not expected in reality, the following cycle control elements were chosen as actuators for maximizing electricity production. It is possible to control the tube side pressure of the heating train using a by-pass valve to circumvent hydrocarbon vapors and possibly a small fraction of condensate. This helps ensure operation within the design pressures and will also be used to adjust the liquid fraction entering the heat exchanger to control the transfer of energy. Since the sea is considered an isothermal heat sink and abrupt operational changes are not expected, using isolation valves for the sectioned cooling manifold will most likely suffice for regulating the condensation process. These can potentially function as cycle actuators for the condenser outlet temperature if replaced with chokes for precise day-to-day operational control, or it is possible to use a by-pass cooling system instead for a similar result. It is required to have a high level of accuracy on the cycle pressure state and working fluid mass rate, of which the main control element is the pump speed. By controlling the duty supplied to the pump the boosting of the working fluid is actuated, and as mentioned, pressure drops of the other cycle elements are controlled by the different by-passes. The final two main control elements required for the subsea ORC are a turbine by-pass valve and a rotor speed controller. The rotor speed is a direct way of controlling the energy state of the working fluid at expander outlet and a gear box is also proposed for determining the frequency of the produced electricity. The turbine by-pass is not meant to be regulated from day to day, as it is there to be opened in the event of working fluid condensate droplets appearing in the expander.

The quantitative thermal feasibility assessment showed that it is possible to achieve the same thermal efficiency subsea as in onshore ORCs. The main challenge is to design an efficient heating system when the heat source is a low temperature geothermal resource. In the qualitative analysis it was worked under the assumption that 46.5 MW worth of heat would be transferred into the subsea power generation unit, which would bring the wellstream down to an evaporator outlet temperature of 20°C. During the quantitative work it was shown that a heat transfer of 23.2 MW is a more realistic value for energy transfer between two fluids using an evaporator at Tordis. With a net power output of 2.1 MW it can not sufficiently cover boosting duties at 4 MW, and the quantitative thermal feasibility is therefore deemed as low. There are possible improvements to the energy conversion system which can potentially increase the net output to desired level. For example through the use of a dual in-line cycle, where the wellstream flows from evaporator outlet into a secondary ORC that operates with a working fluid with even lower boiling point.

5.2 Discussion

The raw thermal power potential of the Tordis wellsteam over field lifetime were calculated based on NPD data of monthly average oil production, GOR, WC and $\Delta T = 50°C$. The result showed that a significant increase in thermal power potential took place as water started to flow with the wellstream, which happened around year 1999. Up until that point, Tordis produced with a relatively steady oil rate at approximately 12×10^3 Sm^3/d while the gas oil ratio increased from 91 to 105 Sm^3/Sm^3 during the same period. The results from the thermal potential calculation over the duration show a congregated data interval of similar valued data points (with very few outliers), suggesting that the GOR increase has very little effect on the thermal potential. A big impact on the potential calculation is seen once water influx takes place into the wellstream. The water cut increases from 20% at the start of year 2000 to a value of approximately 70% at the beginning of 2008, and during the same time the raw potential is relatively stable with a slight upwards slope from around 25 MW to 31 MW. One might have expected a higher thermal power potential increase over the time period since the water cut increased immensely, but total oil production were decreased from approximately 13×10^3 Sm^3/d to around 3.5×10^3 Sm^3/d in 2008. This means that while WC were indeed very much increased, the total volumes of heat energy carrying liquids were not increased by much. In the problem formulation of this thesis it were mentioned that *[...] as increasing water cut leads to more thermal energy potential over time, a positive synergy effect would be if the heat energy could be used to supply duty to submerged boosters [...]*, since boosting requirements increase as fields grow old. These results point to that while that statement can be true, in reality the thermal potential is not necessarily increasing much between the time of water break through and end of field life. It should be noted that this assessment were based on past field data and the Tordis production engineers has worked on minimizing the amount of water produced, as they have had no reason to produce more significant volumes of liquid water. This means that it is possible to produce more water with the aim of harvesting geothermal energy, but doing so will most likely not be beneficial due to depletion of the reservoir pressure. Another possibility is to make use of dry confined wells in the area for geothermal energy production, instead of abandoning them.

In Figure 4.6 the raw power potential of the gas producer Midgard were compared with Tordis oil and regular water, using the same mass rates, wellhead and outlet temperatures. At 75°C the relative difference were around 1.40, with the raw potential of Tordis being 42 MW while Midgard is at 30 MW. As WHT is increased the benefit from using a liquid based wellstream is enhanced. At 105°C the relative difference is 1.44, which points to oil based reservoirs having higher thermal potential for any wellhead temperature when the mass rates are equalized. There are multiple reasons for the increase in energy potential, and it involves phenomena that were discussed in the general theory chapter of this thesis. When the WHT is increased more of

the water, hydrocarbon and non-condensable gas molecules become into an *excited* vibrational and rotational state, making it possible to get a higher meaningful heat transfer upon cooling the fluid. It should be noted that a gas in general has more entropy (and energy) than a liquid, but it does not translate into a higher raw potential heat output in our model because it would be required to condense the gas to harvest the energy as latent heat of condensation.

Selecting an appropriate working fluid in addition to suitable operating parameters for the ORC is the most important and challenging tasks of all. The choice has a direct impact on the thermal efficiency, environmental friendliness and final cost of the ORC. Since every application of an ORC will have a certain amount of available waste heat based on its individual mass flow rates, heating and cooling temperatures, it is necessary to design the ORC with working fluid and operating parameters for each specific case. In Figure 4.7 the results from a general working fluid screening based on the Tordis field parameters with $\Delta T = [T_{WHT} - 20°C]$ are plotted. The wellhead temperatures that are examined ranges from 50°C-115°C, which essentially means that the heat source can be classified as a low temperature geothermal resource. When WHT is as low as this it means that certain substances can not function in a subcritical ORC, because it is not possible to evaporate them with the heating system. The problem is not with the total amount of raw heat energy since the mass rates are high, the problem is rather that we can not allow a temperature cross in the evaporator. The plotted results show five fluids that performed well in the fluid screening, meaning that they could be evaporated with no temperature cross in the heat exchanger, would be condensed by heat exchange with brine at 9°C and all this while keeping a vapor fraction of 1 through the expander. R134a is a very commonly used working fluid in LTORCs in the industry, and also performed with the highest thermal efficiency in this general screening. When simulated at WH temperatures ranging from 105°C-115°C it was seen that the thermal efficiency of R134a dropped, this because of the expander pressure becoming too high due to the expansion of the substance, resulting in liquid droplets appearing at the expander outlet. Therefore, R134a can be credited as the most suited working fluid if WHT is in the range of 50°C to 105°C. i-Butane and n-Butane are easily accessible substances that are contained in the natural Tordis wellstream, and it can be seen that these hydrocarbons performed really well at these constraints. No problems occurred when the butanes were subjected to the entire temperature range, and it can be seen that the butanes net power output curves are becoming increasingly steep as WHT is increased. The pentanes and hexane also technically fit the ORC model, but with considerably lower net power output potential.

The ORC thermal efficiency represents the relative fraction of generator energy output to pump duty and is plotted in Figure 4.8 for the WHT range. At the real Tordis WHT at 75°C it can be seen that R134a operates with 11.4% thermal efficiency while i-Butane is at 10.1%, which are values

that seem very good. The calculated thermal efficiencies in the plot should not be analyzed as absolutes values, but instead only used for direct comparison between the fluids. The reason is that it were not taken into account isentropic efficiencies of the pump and turbine when the data was calculated, which means in an application real cycle efficiency would be lower. Figure 4.9 show how the expander inlet pressure reacts to varied WHT for the five potential working fluids. It is easily seen that the pressure increase of R134a is much higher than the others as WHT is increased, and as mentioned this eventually leads to condensation of liquid droplets from the gaseous phase. An interesting observation is that the expander inlet pressure ratio over the temperature range is very similar for the different working fluids. At 50°C WHT it is seen that R134a is at around 11.9 bars once evaporated and at 105°C the pressure has increased to almost 40 bars, which equates to a pressure ratio of 3.36 over the WHT range. i-Butane is at 6 bars at 50°C WHT and almost 20 when subjected to 105°C WHT, effectively 3.33 as its pressure ratio across the temperature range. By looking at the expander inlet pressures at 75°C WHT it can be seen that for hexane, pentanes and butanes increasing the evaporator outlet pressure to higher than 10 bars would start forcing the working fluid back into liquid state, since they are saturated with low degree of superheat. The Tordis wellheads are placed at approximately 250 meters depth, which means the subsea ambient pressure is around 26 bars. No ORCs in the industry today are exposed to such a level of natural pressure, and it was found that the recommended working fluids for LTORC are not really suited for a subsea application. Since the cycle minimum pressure subsea at Tordis should be at least 26 bars, the freedom of choice for subsea ORC is lower than onshore, making finding a suited working fluid much more of a challenge. In the analysis for ORC topside it was possible to adjust the pressure minimum using the pump duty to maximize the thermal efficiency, but as we start looking at subsea specifically the mindset is changed. The ORC working fluid selection can no longer be solely based on available waste heat, heat source mass rate and temperature, but it has to be chosen based on how it suits subsea pressures as well. In the subsea screening model, the pump speed adjusts working fluid mass rate and cycle pressure minimum to a level above subsea ambient. A suited working fluid that would condense when subjected to 9°C coolant at [26 bar+ΔP_{pump}] while evaporating based on energy from the Tordis wellstream has to be used in the ORC.

In Figure 4.10 the PT-phase curves of five light fluids present in the Tordis wellstream are plotted, namely methane, CO_2, ethane, propane and i-butane. Some extra tick points have been drawn onto the plot, these being at 14°C, 70°C and 26 bars. An assumption here was that a condenser heat exchanger would be able to cool the working fluid to within five degrees different from the temperature of the coolant, so as the sea water is 9°C the minimum working fluid temperature of the cycle would potentially be 14°C. Same assumption were made for the heating system, the potential highest expected working fluid temperature would be around 70°C since WHT is

75°C. The first observation made from the phase curves was that methane is not eligible as a working fluid for the cycle, as it will require a far lower condensation temperature than what is available. At 14°C, 50 bars of pressure would be required to condense CO_2 and approximately 35 bars would condense ethane. It were preferred to use a working fluid that would not necessitate condensation pressure far higher than the ambient, therefore ethane was seen as a more suited candidate than CO_2 at this point in the analysis. From the phase curve for propane it is seen that condensation at these conditions poses no issues, but evaporation at 70°C with a pressure level higher than 26 bars is not possible. Since none of the pure fluids had qualities perfectly suited for the Tordis ORC operating range, it was investigated if the use of a binary mixture as subsea cycle working fluid could be utilized to make a system with high thermal efficiency. Even though usage of multi-component ORC working fluids is not currently seen in the industry, it had to be evaluated as Dong et al. (2017) showed that it is possible and may increase thermal efficiency of a cycle. Based on the phase curves of the five light fluids it were clear that a functioning binary mixture could either be mainly based on CO_2 or ethane, as these two fluids only need slightly increased cycle pressure minimums to condense while being easily evaporated at 70°C, even for extremely high pressures. In Figure 4.11 the results from a pressure sensitivity calculation for CO_2 and ethane are plotted, where the net power output potential from using the fluids were compared. The maximum output seen were from a CO_2 cycle operating at 111 bars expander inlet pressure, generating around 3.1 MW. Ethane required much less cycle pressure to produce almost the same amount of net output, this being 3.0 MW. Both cycle pressure states are realistically achievable using modern submerged pumps, but since usage of CO_2 upsets the pressure equilibrium with the ambient at a much larger degree with very little reward, ethane was chosen as base fluid for the binary working fluid mixture. To see the effect on cycle pressure state by blending CO_2 or propane with ethane, it were analyzed what expander inlet pressures would be necessary to maximize the cycle net power output. The results are shown in Figure 4.12 and it can be seen that the potential of the different binary mixes are very similar, but the working fluid mixes with higher density require less cycle pressure, just as one would expect. Ethane with 10 mol-% propane has peak output when the maximum pressure of the cycle is 65 bars, if the pressure were any higher liquid condensate would be seen in the expander and corresponding thermal efficiency plummets. Ethane with 10 mol-% CO_2 has its peak power output when the cycle pressure maximum is at 75 bars and exhibits a very similar trend to pure ethane. In Figure 4.13 bubble point and dew point lines of a binary mixture of ethane with 18 mol-% is plotted. This working fluid composition puts the bubble point line straight through the point where pressure is 26 bars and temperature is 14°C, while keeping the two-phase region short in respect to pressure. This means that a subsea ORC running using the mixture as working fluid would have saturated condensate at cooler outlet if cycle minimum pressure were equal to the natural pressure of 26 bars. Even though this is a situation where pump duty is minimized, it

is opted to design a cycle that operates on slightly higher pressure minimum than 250 meters equivalent, so that there will be a safety margin between condensation pressure and the ambient.

The final operating conditions for the proposed subsea ORC is listed in Table 4.6. The working fluid selected for modelling were a binary mix of ethane with 10 mol-% propane, which condenses at cooling manifold outlet pressure 30 bars and 14.4°C. The model uses realistic values for isentropic efficiencies of the rotating equipment and the duty from the heat exchangers are now based on numerical models. The cycle operates at a thermal efficiency of 9%, with a net power output of 23260.7 kW from the generator. As 9% thermal efficiency is decent for any ORC, it is clear that it is not a high pump duty that is bottle necking the energy production. In fact, the energy transfer from wellstream to working fluid was found to be the limiting factor once a detailed evaporator model was implemented in the simulation. A shell and tube evaporator were designed in detail in Section 4.7.1 based on the selected working fluid, the Tordis wellstream and required inlet/outlet conditions. Initial assumptions for the evaporator design were to use TEMA type BEM made of carbon steel with 25 mm tubes and 31.25 pitch, installed in triangular tube pattern. Aspen EDR were used to optimize the design with respect to heat transfer, and it was found that a series of 5 shells with 6 baffles, 2 passes and 700 tubes in each shell would give the best result. As mentioned earlier, the proposed heating system would give a meaningful heat transfer of 23.2 MW. This heating duty represents the highest achievable with this setup, as fouling is likely to occur tube side over time. Net power output potential of the subsea cycle is estimated to 2.1 MW, which is lower than the target output at 4 MW. To bring the net output to target level using ORC technology, it would not be enough to change cycle configuration as it would only slightly increase the thermal efficiency. Instead the engineers would need to increase the amount of energy that flows from wellstream to cycle. When the wellstream flows out of the evaporator outlet with the current ORC design, it has an estimated temperature of 44.78°C. This means that it is still at an enthalpy level where the ΔT between wellstream and the sea is significant, meaning it is possible to induce additional heat transfer with a secondary cycle, a so called *dual in-line* cycle. The secondary cycle would have Tordis field fluids at 44.78°C as a energy source and would require a well suited working fluid that can allow operation within a very small temperature window, approximately between 14-39°C. The design of a dual in-line cycle has not been considered in this thesis, but it is plausible that the target output of 4 MW could be met with such a system. In a feasibility analysis assessing reservoir fluids cooled to such an extent a big focus should be on flow assurance, as things like hydrates, wax and silica deposition pose big challenges in a real subsea build.

5.3 Recommendations for Further Work

There is a lot of work remaining before one can determine whether ORC technology has a future offshore or not. The analysis conducted in this thesis has shown that the amount of available power is in the mega-watt range, and the potential power output may be acceptable for certain applications. The author wishes to use this final section to recommend short-, medium- and long-term extensions to the work presented in this thesis, that is needed to determine if the thermal energy conversion project would be successful or not.

Short term

A fluid characterization study should be carried out as early as possible. Analyzing the fluid can provide additional information that would give a more accurate description of the hypotethical components used in the thermodynamic models. An even more important reason to further studying the resource (both brine and hydrocarbons) is to get an overview over how big of a temperature drop that can be allowed before precipitation of solids occur. As petroleum engineers, the focus is usually on staying above the hydrate formation curve or to avoid wax deposition, but dealing with this technology it must also be ensured that silica, stibnite or similar solids do not deposit from the chilling brine. If the results from the fluid analysis show that the wellstream can be cooled the required amount without issues, it is proposed to approach dealers in the industry to get early cost estimates for the various components of the cycle. The Tordis wellstream offer two things "for free", the energy potential and the chosen working fluid (can be separated from the gaseous phase), all other equipment must be bought custom designed for the operating conditions. The information gathered at this point should suffice to determine costs related to operation and annual maintenance, and finally estimate the payback period for the project.

Medium term

The medium-term objective recommendation is rather simple. After cooling capabilities of the working fluid and rate of return have been estimated with acceptable degree of accuracy, one can revisit the cycle configuration. If the wellstream fluid can be cooled to a larger extent than the proposed ORC system is designed for, and the costs are reasonable, it is possible that a dual in-line ORC can be considered. The dual in-line cycle operates in the same fashion as basic ORC, but is really a series of two basic cycles. The added cycle uses a working fluid with lower boiling point than the current and will make it viable to cool the Tordis wellstream to a lower value than 44.7°C. The result would essentially be larger heat transfer from wellstream to the cycles, and the net power output would increase.

Long term

The final stage is to design everything in detail. The cost estimates from the short-term work were approximates which helped decide final cycle configuration and get an idea of the pay back period. Requesting tender offers from industrial providers for specific turbines, heat exchangers and pumps will be part of determining the final costs. If willing to proceed with the project, a risk assessment based on the proposed equipment design has to be performed. For example, it has to be quantified how much working fluid is expected to leak from the turbine shaft and which environmental impact the leak poses. The risk assessment also quantifies financial risks. An example of a financial risk scenario could be to determine the impact of having a delay in the delivery of a vital cycle component. If the ORC were expected to supply energy for boosting a field, and installation is delayed, the impact could be massive. Once a detailed plan and risk assessment for commercializing subsea ORC at Tordis is finalised, the true feasibility can be accurately judged.

Appendix A

Code associated with the Raw Power Model

A.1 Introduction

The following Excel VBA programs was written to link Excel with Aspen HYSYS in order to calculate raw thermal power potential from a fluid stream, to see effects of GOR and WHT changes along with potential development over a fields lifetime.

A.1.1 Tordis power potential over its lifetime VBA

This script was only included for reference, and will be impossible to run without the corresponding Excel document and HYSYS file. Therefore no "cleaning" of the code was performed before attachment.

Listing A.1: Visual basic code used for Tordis field lifetime calculation.

```
Option Explicit
Public hyApp As HYSYS.Application
Public simCase As SimulationCase
Public pStream As ProcessStream
Public Stream_1 As ProcessStream
Public Stream_2 As ProcessStream
Public giStream As ProcessStream
Public oiStream As ProcessStream
Public g0Stream As ProcessStream
Public o0Stream As ProcessStream
Public mixedStream As ProcessStream
Public InletStream As ProcessStream
Public waterStream As ProcessStream
Public feed1Stream As ProcessStream
```

```
15 Public out1Stream As ProcessStream
16 Public q1Stream As ProcessStream
17
18
19 Public filename As String
20 Public ITEM As Integer
21 Public SS As Object
22 Dim hyPhase As FluidPhase
23 Dim hyPhases As FluidPhases
24 Dim hyFluid As Fluid
25 Dim feed1hyFluid As Fluid
26 Dim out1hyFluid As Fluid
27 Dim hyPhaseOut As FluidPhase
28 Dim hyPhasesOut As FluidPhases
29 Dim hyFluidOut As Fluid
30 Dim i As Integer
31 Dim itr As Integer
32 Public Sub StartHYSYS_SurfaceProcessing()
33 Dim filename As String
34 Dim ITEM As Integer
35 Dim Compositions As Variant
36 Dim gasCompositions As Variant
37 Dim oilCompositions As Variant
38 Dim feedCompositions As Variant
39 Dim GOR As Integer
40 Dim rad As Integer
41 Dim qo As Variant
42 Dim qo_temp As Variant
43 Dim factor As Variant
44
45 'Load HYSYS  file
46 Set hyApp = CreateObject("HYSYS.Application")
47 hyApp.Visible = True
48 Set simCase = hyApp.ActiveDocument
49 If simCase Is Nothing Then
50           filename = Worksheets("HYSYS_PowerVsTime_Norne").
               Range("C4").Text
51 If filename <> "False" And simCase Is Nothing Then
```

```
52            Set simCase = GetObject(filename, "HYSYS.
                 SimulationCase")
53            simCase.Visible = True
54 End If
55 End If
56
57 'Code to read data from Excel into HYSYS components
58 Set pStream = simCase.Flowsheet.MaterialStreams.ITEM("
     InitialComp")
59 Set InletStream = simCase.Flowsheet.MaterialStreams.ITEM("Inlet
      stream")
60 Set Stream_1 = simCase.Flowsheet.MaterialStreams.ITEM("1")
61 Set Stream_2 = simCase.Flowsheet.MaterialStreams.ITEM("2")
62 Set giStream = simCase.Flowsheet.MaterialStreams.ITEM("g-i")
63 Set oiStream = simCase.Flowsheet.MaterialStreams.ITEM("o-i")
64 Set g0Stream = simCase.Flowsheet.MaterialStreams.ITEM("g-0")
65 Set o0Stream = simCase.Flowsheet.MaterialStreams.ITEM("o-0")
66 Set feed1Stream = simCase.Flowsheet.MaterialStreams.ITEM("FEED
     -1")
67 Set out1Stream = simCase.Flowsheet.MaterialStreams.ITEM("OUT-1"
     )
68 Set q1Stream = simCase.Flowsheet.EnergyStreams.ITEM("Q-1")
69 Set waterStream = simCase.Flowsheet.MaterialStreams.ITEM("Water
     ")
70
71 'Feed fluid
72 Set hyFluid = pStream.DuplicateFluid
73 Set hyPhases = hyFluid.FluidPhases
74
75 'For Z factor retrieval
76 Set feed1hyFluid = feed1Stream.DuplicateFluid
77 Set out1hyFluid = out1Stream.DuplicateFluid
78
79 'Compositions = pStream.ComponentMolarFractionValue
80 'gasCompositions = g0Stream.ComponentMolarFractionValue
81 'oilCompositions = o0Stream.ComponentMolarFractionValue
82 'For ITEM = 0 To 11        'collecting composition data as
     variant
```

```
'          Compositions(ITEM) = Worksheets("HYSYS_SurfaceProcessing").Range("D" & ITEM + 7).Value
'Next ITEM


'For ITEM = 0 To 11        'collecting composition data as variant
'          Cells(ITEM + 7, 8) = giStream.ComponentMolarFractionValue(ITEM)
'          Cells(ITEM + 7, 12) = oiStream.ComponentMolarFractionValue(ITEM)
'          gasCompositions(ITEM) = Worksheets("HYSYS_SurfaceProcessing").Range("H" & ITEM + 7).Value
'          oilCompositions(ITEM) = Worksheets("HYSYS_SurfaceProcessing").Range("L" & ITEM + 7).Value
'Next ITEM

' apply composition data
'pStream.ComponentMolarFraction.Values = Compositions
'g0Stream.ComponentMolarFraction.Values = gasCompositions
'o0Stream.ComponentMolarFraction.Values = oilCompositions

'g0Stream.MolarFlow.SetValue Cells(21, 8), "m3/d_(gas)"
'o0Stream.MolarFlow.SetValue Cells(21, 12), "m3/d_(gas)"
'g0Stream.MolarFlow.SetValue Cells(21, 8), "kgmole/h"
'o0Stream.MolarFlow.SetValue Cells(21, 12), "kgmole/h"


'WH Temperature and Pressure and flow rate from Excel
pStream.TemperatureValue = Cells(23, 4)
pStream.Pressure.SetValue Cells(24, 4), "bar"

'InletStream.TemperatureValue = Cells(23, 4)
InletStream.Pressure.SetValue Cells(24, 4), "bar"

g0Stream.TemperatureValue = Cells(23, 4)
g0Stream.Pressure.SetValue Cells(24, 4), "bar"
o0Stream.TemperatureValue = Cells(23, 4)
```

```
115 o0Stream.Pressure.SetValue Cells(24, 4), "bar"
116
117 Stream_1.TemperatureValue = Cells(25, 4)
118 Stream_1.Pressure.SetValue Cells(26, 4), "bar"
119 Stream_2.TemperatureValue = Cells(27, 4)
120 Stream_2.Pressure.SetValue Cells(28, 4), "bar"
121
122 feed1Stream.TemperatureValue = Cells(23, 4)
123 feed1Stream.Pressure.SetValue Cells(24, 4), "bar"
124 out1Stream.TemperatureValue = feed1Stream.TemperatureValue -
      Cells(4, 16) 'Out Temp = In Temp minus dT
125 out1Stream.Pressure.SetValue Cells(32, 4), "bar"
126
127
128 feedCompositions = feed1Stream.ComponentMolarFractionValue
129 Set SS = simCase.Flowsheet.Operations.ITEM("SS_GOR")
130 'Initial value for produced molerate of oil
131 o0Stream.MolarFlow.SetValue 400, "kgmole/h"
132 g0Stream.MolarFlow.SetValue 200, "kgmole/h"
133 For rad = 40 To 296
134 SS.Cell("C2").CellValue = Cells(rad, 3) 'Defining GOR in SS_GOR
      in HYSYS
135
136 'Find qo
137 SS.Cell("C5").CellValue = Cells(rad, 5)
138 'Find wc
139 SS.Cell("D2").CellValue = Cells(rad, 4)
140
141
142 While SS.Cell("A2").CellValue * 3600 < SS.Cell("C5").CellValue
143   SS.Cell("A4").CellValue = o0Stream.MolarFlow.GetValue("kgmole
        /h")
144   o0Stream.MolarFlow.SetValue (SS.Cell("A4").CellValue + 10), "
        kgmole/h"
145   Application.Wait Now + 1 / (24 * 60 * 60# * 2)
146 Wend
147
148
```

```
'Store value for molerate of oil in spreadsheet
For ITEM = 0 To 22        'collecting composition data as variant
          feedCompositions(ITEM) = InletStream.ComponentMolarFractionValue(ITEM)
Next ITEM
Application.Wait Now + 1 / (24 * 60 * 60# * 2)
waterStream.StdLiqVolFlow.Value = SS.Cell("D7").CellValue
feed1Stream.ComponentMolarFraction.Values = feedCompositions
feed1Stream.MolarFlow.Value = InletStream.MolarFlow.Value 'Flow rate from "Inlet stream" to "FEED-1"
Cells(rad, 6) = feed1Stream.MassFlow.GetValue("kg/h")
Cells(rad, 7) = q1Stream.HeatFlow.GetValue("kJ/h")
'Enthalpy
Cells(rad, 8) = feed1Stream.MassEnthalpyValue
Cells(rad, 9) = out1Stream.MassEnthalpyValue
'Deviation factor (Z factor)
Cells(rad, 10) = feed1hyFluid.VapourPhase.CompressibilityValue
Cells(rad, 11) = out1hyFluid.VapourPhase.CompressibilityValue

'Reset to low production values to make sure while sentence will work
While SS.Cell("A2").CellValue * 3600 > Cells(rad + 1, 5)
    'While o0Stream.MolarFlow.GetValue("kgmole/h") > 4500
    o0Stream.MolarFlow.SetValue (o0Stream.MolarFlow.GetValue("kgmole/h") - 30), "kgmole/h"
    Application.Wait Now + 1 / (24 * 60 * 60# * 2)
Wend



Next rad


ThisWorkbook.Save

End Sub
```

A.1.2 Code for quick heat transfer calculation based on ΔT and fluid composition

This script was only included for reference, and will be impossible to run without the corresponding Excel document and HYSYS file. Therefore no "cleaning" of the code was performed before attachment.

Listing A.2: Visual basic code for estimating raw power potential when WHT is fixed.

```
Option Explicit
Public hysApp As HYSYS.Application
Public simCase As SimulationCase
Public filename As String
Public Sub HYSYS_Raw_Potential()
Dim WATERinStream As ProcessStream
Dim HCinStream As ProcessStream
Dim WELLSTREAMinStream As ProcessStream
Dim WELLSTREAMoutStream As ProcessStream
Dim RawPotentialStream As ProcessStream

'Code to load HYSYS simulation file
Set hysApp = CreateObject("HYSYS.Application")
hysApp.Visible = True
Set simCase = hysApp.ActiveDocument
If simCase Is Nothing Then
          filename = Worksheets("Raw_Potential_Tordis").Range("
             B2").Text
If filename <> "False" And simCase Is Nothing Then
          Set simCase = GetObject(filename, "HYSYS.
             SimulationCase")
          simCase.Visible = True
End If
End If

'Code to specify input data from Excel into HYSYS components
'Material streams
Set WATERinStream = simCase.Flowsheet.MaterialStreams.Item("HT-
    Water")
Set HCinStream = simCase.Flowsheet.MaterialStreams.Item("HT-HC"
    )
```

```
'Set WELLSTREAMinStream = simCase.Flowsheet.MaterialStreams.
    Item("HT-Wellstream")
Set WELLSTREAMoutStream = simCase.Flowsheet.MaterialStreams.
    Item("LT-Wellstream")
'Energy streams
Set RawPotentialStream = simCase.Flowsheet.EnergyStreams.Item("
    Raw Potential")

'Inlet Temperature and Pressure and flow rate from Excel
WATERinStream.TemperatureValue = Cells(5, 2)
WATERinStream.Pressure.SetValue Cells(6, 2), "bar"
WATERinStream.MassFlow.Value = Cells(7, 2)
HCinStream.TemperatureValue = Cells(5, 2)
HCinStream.Pressure.SetValue Cells(6, 2), "bar"
HCinStream.MassFlow.Value = Cells(8, 2)

'Outlet Temperature and Pressure and flow rate from Excel
WELLSTREAMoutStream.TemperatureValue = Cells(9, 2)
WELLSTREAMoutStream.Pressure.SetValue Cells(10, 2), "bar"

'Print raw potential to Excel spreadsheet
Cells(13, 2) = RawPotentialStream.HeatFlow.GetValue("MW")
End Sub
```

A.1.3 Code for quick heat transfer calculation based on ΔT and fluid composition over entire WHT range

This script was only included for reference, and will be impossible to run without the corresponding Excel document and HYSYS file. Therefore no "cleaning" of the code was performed before attachment.

Listing A.3: Visual basic code for estimating raw power potential when WHT is varied.

```
Public Sub HYSYS_Raw_Potential_Sensitivity()
Dim WATERinStream As ProcessStream
Dim HCinStream As ProcessStream
Dim WELLSTREAMinStream As ProcessStream
Dim WELLSTREAMoutStream As ProcessStream
Dim RawPotentialStream As ProcessStream
Dim i As Integer

'Code to load HYSYS simulation file
Set hysApp = CreateObject("HYSYS.Application")
hysApp.Visible = True
Set simCase = hysApp.ActiveDocument
If simCase Is Nothing Then
          filename = Worksheets("Raw_Potential_Tordis").Range("
             B2").Text
If filename <> "False" And simCase Is Nothing Then
          Set simCase = GetObject(filename, "HYSYS.
             SimulationCase")
          simCase.Visible = True
End If
End If

'Code to specify input data from Excel into HYSYS components
'Material streams
Set WATERinStream = simCase.Flowsheet.MaterialStreams.Item("HT-
   Water")
Set HCinStream = simCase.Flowsheet.MaterialStreams.Item("HT-HC"
   )
'Set WELLSTREAMinStream = simCase.Flowsheet.MaterialStreams.
   Item("HT-Wellstream")
Set WELLSTREAMoutStream = simCase.Flowsheet.MaterialStreams.
```

```
    Item("LT-Wellstream")
'Energy streams
Set RawPotentialStream = simCase.Flowsheet.EnergyStreams.Item("
    Raw Potential")

'Inlet Pressure and flow rate from Excel
WATERinStream.Pressure.SetValue Cells(6, 2), "bar"
WATERinStream.MassFlow.Value = Cells(7, 2)
HCinStream.TemperatureValue = Cells(5, 2)
HCinStream.Pressure.SetValue Cells(6, 2), "bar"
HCinStream.MassFlow.Value = Cells(8, 2)

'Outlet Temperature and Pressure and flow rate from Excel
WELLSTREAMoutStream.TemperatureValue = Cells(9, 2)
WELLSTREAMoutStream.Pressure.SetValue Cells(10, 2), "bar"

For i = 0 To (Cells(20, 3) - Cells(20, 2))
Cells(23 + i, 1) = Cells(20, 2) + i 'Printing temperature range
    from A23
Cells(23 + i, 2) = i + 1 'Printing iteration number from B23
'Inlet Temperature and Pressure and flow rate from Excel
WATERinStream.TemperatureValue = Cells(23 + i, 1)
HCinStream.TemperatureValue = Cells(23 + i, 1)
'Print raw potential to Excel spreadsheet
Cells(23 + i, 3) = RawPotentialStream.HeatFlow.GetValue("MW")
Next i

End Sub
```

Appendix B

Code associated with the Subsea ORC Model

B.1 Introduction

The following Excel VBA programs was written to link Excel with Aspen HYSYS in order to calculate ORC basic cycle properties based on specifications defined in the spreadsheet and print the results. The code calls based on a lot of cell coordinates which correspond to those shown in Figure B.1.

Cell coordinates referenced in code

	A	B	C	D	E
1	**Stream**	**Temperature**	**Pressure**	**Vapor Fraction**	**Rate**
2	**Condensate**	**14.00 C**	4.713 bar	**0.0000**	213.6 kg/s
3	**HP-Liquid**	15.21 C	22.28 bar	0.0000	
4	**HP-Gas**	**70.00 C**	21.28 bar	**1.0000**	
5	**Turbine Exhaust**	20.07 C	5.713 bar	0.9956	
6					
7		**Duties**		**Power**	**Efficiency**
8	**Boiler**	**4.577e+004 kJ/s**	**Turbine**	4752 kW	**85.0000**
9	**Condenser**	4.140e+004 kJ/s	**Pump**	377.9 kW	**80.00**
10			**Net Produced**	*4374 kW*	
11			**Thermal Efficiency**	*9.555*	

Figure B.1: The scripts in Appendix B references the variables in this figure.

B.1.1 Code for calculation of basic ORC properties

This script was only included for reference, and will be impossible to run without the corresponding Excel document and HYSYS file. Therefore no "cleaning" of the code was performed before attachment.

Listing B.1: Visual basic code for estimation and print basic ORC properties

```
Public Sub HYSYS_Basic_Cycle()
Dim SS As Object
Dim Compositions As Variant
Dim WF As Integer
Dim condensateStream As ProcessStream

'Code to load HYSYS simulation file
Set hysApp = CreateObject("HYSYS.Application")
hysApp.Visible = True
Set simCase = hysApp.ActiveDocument
If simCase Is Nothing Then
          filename = Worksheets("Raw_Potential_Tordis").Range("
             B2").Text
If filename <> "False" And simCase Is Nothing Then
          Set simCase = GetObject(filename, "HYSYS.
             SimulationCase")
          simCase.Visible = True
End If
End If

Set condensateStream = simCase.Flowsheet.MaterialStreams.Item("
   Condensate (3)")
Compositions = condensateStream.ComponentMolarFractionValue
For WF = 0 To 43      'collecting composition data as variant
          Compositions(WF) = Worksheets("Raw_Potential_Tordis")
             .Range("I" & WF + 23).Value
Next WF
' apply composition data
condensateStream.ComponentMolarFraction.Values = Compositions

Set SS = simCase.Flowsheet.Operations.Item("Cycle Summary")
SS.Cell("B2").CellValue = Cells(6, 12)
```

```
SS.Cell("B4").CellValue = Cells(8, 12)
SS.Cell("B8").CellValue = Cells(12, 12)
'SS.Cell("C4").CellValue = Cells(8, 13) * 100
Cells(8, 13) = SS.Cell("C4").CellValue * 0.01
SS.Cell("D2").CellValue = Cells(6, 14)
SS.Cell("D4").CellValue = Cells(8, 14)
SS.Cell("E8").CellValue = Cells(16, 14)
SS.Cell("E9").CellValue = Cells(17, 14)
Cells(7, 12) = SS.Cell("B3").CellValue
Cells(9, 12) = SS.Cell("B5").CellValue
Cells(13, 12) = SS.Cell("B9").CellValue
Cells(6, 13) = SS.Cell("C2").CellValue * 0.01
Cells(7, 13) = SS.Cell("C3").CellValue * 0.01
Cells(9, 13) = SS.Cell("C5").CellValue * 0.01
Cells(7, 14) = SS.Cell("D3").CellValue
Cells(9, 14) = SS.Cell("D5").CellValue
Cells(16, 12) = SS.Cell("D8").CellValue
Cells(17, 12) = SS.Cell("D9").CellValue
Cells(18, 12) = SS.Cell("D10").CellValue
Cells(19, 12) = SS.Cell("D11").CellValue
End Sub
```

B.1.2 Code for calculation of basic ORC properties when WHT is varied.

This script was only included for reference, and will be impossible to run without the corresponding Excel document and HYSYS file. Therefore no "cleaning" of the code was performed before attachment.

Listing B.2: Visual basic code for estimation and print basic ORC properties for a series of WHT values.

```
Public Sub HYSYS_Basic_Cycle_Sensitivity()
Dim SS As Object
Dim j As Integer
Dim Compositions As Variant
Dim WF As Integer
Dim condensateStream As ProcessStream

'Code to load HYSYS simulation file
Set hysApp = CreateObject("HYSYS.Application")
```

```
hysApp.Visible = True
Set simCase = hysApp.ActiveDocument
If simCase Is Nothing Then
          filename = Worksheets("Raw_Potential_Tordis").Range("
             B2").Text
If filename <> "False" And simCase Is Nothing Then
          Set simCase = GetObject(filename, "HYSYS.
             SimulationCase")
          simCase.Visible = True
End If
End If

Set condensateStream = simCase.Flowsheet.MaterialStreams.Item("
   Condensate (3)")
Compositions = condensateStream.ComponentMolarFractionValue
For WF = 0 To 43       'collecting composition data as variant
          Compositions(WF) = Worksheets("Raw_Potential_Tordis")
             .Range("I" & WF + 23).Value
Next WF
condensateStream.ComponentMolarFraction.Values = Compositions

Set SS = simCase.Flowsheet.Operations.Item("Cycle Summary")
SS.Cell("B2").CellValue = Cells(6, 12)
SS.Cell("B4").CellValue = Cells(8, 12)
SS.Cell("B8").CellValue = Cells(12, 12)
'SS.Cell("C4").CellValue = Cells(8, 13) * 100

SS.Cell("D2").CellValue = Cells(6, 14)
SS.Cell("D4").CellValue = Cells(8, 14)
SS.Cell("E8").CellValue = Cells(16, 14)
SS.Cell("E9").CellValue = Cells(17, 14)

'to reset
SS.Cell("B4").CellValue = Cells(8, 12)
Cells(23 + 0, 11) = Cells(20, 2) + 0 'Printing temperature
   range from A23
Cells(23 + 0, 12) = 0 + 1 'Printing iteration number from B23
Cells(23 + 0, 13) = Cells(23 + 0, 3) * 1000 'Boiler duty
```

```
Cells(12, 12) = Cells(23 + 0, 3) * 1000
Cells(8, 12) = Cells(23 + 0, 1) - Cells(21, 12) 'Pinch
Application.Wait Now + #12:00:01 AM#
Cells(23 + 0, 14) = SS.Cell("D10").CellValue
Cells(23 + 0, 15) = SS.Cell("D11").CellValue
Cells(23 + 0, 16) = SS.Cell("C4").CellValue * 0.01 'Turbine
    inlet pressure
'end reset

For j = 0 To (Cells(20, 3) - Cells(20, 2))
Cells(23 + j, 11) = Cells(20, 2) + j 'Printing temperature
    range from A23
Cells(23 + j, 12) = j + 1 'Printing iteration number from B23
Cells(23 + j, 13) = Cells(23 + j, 3) * 1000 'Boiler duty
Cells(12, 12) = Cells(23 + j, 3) * 1000
Cells(8, 12) = Cells(23 + j, 1) - Cells(21, 12) 'Pinch
Application.Wait Now + #12:00:01 AM#
Cells(23 + j, 14) = SS.Cell("D10").CellValue
Cells(23 + j, 15) = SS.Cell("D11").CellValue
Cells(23 + j, 16) = SS.Cell("C4").CellValue * 0.01 'Turbine
    inlet pressure
Cells(23 + j, 17) = SS.Cell("D5").CellValue 'Turbine Exhaust
    Vapor Fraction
SS.Cell("B4").CellValue = Cells(8, 12)
SS.Cell("B8").CellValue = Cells(12, 12)
Next j

Cells(8, 13) = SS.Cell("C4").CellValue * 0.01
Cells(7, 12) = SS.Cell("B3").CellValue
Cells(9, 12) = SS.Cell("B5").CellValue
Cells(13, 12) = SS.Cell("B9").CellValue
Cells(6, 13) = SS.Cell("C2").CellValue * 0.01
Cells(7, 13) = SS.Cell("C3").CellValue * 0.01
Cells(9, 13) = SS.Cell("C5").CellValue * 0.01
Cells(7, 14) = SS.Cell("D3").CellValue
Cells(9, 14) = SS.Cell("D5").CellValue
Cells(16, 12) = SS.Cell("D8").CellValue
Cells(17, 12) = SS.Cell("D9").CellValue
```

```
77 Cells(18, 12) = SS.Cell("D10").CellValue
78 Cells(19, 12) = SS.Cell("D11").CellValue
79
80 End Sub
```

B.1.3 Code used for calculation of basic subsea model ORC properties.

This script was only included for reference, and will be impossible to run without the corresponding Excel document and HYSYS file. Therefore no "cleaning" of the code was performed before attachment.

Listing B.3: Visual basic code for estimation and print properties subsea ORC model.

```
1  Public Sub HYSYS_Subsea_Cycle_Sensitivity()
2  Dim SS As Object
3  Dim j As Integer
4  Dim Compositions As Variant
5  Dim WF As Integer
6  Dim condensateStream As ProcessStream
7
8  'Code to load HYSYS simulation file
9  Set hysApp = CreateObject("HYSYS.Application")
10 hysApp.Visible = True
11 Set simCase = hysApp.ActiveDocument
12 If simCase Is Nothing Then
13           filename = Worksheets("Raw_Potential_Tordis").Range("
               B2").Text
14 If filename <> "False" And simCase Is Nothing Then
15           Set simCase = GetObject(filename, "HYSYS.
               SimulationCase")
16           simCase.Visible = True
17 End If
18 End If
19
20 'Set condensateStream = simCase.Flowsheet.MaterialStreams.Item
     ("Condensate (3)")
21 'Compositions = condensateStream.ComponentMolarFractionValue
22 'For WF = 0 To 41       'collecting composition data as variant
23 '          Compositions(WF) = Worksheets("Raw_Potential_Tordis
```

```
    ").Range("I" & WF + 23).Value
'Next WF
'condensateStream.ComponentMolarFraction.Values = Compositions

Set SS = simCase.Flowsheet.Operations.Item("Cycle Summary")
SS.Cell("B2").CellValue = Cells(102, 2)
'SS.Cell("B4").CellValue = Cells(104, 2)
SS.Cell("B8").CellValue = Cells(108, 2)
'SS.Cell("C4").CellValue = Cells(8, 13) * 100

SS.Cell("D2").CellValue = Cells(102, 4)
SS.Cell("D4").CellValue = Cells(104, 4)
SS.Cell("E8").CellValue = Cells(108, 5)
SS.Cell("E9").CellValue = Cells(109, 5)

'to reset
SS.Cell("B4").CellValue = Cells(114, 1)
'Cells(114 + 0, 11) = Cells(20, 2) + 0 'Printing temperature
    range from A23
'Cells(114 + 0, 12) = 0 + 1 'Printing iteration number from B23
'Cells(114 + 0, 13) = Cells(23 + 0, 3) * 1000 'Boiler duty
'Cells(114, 12) = Cells(23 + 0, 3) * 1000
'Cells(8, 12) = Cells(23 + 0, 1) - Cells(21, 12) 'Pinch
Application.Wait Now + #12:00:01 AM#
Cells(114 + 0, 2) = SS.Cell("D10").CellValue
Cells(114 + 0, 3) = SS.Cell("B3").CellValue
Cells(114 + 0, 4) = SS.Cell("B4").CellValue
Cells(114 + 0, 5) = SS.Cell("C2").CellValue * 0.01
Cells(114 + 0, 6) = SS.Cell("C3").CellValue * 0.01
Cells(114 + 0, 7) = SS.Cell("C4").CellValue * 0.01
Cells(114 + 0, 8) = SS.Cell("C5").CellValue * 0.01
Cells(114 + 0, 9) = SS.Cell("D2").CellValue
Cells(114 + 0, 10) = SS.Cell("D3").CellValue
Cells(114 + 0, 11) = SS.Cell("D4").CellValue
Cells(114 + 0, 12) = SS.Cell("D5").CellValue
Cells(114 + 0, 13) = SS.Cell("E2").CellValue
Cells(114 + 0, 14) = SS.Cell("B8").CellValue
Cells(114 + 0, 15) = SS.Cell("B9").CellValue
```

```
Cells(114 + 0, 16) = SS.Cell("D8").CellValue
Cells(114 + 0, 17) = SS.Cell("D9").CellValue
Cells(114 + 0, 18) = SS.Cell("D11").CellValue
'Cells(114 + 0, 16) = SS.Cell("C4").CellValue * 0.01 'Turbine
    inlet pressure
'end reset

For j = 0 To 76 ' (Cells(20, 3) - Cells(20, 2))
SS.Cell("B4").CellValue = Cells(114 + j, 1)
'Cells(114 + 0, 11) = Cells(20, 2) + 0 'Printing temperature
    range from A23
'Cells(114 + 0, 12) = 0 + 1 'Printing iteration number from B23
'Cells(114 + 0, 13) = Cells(23 + 0, 3) * 1000 'Boiler duty
'Cells(114, 12) = Cells(23 + 0, 3) * 1000
'Cells(8, 12) = Cells(23 + 0, 1) - Cells(21, 12) 'Pinch
Application.Wait Now + #12:00:01 AM#
Cells(114 + j, 2) = SS.Cell("D10").CellValue
Cells(114 + j, 3) = SS.Cell("B3").CellValue
Cells(114 + j, 4) = SS.Cell("B4").CellValue
Cells(114 + j, 5) = SS.Cell("C2").CellValue * 0.01
Cells(114 + j, 6) = SS.Cell("C3").CellValue * 0.01
Cells(114 + j, 7) = SS.Cell("C4").CellValue * 0.01
Cells(114 + j, 8) = SS.Cell("C5").CellValue * 0.01
Cells(114 + j, 9) = SS.Cell("D2").CellValue
Cells(114 + j, 10) = SS.Cell("D3").CellValue
Cells(114 + j, 11) = SS.Cell("D4").CellValue
Cells(114 + j, 12) = SS.Cell("D5").CellValue
Cells(114 + j, 13) = SS.Cell("E2").CellValue
Cells(114 + j, 14) = SS.Cell("B8").CellValue
Cells(114 + j, 15) = SS.Cell("B9").CellValue
Cells(114 + j, 16) = SS.Cell("D8").CellValue
Cells(114 + j, 17) = SS.Cell("D9").CellValue
Cells(114 + j, 18) = SS.Cell("D11").CellValue
Next j

'Cells(8, 13) = SS.Cell("C4").CellValue * 0.01
'Cells(7, 12) = SS.Cell("B3").CellValue
'Cells(9, 12) = SS.Cell("B5").CellValue
```

```
'Cells(13, 12) = SS.Cell("B9").CellValue
'Cells(6, 13) = SS.Cell("C2").CellValue * 0.01
'Cells(7, 13) = SS.Cell("C3").CellValue * 0.01
'Cells(9, 13) = SS.Cell("C5").CellValue * 0.01
'Cells(7, 14) = SS.Cell("D3").CellValue
'Cells(9, 14) = SS.Cell("D5").CellValue
'Cells(16, 12) = SS.Cell("D8").CellValue
'Cells(17, 12) = SS.Cell("D9").CellValue
'Cells(18, 12) = SS.Cell("D10").CellValue
'Cells(19, 12) = SS.Cell("D11").CellValue

End Sub
```

B.1.4 Code used for calculation of basic ORC properties at higher pressure levels.

This script was only included for reference, and will be impossible to run without the corresponding Excel document and HYSYS file. Therefore no "cleaning" of the code was performed before attachment.

Listing B.4: Visual basic code for estimation and print properties subsea ORC model, expander inlet pressure varied.

```
Public Sub HYSYS_Subsea_Cycle_Pump_Sensitivity()
Dim SS As Object
Dim j As Integer
Dim Compositions As Variant
Dim WF As Integer
Dim condensateStream As ProcessStream

'Code to load HYSYS simulation file
Set hysApp = CreateObject("HYSYS.Application")
hysApp.Visible = True
Set simCase = hysApp.ActiveDocument
If simCase Is Nothing Then
          filename = Worksheets("Raw_Potential_Tordis").Range("
             B2").Text
If filename <> "False" And simCase Is Nothing Then
          Set simCase = GetObject(filename, "HYSYS.
```

```
                SimulationCase")
            simCase.Visible = True
End If
End If

'Set condensateStream = simCase.Flowsheet.MaterialStreams.Item
    ("Condensate (3)")
'Compositions = condensateStream.ComponentMolarFractionValue
'For WF = 0 To 41        'collecting composition data as variant
'           Compositions(WF) = Worksheets("Raw_Potential_Tordis
    ").Range("I" & WF + 23).Value
'Next WF
'condensateStream.ComponentMolarFraction.Values = Compositions

Set SS = simCase.Flowsheet.Operations.Item("Cycle Summary")
SS.Cell("B2").CellValue = Cells(197, 2)
'SS.Cell("B4").CellValue = Cells(104, 2)
SS.Cell("B8").CellValue = Cells(203, 2)
'SS.Cell("C4").CellValue = Cells(8, 13) * 100

'SS.Cell("D2").CellValue = Cells(197, 4)
'SS.Cell("D4").CellValue = Cells(199, 4)
'SS.Cell("E8").CellValue = Cells(203, 5)
'SS.Cell("E9").CellValue = Cells(204, 5)

'to reset
'SS.Cell("B4").CellValue = Cells(209, 1)
'Cells(114 + 0, 11) = Cells(20, 2) + 0 'Printing temperature
    range from A23
'Cells(114 + 0, 12) = 0 + 1 'Printing iteration number from B23
'Cells(114 + 0, 13) = Cells(23 + 0, 3) * 1000 'Boiler duty
'Cells(114, 12) = Cells(23 + 0, 3) * 1000
'Cells(8, 12) = Cells(23 + 0, 1) - Cells(21, 12) 'Pinch
SS.Cell("C4").CellValue = Cells(209, 1) * 100
Application.Wait Now + #12:00:01 AM#
Cells(209 + 0, 2) = SS.Cell("D10").CellValue
Cells(209 + 0, 3) = SS.Cell("B3").CellValue
Cells(209 + 0, 4) = SS.Cell("B4").CellValue
```

```
Cells(209 + 0, 5) = SS.Cell("C2").CellValue * 0.01
Cells(209 + 0, 6) = SS.Cell("C3").CellValue * 0.01
Cells(209 + 0, 7) = SS.Cell("C4").CellValue * 0.01
Cells(209 + 0, 8) = SS.Cell("C5").CellValue * 0.01
Cells(209 + 0, 9) = SS.Cell("D2").CellValue
Cells(209 + 0, 10) = SS.Cell("D3").CellValue
Cells(209 + 0, 11) = SS.Cell("D4").CellValue
Cells(209 + 0, 12) = SS.Cell("D5").CellValue
Cells(209 + 0, 13) = SS.Cell("E2").CellValue
Cells(209 + 0, 14) = SS.Cell("B8").CellValue
Cells(209 + 0, 15) = SS.Cell("B9").CellValue
Cells(209 + 0, 16) = SS.Cell("D8").CellValue
Cells(209 + 0, 17) = SS.Cell("D9").CellValue
Cells(209 + 0, 18) = SS.Cell("D11").CellValue
'Cells(114 + 0, 16) = SS.Cell("C4").CellValue * 0.01 'Turbine
    inlet pressure
'end reset

For j = 0 To 100 '  (Cells(20, 3) - Cells(20, 2))
'SS.Cell("B4").CellValue = Cells(209 + j, 1)
SS.Cell("C4").CellValue = Cells(209 + j, 1) * 100
'Cells(114 + 0, 11) = Cells(20, 2) + 0 'Printing temperature
    range from A23
'Cells(114 + 0, 12) = 0 + 1 'Printing iteration number from B23
'Cells(114 + 0, 13) = Cells(23 + 0, 3) * 1000 'Boiler duty
'Cells(114, 12) = Cells(23 + 0, 3) * 1000
'Cells(8, 12) = Cells(23 + 0, 1) - Cells(21, 12) 'Pinch
Application.Wait Now + #12:00:01 AM#
Cells(209 + j, 2) = SS.Cell("D10").CellValue
Cells(209 + j, 3) = SS.Cell("B3").CellValue
Cells(209 + j, 4) = SS.Cell("B4").CellValue
Cells(209 + j, 5) = SS.Cell("C2").CellValue * 0.01
Cells(209 + j, 6) = SS.Cell("C3").CellValue * 0.01
Cells(209 + j, 7) = SS.Cell("C4").CellValue * 0.01
Cells(209 + j, 8) = SS.Cell("C5").CellValue * 0.01
Cells(209 + j, 9) = SS.Cell("D2").CellValue
Cells(209 + j, 10) = SS.Cell("D3").CellValue
Cells(209 + j, 11) = SS.Cell("D4").CellValue
```

```
86  Cells(209 + j, 12) = SS.Cell("D5").CellValue
87  Cells(209 + j, 13) = SS.Cell("E2").CellValue
88  Cells(209 + j, 14) = SS.Cell("B8").CellValue
89  Cells(209 + j, 15) = SS.Cell("B9").CellValue
90  Cells(209 + j, 16) = SS.Cell("D8").CellValue
91  Cells(209 + j, 17) = SS.Cell("D9").CellValue
92  Cells(209 + j, 18) = SS.Cell("D11").CellValue
93  Next j
94
95  'Cells(8, 13) = SS.Cell("C4").CellValue * 0.01
96  'Cells(7, 12) = SS.Cell("B3").CellValue
97  'Cells(9, 12) = SS.Cell("B5").CellValue
98  'Cells(13, 12) = SS.Cell("B9").CellValue
99  'Cells(6, 13) = SS.Cell("C2").CellValue * 0.01
100 'Cells(7, 13) = SS.Cell("C3").CellValue * 0.01
101 'Cells(9, 13) = SS.Cell("C5").CellValue * 0.01
102 'Cells(7, 14) = SS.Cell("D3").CellValue
103 'Cells(9, 14) = SS.Cell("D5").CellValue
104 'Cells(16, 12) = SS.Cell("D8").CellValue
105 'Cells(17, 12) = SS.Cell("D9").CellValue
106 'Cells(18, 12) = SS.Cell("D10").CellValue
107 'Cells(19, 12) = SS.Cell("D11").CellValue
108
109 End Sub
```

Appendix C

Heat Exchanger Design Illustration

The design illustrations shown in Appendix C were generated using Aspen HYSYS. The optimization was performed using the built in tool Aspen EDR Design and Rating. Component wise a build as simple as possible was preferred, proposing models with a maximum of two passes.

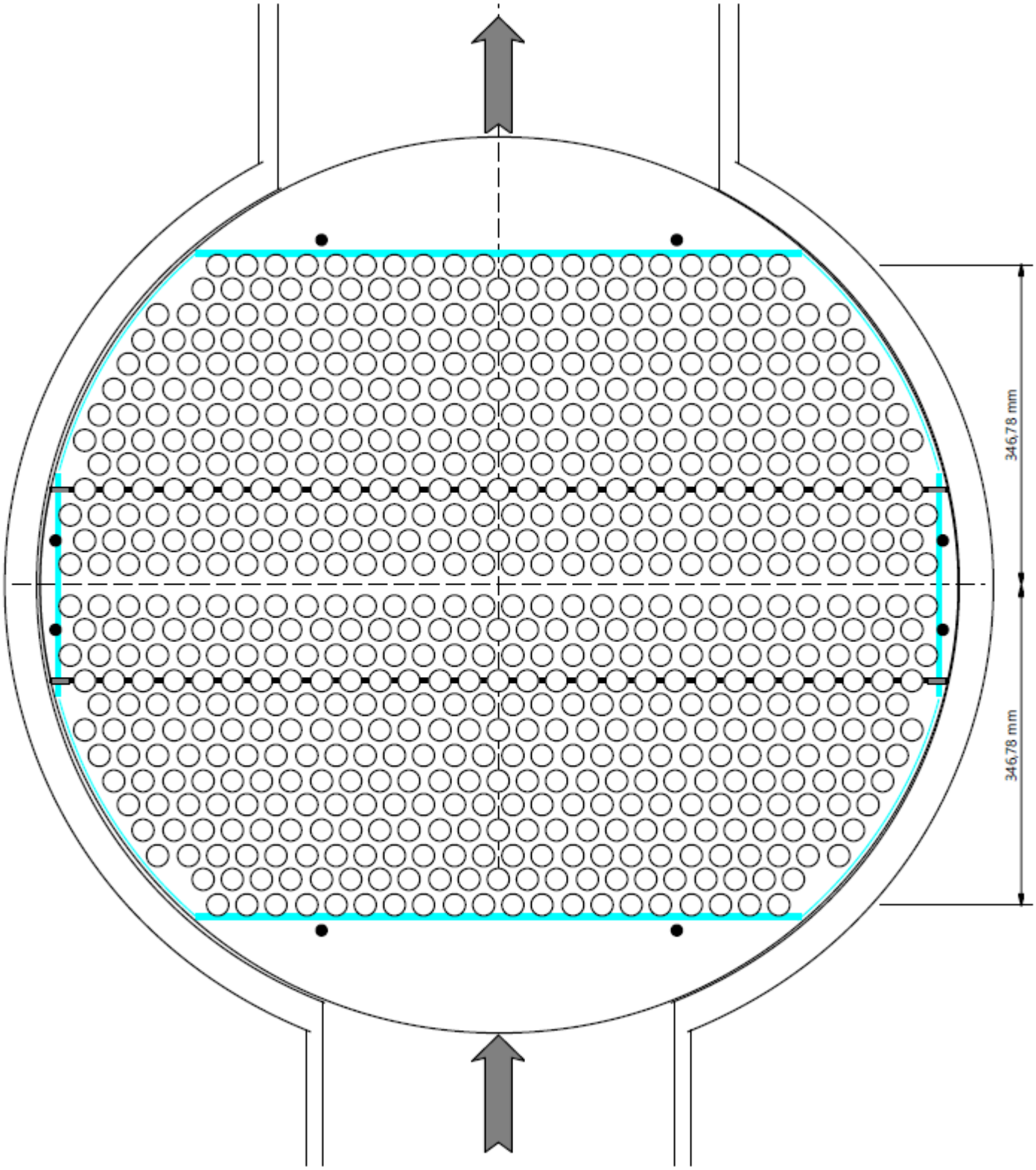

Figure C.1: Full cross section of the evaporator with 692 tubes installed using triangular pattern. Illustration generated using Aspen EDR.

Bibliography

Astolfi, M. and Macchi, E. (2017). *Organic rankine cycle (ORC) power systems: technologies and applications*. Number 107 in Energy. Woodhead Publishing, 1 edition.

Bai, Q. and Bai, Y. (2014). *Subsea Pipeline Design, Analysis, and Installation*. Gulf Professional Publishing, 1 edition.

Baumann, K. (1921). Some recent developements in large steam turbine practice. *I.E.E Journal*, 59(302):565 – 623.

Churchill, S. W. and Chu, H. H. (1975a). Correlating equations for laminar and turbulent free convection from a horizontal cylinder. *International Journal of Heat and Mass Transfer*, 18(9):1049 – 1053.

Churchill, S. W. and Chu, H. H. (1975b). Correlating equations for laminar and turbulent free convection from a vertical plate. *International Journal of Heat and Mass Transfer*, 18(11):1323 – 1329.

DiPippo, R. (2016). *Geothermal Power Plants, Fourth Edition: Principles, Applications, Case Studies and Environmental Impact*. Butterworth-Heinemann, 4 edition.

Dong, B., Xu, G., Luo, X., Zhuang, L., and Quan, Y. (2017). Potential of low temperature organic rankine cycle with zeotropic mixtures as working fluid. *Energy Procedia*, 105:1489–1494.

Efstathiadis, T., Kalfas, A., Seferlis, P., Kyprianidis, K., and Rivarolo, M. (2015). Geometry optimization of power production turbine for a low enthalpy (≤ 100°c) orc system. *Energy Procedia*, 75:1624 – 1630. Clean, Efficient and Affordable Energy for a Sustainable Future: The 7th International Conference on Applied Energy (ICAE2015).

Gleditsch, R. (2017). *Thermal Energy Conversion Methods for Subsea Power Generation*. TPG4560 Petroleum Engineering, Specialization Project.

Hettiarachchi, H. M., Golubovic, M., Worek, W. M., and Ikegami, Y. (2007). Optimum design criteria for an organic rankine cycle using low-temperature geothermal heat sources. *Energy*, 32(9):1698 – 1706.

Murty, V. D. (2018). *Turbomachinery Concepts, Applications, and Design*. CRC Press, 1 edition.

Nitsche, M. and Gbadamosi, R. O. (2016). *Heat Exchanger Design Guide: A Practical Guide for Planning, Selecting and Designing of Shell and Tube Exchangers*. Butterworth-Heinemann, 1 edition.

NORSOK P-002 (2014). Process system design. Standard, Standard Norge, Oslo.

Rudh, M., Fritz Jahnsen, O., and Hasan, Z. (2016). Subsea cooling; passive, active or sea current controlled? *SPE Asia Pacific Oil Gas Conference and Exhibition*.

Saleh, B., Koglbauer, G., Wendland, M., and Fischer, J. (2007). Working fluids for low-temperature organic rankine cycles. *Energy*, 32(7):1210 – 1221.

SIEMENS (2014). *Pre-designed Steam Turbines*. https://www.siemens.com/press/pool/de/feature/2014/energy/2014-04-orc/pre-designed-steam-turbines-10mw-e.pdf [Accessed: 2018-05-10].

Toffolo, A., Lazzaretto, A., Manente, G., and Paci, M. (2014). A multi-criteria approach for the optimal selection of working fluid and design parameters in organic rankine cycle systems. *Applied Energy*, 121:219–232.